

https://dspace.org/

Leaching of a copper-nickel flotation concentrate in choline-chloride based deep eutectic solvents

Kalake, Biki Tebogo

2025-09
University of the Witwatersrand, Johannesburg
https://hdl.handle.net/10539/49715

Kalake, Biki Tebogo. (2025). Leaching of a copper-nickel flotation concentrate in choline-chloride based deep eutectic solvents. [Master's dissertation, University of the Witwatersrand, Johannesburg]. WIReDSpace. https://hdl.handle.net/10539/49715

Downloaded from a DSpace repository. https://dspace.org/



LEACHING OF A COPPER-NICKEL FLOTATION CONCENTRATE IN CHOLINE CHLORIDE BASED DEEP EUTECTIC SOLVENTS

Biki Tebogo Kalake

A dissertation submitted to the Faculty of Engineering and the Built Environment, University of Witwatersrand, Johannesburg, in fulfilment of the requirements for the degree of Master of Science in Engineering.

Johannesburg, 2025

DECLARATION

I declare that this dissertation is my own unaided work. It is being submitted for the degree of Master of Science in Engineering to the University of the Witwatersrand, Johannesburg. It has not been submitted before for any other degree or examination in any other University.



Biki Tebogo Kalake

9th day of September 2025

ABSTRACT

The quest for sustainable and environmentally friendly metal extraction has driven the exploration of reagents such as deep eutectic solvents (DESs) as alternatives to conventional leaching reagents. This study investigated the leaching of nickel (Ni), copper (Cu), and cobalt (Co) from copper-nickel sulphide ore concentrates using three choline chloride-based DESs: ethaline, reline, and maline. Ethaline demonstrated the highest nickel recovery (56.34%) in factor screening experiments, while copper recoveries varied, with maline achieving the highest copper recovery of 19.61%. Cobalt recoveries were relatively low, peaking at 16% and showing minimal variation across the solvents. All solvents selectively recovered nickel, highlighting the potential of DESs as lixiviants for targeted metal dissolution.

Pulp density was identified as the most critical factor influencing nickel recovery in ethaline, with lower densities improving nickel extraction. Although the stirring rate was not independently significant, its interaction with temperature and leaching time was statistically significant. Optimal leaching conditions, of 0.5% pulp density, 600 rpm stirring rate, 25°C, and 1-hour leaching time, resulted in a nickel recovery of 59.06%, closely matching the response surface methodology (RSM) predicted maximum recovery of 58.12%. The process's rapid kinetics (1 hour) at near-ambient temperatures underscores its potential efficiency and scalability for sustainable metal extraction.

Kinetic studies revealed that the nickel dissolution is primarily controlled by mass transport, as indicated by a low activation energy of 12.24 kJ/mol. Activation energy calculations further showed copper dissolution was governed by mixed control mechanism. The nickel and cobalt kinetic data were fitted by a hybrid shrinking core model coupled with pseudo-second-order kinetics (R^2 > 80%), capturing the dynamic interactions of mass transfer and surface reactions.

The study further found that adding ethylene glycol as a diluent to reduce solvent viscosity did not enhance metal recoveries, with neat solvents showing superior performance.

This study highlights the potential of DESs, particularly ethaline, for selective and efficient nickel recovery from sulphide ores, providing sustainable insights into key operational parameters.

PUBLICATIONS AND PRESENTATIONS

Journal Publications

1. **Kalake, B.T.**, Ndlovu, S., Mapolelo, M.M., 2025. Comparative evaluation of choline chloride-based DESs for the leaching of base metals from copper-nickel sulphide ore, (Manuscript under preparation).

Conference Presentations

1. **Kalake, B.T.**, Ndlovu, S., Mapolelo, M.M., 2024. Leaching of a copper-nickel flotation concentrate in choline chloride-based deep eutectic solvents. Presented at Hydrometallurgy Conference 2024, SAIMM Southern Africa, Stellenbosch, South Africa, September 01 – 03.

DEDICATION

Dedicated to my late mother for instilling in me the value of education, and my late father for being a pillar of strength and support. To my wife and son for their love and understanding

ACKNOWLEDGEMENTS

“Wisdom is like a baobab tree; no one individual can embrace it’’. Throughout the course of this work, I encountered numerous challenges, but somehow, I managed to overcome them, largely due to the invaluable support of others. The attainment of true knowledge and wisdom requires walking a vast and complex road that requires the collective understanding and contributions of many people.

My deepest gratitude goes to my academic supervisor Prof Selo Ndlovu, for her insightful guidance and thought-provoking questions that greatly enriched the research presented in this dissertation. Her mentorship and unwavering support were essential to this research and are greatly appreciated.

I am equally grateful to my workplace supervisor Dr Mmilili Mapolelo for his guidance and always keeping me on track. His meticulous review of my work provided clarity and direction, ensuring that the quality of this research met the highest standards.

This study materialised due to the financial support of my employer the Botswana Institute for Technology Research and Innovation (BITRI). Its financial support, which was instrumental in the success of this study, is acknowledged and sincerely appreciated. BITRI further provided access to its state-of-the-art laboratory facilities where most of this study was conducted.

Special thanks are also due to the Hydrometallurgy Research Group at the School of Chemical and Metallurgical Engineering for the teamwork, and constructive feedback during group meetings.

.

TABLE OF CONTENTS

Declaration ii
Abstract iii
Publications and Presentations v
Dedication vi
Acknowledgements vii
List of Figures xiii
List of Tables xv
CHAPTER ONE 1
1 INTRODUCTION 1
1.1 Introduction 1
1.2 Problem Statement 5
1.3 Research Objectives 6
1.4 Research Methodology 7
1.5 Dissertation Layout 7
1.6 Summary 8
CHAPTER TWO 9
2 LITERATURE REVIEW 9
2.1 General Introduction 9
2.2 Mineralogy and Occurrence of Sulphide Deposits 10
2.2.1 Origin of the Sulphide Ore 11
2.2.2 Production of the Ore concentrate 12
2.3 Sulphide Ore Processing Methods 12
2.3.1 Beneficiation 12
2.3.2 Pyrometallurgy 14
2.3.3 Hydrometallurgy 15

2.4 Deep Eutectic Solvent Leaching 21
2.4.1 Introduction 21
2.4.2 Description and Formulation of Deep Eutectic Solvents 22
2.4.3 Properties of DESs 24
2.4.4 Ionometallurgy 25
2.5 Kinetics of Leaching Reactions 30
2.5.1 Models and Mechanisms 31
2.5.2 Influence of Leaching Variables 36
2.6 Summary 42
CHAPTER THREE 43
3 MATERIALS AND METHODS 43
3.1 Introduction 43
3.2 Materials 43
3.2.1 Copper-Nickel Sulphide Ore Concentrate 43
3.2.2 Reagents 46
3.2.3 Synthesis of DESs 46
3.3 Experimental Methods 47
3.3.1 Design of Experiments 47
3.3.2 Factor Settings 48
3.3.3 Apparatus and Experimentation 49
3.4 Analytical Techniques: Chemical Analysis 50
3.4.1 Sample Digestion 50
3.4.2 Atomic Emission Spectroscopy 51
3.4.3 X-Ray Fluorescence Spectroscopy 52
3.5 Mineral Analysis 53
3.5.1 X-ray Diffraction 53
3.5.2 AutoSEM Analyses – by TIMA-X 55

3.6 Data Analysis 56
3.7 Summary 56
CHAPTER FOUR 57
4 CHARACTERIZATION OF SULPHIDE ORE CONCENTRATE 57
4.1 Introduction 57
4.2 Results and Discussions 58
4.2.1 Chemical Analysis Results 58
4.2.2 Auto SEM: Bulk Mineralogy Analysis 58
4.2.3 Ni and Cu Deportment 59
4.2.4 Grain Size Distribution of Ni and Cu Bearing Minerals 60
4.2.5 Liberation Analysis 62
4.2.6 Associations of Minerals 64
4.3 Summary 65
CHAPTER FIVE 66
5 SCREENING OF SIGNIFICANT FACTORS AND SOLVENT ALTERNATIVES 66
5.1 Introduction 66
5.2 Experimental Factor Levels 67
5.3 Methodology for Data Analysis 68
5.3.1 Half-Normal Probability Plot of Effects 68
5.3.2 Pareto Chart 69
5.3.3 Analysis of Variance (ANOVA) 70
5.3.4 Diagnostic Plots (Residual analysis) 70
5.3.5 Model Graphs 71
5.4 Screening Experiments 72
5.4.1 Fractional Factorial Design 72
5.4.2 Full Factorial Design 79
5.5 Summary 88

CHAPTER SIX 89
6 PARAMETER OPTIMIZATION 89
6.1 Introduction 89
6.2 Model Derivation 90
6.3 Evaluating the Validity of the Model 92
6.4 Statistical Properties of the Model 94
6.5 Normal Plot of Residuals 95
6.6 Residuals vs Predicted 95
6.7 Model Graphs 96
6.8 Comparing Cubic to Quadratic model 98
6.9 Standard Error of Design 99
6.10 Determination of Optimum Conditions 100
6.11 Numerical Optimization 101
6.12 Response Prediction and Confirmation 104
6.13 Summary 106
CHAPTER SEVEN 108
7 KINETIC STUDY 108
7.1 Introduction 108
7.2 Extraction Profiles 109
7.2.1 Nickel Dissolution 110
7.2.2 Cobalt Dissolution 111
7.2.3 Copper Dissolution 112
7.3 SCM rate controlling mechanisms 113
7.3.1 Modelling Framework and Assumptions 114
7.3.2 Experimental Conditions 115
7.3.3 Results and Analysis 115
7.3.4 Discussion 119

7.4 Shrinking Particle Model Coupled with Pseudo-Second-Order Kinetics 120
7.5 Results and Discussion 122
7.6 Activation Energy 125
7.6.1 Results and Discussion 126
7.7 Summary 129
CHAPTER EIGHT 130
8 CONCLUSIONS AND RECOMMENDATIONS 130
8.1 Conclusions 130
8.1.1 Introduction 130
8.1.2 Screening of significant factors and solvent alternatives 131
8.1.3 Parameter Optimization 133
8.1.4 Kinetic study 134
8.1.5 Potential Application in Industry 135
8.2 Recommendations 136
8.2.1 Inert Atmosphere Experiments 136
8.2.2 Multiple Leaching Stages 137
8.2.3 Oxidative Leaching 137
REFERENCES 138
APPENDIX A 147
APPENDIX B 153
APPENDIX C 157

LIST OF FIGURES

Figure 1-1 Dissertation layout..... 8
Figure 2-1 Examples of hydrogen bond donors and hydrogen..... 23
Figure 2-2 Basic formula for quaternary ammonium salt-based DES (García Álvarez, 2014)..... 23
Figure 2-3 Graphic representation of leaching steps..... 32
Figure 2-4 Leaching of particles based on the Shrinking-Core-Model – Constant Size..... 34
Figure 2-5 Effect of solids to liquid ratio (pulp density) on the extraction of base metals from converter slag (Topçu, Rüşen and Küçük, 2021)..... 41
Figure 3-1 Leaching test setup..... 50
Figure 3-2 The Agilent 4200 Microwave-Plasma Atomic Emission Spectrometer (MP-AES)..... 52
Figure 3-3 A diagram representing a transverse-cut polished block..... 55
Figure 4-1 Explanation of grain versus particle..... 61
Figure 4-2 A schematic representation showing how a grain of interest can occur in varying..... 62
Figure 4-3 Liberation of Ni-bearing Minerals..... 63
Figure 4-4 Liberation of Cu-bearing Minerals..... 63
Figure5-1 Half Normal plot of estimated factor effects of Ni recovery using ethaline..... 73
Figure5-2 Pareto chart for ranking of main and interactive effects (Ni recovery)..... 73
Figure 5-3 Pareto chart for ranking of main and interactive effects (Co recovery)..... 74
Figure 5-4 Normal plot of residuals for Cu recovery..... 76
Figure 5-5 Half normal plot for Ni recovery..... 81
Figure 5-6 Pareto chart for ranking of effects on Ni recovery..... 82
Figure 5-7 Diagnostic plots, top left (Normal plot of residuals), top right (Residuals vs Predicted), bottom left (Residuals vs Run) and bottom right (Box-Cox Plot)..... 85
Figure 5-8 An interaction plot of pulp density vs Ni recovery..... 86
Figure 5-9 Two-way interaction plot for Ni recovery vs stirring rate..... 87
Figure 5-10 Cube plot for Ni recovery..... 87
Figure 6-1 Derivation of residuals..... 94
Figure 6-2 Normal plot of residuals for Ni recovery..... 95
Figure 6-3 Residuals vs Predicted response..... 96
Figure 6-4 Response surface plot for Ni recovery..... 97
Figure 6-5 Response surface plot for Co recovery..... 97

Figure 6-6 Response surface plot for Fe recovery 97
Figure 6-7 FDS plot for cubic model 98
Figure 6-8 FDS plot for quadratic model 98
Figure 6-9 Standard error of design for quadratic model 100
Figure 6-10 Goal is to maximize nickel recovery within the range 103
Figure 6-11 Solution to Ni recovery maximization via numerical optimization 103
Figure 6-12 Numerical optimization graphs indicating the predicted responses and factor levels 104
Figure 7-1 Nickel (pentlandite) dissolution from a polymetallic ore concentrate in terms of recovery at different temperatures 111
Figure 7-2 Cobalt (pentlandite inclusion) dissolution from a polymetallic ore concentrate in terms of recovery at different temperatures 112
Figure 7-3 Copper (chalcopyrite) dissolution from a polymetallic ore concentrate in terms of recovery at different temperatures 113
Figure 7-4 Plots of $1 - 1 - x23$ vs time for Co Dissolution at 25℃ to 60 ℃ 116
Figure 7-5 Plot of $1 - 31 - x23 + 21 - x$ vs time for Cu Dissolution at 25℃ to 60 ℃ 117
Figure 7-6 Plot of $1 - 1 - x13$ vs time for Cu Dissolution at 25℃ - 60℃ 117
Figure 7-7 Plot of $1 - 1 - x23$ vs time for Ni Dissolution at 25℃ - 60℃ 118
Figure 7-8 Plot of 1α vs $1t$ for the proposed SPM-PSO Co kinetic model at 25℃ 122
Figure 7-9 Plot of 1α vs $1t$ for the proposed SPM-PSO Co kinetic model at 60℃ 122
Figure 7-10 Plot of 1α vs $1t$ for the proposed SPM-PSO Ni kinetic model at 25℃ 124
Figure 7-11 Plot of 1α vs $1t$ for the proposed SPM-PSO Ni kinetic model at 60℃ 124
Figure 7-12 Arrhenius plot showing the linear relationship between *lnk* and *1/T* for Ni extraction in the DES, ethaline (1ChCl:2EG). 127
Figure 7-13 Arrhenius plot showing the linear relationship between lnk and 1/T 128

LIST OF TABLES

Table 2-1 Synopsis of base metal oxides/sulphides processed in various DESs with references.. 26
Table 3-1 List of chemicals used in the study 46
Table 3-2 Ethaline (ChCl:2EG) factor level settings 48
Table 3-3 Reline (ChCl:2U: nEG) factor level settings, where n 49
Table 3-4 Maline factor level settings (1ChCl:1MA: nEG),..... 49
Table 4-1 Chemical assay results 58
Table 4-2 Mineralogical Composition of the Samples, as Determined by Auto-SEM..... 59
Table 4-3 Distribution of Ni in Ni-bearing Minerals 60
Table 4-4 Distribution of Cu in Cu-bearing Minerals..... 60
Table 4-5 Size (ranges) at which 80% of mineral Grains will pass 61
Table 4-6 Association of Minerals Present in Sample (* Hem/Mag – Hematite/Magnetite) 64
Table 5-1 Experimental factors and their level settings..... 68
Table 5-2 Base metal recovery results for the $2IV4-1$fractional factorial design (leaching in ethaline)..... 72
Table 5-3 Summary of estimated main and interaction effects and diagnosis for ethaline 74
Table 5-4 ANOVA for the selected Co recovery model..... 75
Table 5-5 Base metal recovery results for the $2III5-2$fractional factorial design (maline). 76
Table 5-6 Summary of estimated main and interaction effects and model diagnosis for reline 77
Table 5-7 Base metal recovery results for the $2III5-2$fractional factorial design (leaching in maline). 77
Table 5-8 Summary of estimated main and interaction effects and model diagnosis for maline .. 78
Table 5-9 Base metal recovery results for the $2V4$fractional factorial design (leaching in ethaline). 80
Table 5-10 ANOVA for the selected Ni recovery model..... 83
Table 5-11 Fit statistics for Ni recovery..... 83
Table 6-1 Base metal recovery results for the I-optimal design 90
Table 6-2 Response information 91
Table 6-3 ANOVA for Ni recovery model 92
Table 6-4 Coefficients in Terms of Coded Factors 93
Table 6-5 Model Summary statistics (Ni Recovery)..... 93
Table 6-6 Model terms for cubic model..... 98

Table 6-7 Confirmation of Ni recovery at optimum leaching conditions 105
Table 6-8 Final optimum leaching conditions..... 107
Table 7-1 R-squared values for SCM fits..... 115
Table 7-2 Summary of cobalt SPM-PSO fit results 123
Table 7-3 Summary of nickel SPM-PSO fit results 125

CHAPTER ONE

INTRODUCTION

1.1 Introduction

The invention of lithium-ion batteries, coupled with smart devices, has transformed our way of life. Lithium-ion battery electrodes are constructed from significant quantities of cobalt, nickel, and copper. The accessibility of this trio of metals, particularly cobalt, is probably the defining factor in realizing the predicted "Electric Future". The desire to lower our reliance on fossil fuels and the related atmospheric pollution, by switching, a portion of traditional transportation to electric cars, has caused a surge in the demand for lithium-ion batteries and the associated raw materials. According to present-day production records, identified onshore reserves of cobalt may be depleted in seventy years, and those for copper and nickel in about forty years (Harris, 2019). Any surge in demand is predicted to significantly shrink this time frame. Competition for these metals, at least nickel, is partly driven by the steel industry, as it consumes seventy-one per cent of primary nickel production, with demand anticipated to grow at a rate of 5.7% per annum (Golroudbary *et al*, 2023).

To address the challenges posed by increasing demand and finite resources, advancements in processing technologies have become critical (Xie *et al*, 2005; Panayotova and Panayotov, 2020). The metals industry has favoured the advancement of aqueous-based or hydrometallurgical processes to meet these recent challenges. The hydrometallurgical processes are distinguishable from the conventional pyrometallurgical process routes by their lower operating temperatures, better environmental benignity, reduced unit costs and chemical selectivity (Smit, 2001).

Despite the benefits of hydrometallurgical processes, many existing operations still rely on traditional pyrometallurgical methods, which pose significant environmental challenges. A notable example of the detriments associated with pyrometallurgy is the case of the insolvent Bamangwato Concessions Limited (BCL Ltd) mine located in north-eastern Botswana. BCL also happens to be the source of ore concentrate used in this study. The company has been mining copper and nickel since the 1970s up until 2016 when it was put under provisional liquidation (Denysschen and Wagner, 2009; Mcrae, 2016; Otunniyi et al, 2016). They produced metal concentrate through froth flotation that was further processed in one of the world's largest flash furnace smelters into a high-grade matte product (Dixon-Warren, 2017).The flotation concentrate comprised of the sulphide ore minerals chalcopyrite, pentlandite and pyrrhotite, assaying between 2.5-3.5 % Ni and 3.2-4.5 % Cu (Simwakwa et al, 2009; Tripathi, Peek and Stroud, 2011).

The smelting of the BCL sulphide concentrate has always been mired in controversy, with various reports indicating the persistent concern of environmental issues associated with the substandard management of waste generated by the mine (Motswaiso, 2019; Ultra Jr and Manyiwa, 2021). Based on some reports, residents of the mining town were continuously exposed to polluted air laden with sulphur dioxide and heavy metals because of the smelting operations. Exposure to contaminated air has been linked to a high rise in cases of respiratory diseases in the nearby town of Selebi-Phikwe (Ekosse, 2007).

Smelting clearly presents several environmental and technical issues. Consequently, there is a growing interest in hydrometallurgical processing of concentrates, particularly for resources where this approach offers clear advantages. Hydrometallurgy involves metal extraction from mineral resources in acidic and alkaline media by use of various techniques such as atmospheric leaching, pressure leaching, heap leaching and more recently, bacterial leaching (Harris, 2019).

Microbial based lixiviants have been demonstrated to be highly successful in leaching chemical resistant gold (the BIOX® Process), but not as effective for certain base metal ore types (BioCOP® and BioNIC®). The BioCOP® process is effective for extracting copper from secondary sulphides like chalcocite but is less amenable to primary sulphides like chalcopyrite. Bioleaching processes also have relatively slower kinetics compared to abiotic systems and can extend leaching times to several weeks or months (van Aswegen, van Niekerk and Olivier, 2007; Gericke, Neale and Staden, 2009; Natarajan, 2018).

Numerous attempts have also been made to come up with nitrate-based circuits for base metals, such as the Nitrox and Redox process, without much success. Nitric acid is highly oxidizing, which makes it hazardous, particularly when combined with reducing agents like metal sulphides, making it susceptible to "runaway" reactions (Harris, 2019).

Despite its obvious advantages, hydrometallurgy is not entirely suited for the extraction of metals from low-grade ores. The acids used are not very selective at low metal concentrations, hence, significant portions of gangue minerals are also dissolved producing contaminated leachates (Binnemans and Jones, 2017). There is a perceptible necessity to come up with more efficient, cost-effective, and greener processes that can recover metals from progressively complex polymetallic ores (Chagnes, 2019).

Solvometallurgy is a promising new alternative in situations where pyrometallurgy or hydrometallurgy cannot satisfactorily recover metals from process streams. Sometimes referred to as non-aqueous metallurgy, solvometallurgy is a relatively new branch of extractive metallurgy that uses solvents such as ionic liquids (ILs), liquid state ammonia, DESs and supercritical carbon dioxide (Binnemans and Jones, 2017).

The initial idea for solvometallurgy can be traced back to the 1950s in the USA when organic mixtures were used to extract uranium from its ores (Bloecher Jr, 1950; Kimball and Ewing, 1957). It was later followed by the application of solvometallurgical techniques for the extraction of copper from chrysocolla (Raghavan and Fuerstenau, 1993). Recent research outputs indicate that process improvements have been made in the application of ILs and DESs for the extraction of non-ferrous metals like copper, nickel, zinc and lead (Tian, Jian and Hua, 2010; Smith, Abbott and Ryder, 2014).

Process intensification is an attractive feature of solvometallurgy. Process intensification refers to the development of innovative technologies and methodologies that make chemical processes more efficient, sustainable, and compact. It aims to enhance performance by reducing equipment size, energy consumption, waste generation, and operational costs. According to Binnemans and Jones (2017) through process intensification, the leaching and solvent extraction (SX) unit operations can effectively be combined into a single step, cutting equipment and operational costs.

Solvent selection is an important consideration in solvometallurgy. Inorganic solvents such as liquid ammonia and concentrated sulfuric acid, in essence, can be utilised as lixiviants. However, they are very unsafe and problematic to handle in practice. Ionic liquids on the other hand are considered excellent solvents but are too expensive for industrial application. An economic alternative to ILs is the wide variety of DESs, the majority of which are composed of choline chloride and a hydrogen bond donor or a hydrated metal salt. A typical DES is formed by a combination of choline chloride (ChCl) with urea (U) or ethylene glycol (EG) in a 1:2 molar ratio (Binnemans and Jones, 2017). ChCl is a cheap readily available animal feed product, which makes it ideal for large scale applications. The DES Ethaline (1mole ChCl: 2 moles EG) in the presence of iodine (I_2) as an oxidizing agent has been used to successfully leach chalcopyrite containing gold ore samples (Jenkin et al., 2016).

The kinetic data from the study showed that some gold grains dissolved completely within 15 minutes whereas the copper-containing grains dissolved more slowly. ChCl/U mixtures have previously been used to leach metals from various mixed metal oxides. The highest metal dissolution rates were observed for oxides of copper, zinc, and lead. These results indicated that the choice of hydrogen bond donor (ethylene glycol vs urea) influences dissolution rate (Abbott *et al*, 2005).

Despite their promise, the industrial application of DESs is still limited by several technical factors, such as their relatively high viscosities. The high viscosities can pose serious pumping and filtration problems. However, these issues might be mitigated using additives such as ethylene glycol to improve the rheological properties (Abbott *et al*, 2009). It seems little is known about the behavior of metal ions in non-aqueous media, in comparison to the vast amount of data on the properties of metal ions in aqueous systems. This knowledge gap needs to be addressed urgently. The technology readiness rating of most solvometallurgical techniques is still very low (Binnemans and Jones, 2017). Although this outlook is not considered good for immediate application, it represents a great opportunity for research and development.

1.2 Problem Statement

Although the extraction of critical battery metals from various minerals using deep eutectic solvents (DESs) has been substantially studied, most research has focused on electrochemical leaching of metal oxides. Limited research exists on the non-redox chemical dissolution of polymetallic sulphides in DESs. Furthermore, while numerous eutectic mixtures have been explored for metal recovery, their performance often results in poor recoveries, and comparative studies to guide solvent selection are almost non-existent. It is hypothesized that novel DES formulations can selectively dissolve polymetallic sulphides, enable the recovery of nickel, copper, and cobalt while avoiding the challenges of sulphur dioxide emissions associated with pyrometallurgy and the toxicity of some aqueous

solvents. By optimizing solvent formulation and processing conditions, high metal recoveries may be achieved.

1.3 Research Objectives

This study aims to develop an eco-efficient approach for the extraction of copper, nickel, and cobalt from a polymetallic sulphide flotation concentrate using environmentally friendly DESs. Unlike previous studies that focused on single minerals like chalcopyrite or emphasized electrochemical-driven leaching, this work investigates the non-redox chemical dissolution of a complex concentrate and provides a comparative analysis of choline chloride-based DES formulations (ethaline, reline, and maline) to optimize metal recovery. The specific objectives for the research study are as follows.

(i) To conduct solvent selection or comparison experiments, to identify the lixiviant (ethaline, reline or maline) that demonstrates the highest extraction of nickel, copper and cobalt.

(ii) Investigation of parameters which promote Ni, Cu and Co dissolution in sulphide concentrate using the DESs

(iii) To establish the optimal conditions for extraction of nickel, copper and cobalt by employing the most effective lixiviant (*i.e.*, optimization studies).

(iv) Derivation of a conceptual reaction kinetic model for Ni, Cu and Co dissolution.

The research questions the study aims to address are as follows.

i) Which choline chloride-based DES (ethaline, reline or maline) demonstrates the highest extraction efficiency for nickel, copper, and cobalt from polymetallic sulphide flotation concentrates?

ii) What are the critical leaching parameters (e.g., temperature, leaching time, pulp density) that significantly affect the dissolution of nickel, copper, and cobalt using DESs?

iii) What are the optimal leaching conditions for maximizing the recovery of nickel, copper, and cobalt from sulphide flotation concentrates using DESs?

iv) What are the reaction kinetics governing the dissolution of nickel, copper, and cobalt in the most effective DES formulation, and how can these be modelled conceptually?

1.4 Research Methodology

The research methodology was carried out over several major steps: literature review, experimental design, laboratory experimentation and data analysis, drawing conclusions from the results and offering recommendations.

1.5 Dissertation Layout

This section offers an overview of the chapters and sections that are contained in this dissertation. Each chapter starts with a brief background that underscores the key points of the various sections in the chapter. A synopsis is given at the end of each chapter to highlight the main takeaways. An overview of the dissertation layout is depicted in the flow diagram in **Figure 1-1**.

Chapter 1 provides motivation for the research, the problem statement, and the overall objectives of the study. Chapter 2 sets out to review related literature on the extraction of base metals in DESs. A general overview of the conventional methods of extraction of copper, nickel and cobalt is given. Also, current literature on processing these metals in DESs is given. Chapter 3 describes the materials and methods used in the study. Chapters 4 to 7: describe the laboratory tests and findings as depicted in **Figure 1-1**. Chapter 8 concludes the dissertation with a summary of the findings and recommendations. Appendices of detailed laboratory test results and other important data are also included.

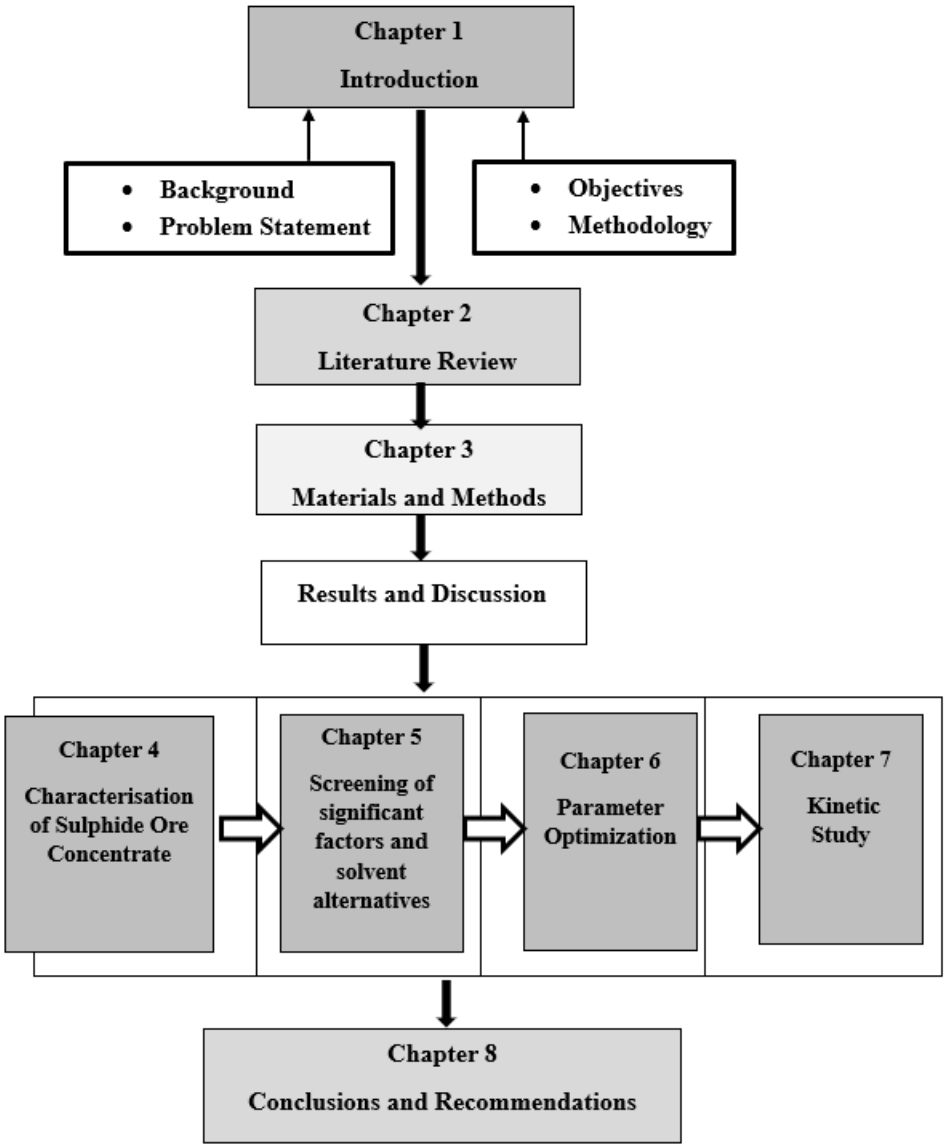


Figure 1-1 Dissertation layout

1.6 Summary

In this introductory chapter, the background, problem statement, research aims and objectives were discussed. This was followed by a short description of the research methodology and thesis outline. The next chapter reviews relevant literature.

CHAPTER TWO

LITERATURE REVIEW

2.1 General Introduction

The burgeoning demand for electric vehicles (EVs) as a remedy for extensive decarbonization of terrestrial transportation systems and as a tactic for alleviating climate change has consequently driven the demand for battery metals and minerals (Manjong *et al.*, 2021). Considerable amounts of metals, such as lithium, manganese, cobalt, nickel, and rare earth elements, are indispensable for emerging technologies, particularly those essential for low-carbon energy. These so-called "critical materials" because of their rising economic significance and important contribution to emerging green technologies have a high risk of supply shortage. At present, lithium-nickel-cobalt-manganese oxide materials are the primary components dominating the EV battery technology. The current demand for these metals is rapidly increasing, with lithium rising by a factor of 18-20, cobalt by 17-19, and nickel by 28-31 from 2020 to 2050. The two main EV battery types, Nickel Cobalt Aluminium (NCA) and Nickel Manganese Cobalt (NMC), predominantly use nickel, accounting for 80% and 50% of their composition, respectively. It is imperative to explore sustainable and alternative sources to fulfil the surging demand for these metals. However, increased production output needs to be balanced with the development of green mineral processing and extraction technologies to mitigate the environmental issues associated with conventional mining methods (Nkrumah *et al.*, 2022).

This literature review aims to obtain a general knowledge of nickel/copper/cobalt sulphide ore mineralogy and its occurrence including the current metallurgical processes and the associated difficulties in the beneficiation of sulphides. The general principles of the leaching processes of ores are also discussed. The importance of DESs in the leaching of metallic sulphide ores is emphasized, as they may offer a greener alternative to conventional lixiviants. In contrast to strong

mineral acids, DESs are less volatile, less corrosive, and in many cases biodegradable, thereby potentially reducing environmental risks such as acid mine drainage and emissions associated with conventional hydrometallurgical and pyrometallurgical processes.

2.2 Mineralogy and Occurrence of Sulphide Deposits

Nickel was first used in alloys called packfong by the Chinese long before it was known in Europe (Weeks, 1932). It was later identified and named by the Swedish chemist and mineralogist Axel Fredrick Cronstedt in 1751. Cronstedt's discovery precipitated from his study of the nickel ore niccolite, at the time believed or mistaken by some scientists to be a type of copper alloy containing cobalt, arsenic, and iron. Niccolite, which happens to be a nickel arsenide, has largely been replaced by pentlandite ores as the primary nickel source in the modern era (Bartow, 1953). Cobalt, like nickel owes its discovery to a Swedish chemist, Georg Brandt. Initially favoured for its ability to colour glass blue, cobalt now has many uses. Its primary minerals include cobaltite (CoAsS) and erythrite ($Co_3(AsO_4)_2$). However, it is important to note that cobalt is commonly found as a byproduct of nickel and copper ore processing (Weeks, 1932). Archaeological findings indicate copper has been used by people for at least 7000 years (Radetzki, 2009). The Romans got most of their copper from the island of Cyprus, hence its name aes cyprium (ore of Cyprus. Today, copper is mainly sourced from the sulphide ores chalcopyrite ($CuFeS_2$), bornite (Cu_6FeS_4),), chalcocite (Cu_2S) and covellite (CuS)) (Dhavalikar, 1997).

Sulphide deposits are broadly classified into three categories, i.e., magmatic deposits: volcanic and sediment-hosted massive sulphide deposits. Magmatic sulphide deposits are the outcome of natural smelting, the ores are created through the concentration of non-miscible sulphide liquid (matte), upgraded with chalcophile metals, acquired from silicate magmas (slags) (Barnes, Holwell and Le Vaillant, 2017).

The enrichment of the metals; Ni, Cu, Au, and the platinum group metals (PGMs) in the matte section have created some of the most important ore deposits on the planet. More than half of global nickel output and 96% of PGM production is linked to sulphide deposits. The Francistown region, in the east of Botswana, holds several such plutonic magmatic deposits, including the already exploited Phoenix, Selebi-Phikwe and Selkirk ore bodies (Maier *et al.*, 2008).

2.2.1 Origin of the Sulphide Ore

The material used in this study originates from the sulphide deposits of the Selebi-Phikwe region. The deposits were originally discovered by the inactive and insolvent mining company, Bamangwato Concessions Limited (BCL) between 1963 and 1966. Among these, the Phikwe deposit is the largest, with an estimated 31 Mt at grades of 1.36% Ni and 1.12% Cu, whereas Tekwane is the smallest, with 0.6 Mt at grades of 1.2% Ni and 0.6% Cu (Maier *et al.*, 2008).

The sulphide mineralization in the deposits occurs in disseminated, massive, and vein-type structures, comprising pyrrhotite, chalcopyrite, and pentlandite. Pentlandite is the primary nickel-bearing mineral, present as lamellae flares and coarse clusters within pyrrhotite, with grain sizes ranging from 8 to 38 microns. Approximately 0.1–1% Ni is found in the pyrrhotite crystal lattice, while cobalt is present primarily in solid solutions in pentlandite (Mulaba -Bafubiandi and Medupe, 2007). The identified PGM minerals include merenskyite, hollingworthite, and sperrylite (Maier *et al.*, 2008). The ore also contains trace amounts of native gold and cobaltite. The main gangue minerals are feldspar, quartz, amphibolite, and mica making up around sixty-eight per cent of the ore composition (Otunniyi et al., 2016).

2.2.2 Production of the Ore concentrate

The mining of the Selebi-Phikwe deposits to recover nickel and copper has been going on since 1973 up until 2016 when the mine was shut down and put under care and maintenance (Otunniyi et al., 2016). The mine produced feed ore at a grade of 0.55–0.71 % Ni, 0.58–0.75 % Cu and 0.05% Co. The beneficiation of run-of-mine ore (ROM) began with a three-stage dry crushing process that produced a -25 mm size fraction that was followed by grinding in separate. The ground ore was upgraded to a concentrate by froth flotation and magnetic separation. Magnetic separation was used to recover pentlandite that is associated with the faintly magnetic pyrrhotite from the flotation tailings. Final concentrate grades have been reported to range between 2.5–3.5 % Ni, 3.2–4.5 % Cu, 30% S, 45% Fe and 8% Si. The flotation concentrate was smelted to produce a high and low sulphur Cu-Ni matte product that was sold to refineries in Norway and Zimbabwe respectively (Mulaba -Bafubiandi and Medupe, 2007; Simwakwa et al., 2009; Tripathi, Peek and Stroud, 2011).

2.3 Sulphide Ore Processing Methods

2.3.1 Beneficiation

The first step in the processing of Ni-Cu sulphide ores involves the physical separation of the values from gangue, typically by froth flotation to obtain a concentrate. Froth flotation separates minerals by exploiting the differences in surface properties. Certain minerals can be rendered hydrophobic using reagents called collectors, allowing them to be floated or separated from an ore slurry. The copper and nickel minerals can be separated by selective flotation in a stepwise fashion to recover copper and nickel as separate concentrates. However, in the case of finely disseminated complex sulphides where liberation is difficult the minerals are often bulk floated to obtain a bulk concentrate, which may undergo further processing.

Bulk flotation offers faster processing times and simple reagent schemes when compared to selective flotation however it comes at the cost of poor selectivity and lower grades.

Flotation recipes are complex and variable. They are generally influenced by the ore mineralogy, hence will vary from place to place. The chalcocite and carrolite mineral fractions of the ores of the DRC are bulk floated at pH 9.2 utilising xanthates as collectors and tri-ethoxybutane as a frothing agent yielding a concentrate assaying 43-53% Cu and 0.5-3% Co. The Cu-Co ores of Zambia are initially conditioned to selectively float the copper minerals using sodium cyanide as a depressant. The depressed cobalt minerals are then activated by sulphuric acid and floated using sodium isopropyl xanthate (Habashi, 1997). Beneficiation of the run of mine (ROM) at BCL mine in Botswana entailed flotation and magnetic separation. The flotation was accomplished using a potassium *n*-butyl xanthate (PNBX) collector and Sasfroth 200 (butyl triglycol ether) as a frother . Magnetic separation was used to recover pentlandite that was associated with the faintly magnetic pyrrhotite from the flotation tailings. Final concentrate grades were reported to range between 2.5–3.5 % Ni, 3.2–4.5 % Cu, 30% S, 45% Fe and 8% Si (Mulaba -Bafubiandi and Medupe, 2007; Simwakwa et al., 2009; Tripathi, Peek and Stroud, 2011).

Froth flotation is generally an effective technique for upgrading polymetallic ores as it is highly selective (Fuerstenau, Jameson and Yoon, 2007). It is also very versatile as it can be applied to both small-scale and large-scale operations. More importantly it facilitates the recovery of valuable metals from previously subeconomic low-grade and polymetallic ores (Gupta and Yan, 2006).

Despite its economic and technical prowess, flotation comes with some environmental and operational challenges. Froth flotation generates sulphide tailings that require stringent environmental management, to mitigate acid-mine drainage (Lottermoser and Lottermoser, 2010).

The process also requires continuous optimization to address ore variability and maximize recovery. There are also challenges with recovery of minor but valuable elements like cobalt which might get lost to tailings without additional processing stages. A study by Shengo (2021) discusses innovative techniques for recovering cobalt and copper from flotation tailings, highlighting its economic potential. Advancements in reagent chemistry, process automation, and environmental management are essential to maximize the benefits and mitigate drawbacks associated with froth flotation.

2.3.2 Pyrometallurgy

The extraction of nickel, copper and cobalt from concentrates is typically accomplished by pyrometallurgical, hydrometallurgical and electrometallurgical methods (Habashi, 1997). Among these, pyrometallurgy plays a central role in the processing of sulphide concentrates, utilizing high temperature processes such as roasting, smelting and converting to drive the necessary chemical reactions for metal recovery (Gupta, 2006). Pyrometallurgy is carried out over a wide temperature spectrum, that ranges from 300 ℃ for lead processing and up to 2000 ℃ to produce ferronickel (Reuter, 2021). For copper processing, sulphide concentrates are typically smelted at temperatures between 1200 and 1500 ℃ to produce a matte, which is further oxidized to yield crude or blister copper (Samadov *et al.*, 2018). Nickel extraction follows a similar route, with roasting used to remove sulphur as sulphur dioxide (SO_2) gas, followed by smelting to produce a nickel-rich phase, and converting to remove residual iron and sulphur (Habashi, 1997).

While pyrometallurgical methods are effective, they come with notable disadvantages. One of the most significant challenges is the environmental impact associated with the production of large quantities of SO_2 gas. This byproduct, if untreated, poses severe environmental hazards. Although SO_2 can be converted into sulfuric acid, this requires additional infrastructure, and the transportation and marketing of the acid can be both hazardous and expensive, adding to the overall

operational costs. Furthermore, pyrometallurgy is highly energy-intensive, necessitating the excessive consumption of fuel to maintain the high temperatures required for smelting and converting. This energy demand not only increases costs but also necessitates the use of complex installations to improve heat economy, which can be cumbersome to manage and maintain (Habashi, 2013).

Another critical drawback of pyrometallurgy is its limited efficiency in processing complex ores. The separation of metals such as cobalt becomes particularly challenging, with substantial losses often occurring to the slag phase. In the case of cobalt recovery, only about 22-30% of the cobalt in the feed concentrate is typically recovered to the matte phase, with the remainder lost to the iron-rich slag. Additionally, the smelting of lower grade ores is often uneconomical due to their high gangue content, which increases the flux requirements and energy consumption disproportionately to the value of the extracted metals. This economic limitation reduces the feasibility of using pyrometallurgical methods for low-grade or highly complex sulphide ores. This is concerning as ore grades have historically been declining and primary ores are also being depleted (Tripathi, Peek and Stroud, 2011).

Despite these challenges, pyrometallurgy remains an established and well-optimized technology to produce high-grade matte and finished metal products. However, its drawbacks highlight the need for alternative or supplementary methods, such as hydrometallurgical and solvometallurgical approaches, which may address some of the environmental and energy concerns associated with pyrometallurgy.

2.3.3 Hydrometallurgy

Hydrometallurgy involves the processing of metallic ores in water-based media. Metal extraction occurs through the interaction of metal-bearing minerals with reactive species in aqueous solutions, transforming the metals into soluble ionic

forms. This solubilization facilitates subsequent purification or recovery processes such as solvent extraction and ion exchange (Free, 2013). The selectivity of lixiviants plays a crucial role in targeting specific minerals and minimizing reagent consumption, thus addressing some limitations of pyrometallurgy. However, the relatively slow kinetics of leaching and the large volumes of solutions required per unit mass of metal are significant drawbacks. Additionally, the generation of sulphate-containing effluents necessitates effective wastewater treatment to mitigate environmental contamination (Habashi, 1997). The following subsections critically evaluate specific hydrometallurgical techniques for treating copper-nickel sulphide ores, highlighting their strengths and limitations.

Ammonia Pressure Leaching

The ammonia pressure leaching process, pioneered by Sherritt Gordon, effectively dissolves nickel, copper, and cobalt as ammonia complexes at moderate temperatures (80–95°C) under high-pressure conditions. CuS is rejected from the nickel liquors through the addition of sulphur and SO_2. Nickel is then recovered as a powder by hydrogen reduction. The reduction end solution is then treated with hydrogen sulphide to precipitate the rest of the nickel and cobalt in sulphide form (Habashi, 1997).

Ammonia leaching offers several advantages over traditional methods. Notably, it boasts lower toxicity and a relatively low cost, particularly due to its ease of recycling. Ammonia leaching also excels in its low reagent consumption for refractory ores and its ability to efficiently dissolve many transition metals into water-soluble complexes. The dissolution kinetics of copper, nickel, and cobalt in ammoniacal solutions have been well-studied (Meng and Han, 1996).

These basic heavy metals are readily soluble in ammoniacal solutions even at room temperature. However, the leaching kinetics of these metals are often controlled by mass transfer of a limiting reactant such as, dissolved oxygen.

The dissolution mechanism is electrochemical in nature, making it susceptible to passivation, a phenomenon that can occur when the solution pH is either too high or too low (Meng and Han, 1996).

Atmospheric Acid leaching

Atmospheric acid leaching has been developed and applied as a relatively low-cost method for processing certain metal sulphides and mattes. A notable example is the atmospheric leach process developed by Outokumpu in Finland in the 1960s for the treatment of low-sulphur matte. This process utilizes air-agitated Pachuca tanks and involves three-stage counter-current leaching at approximately 80°C in an acidic sulphate medium (Habashi, 1997).

Nickel is dissolved in the first stage by reaction with acid and soluble copper, which is cemented from the solution as metal. The residual nickel and a bit of copper are leached in the subsequent leach stages. Overall, nickel recovery from the process is approximately 90%, while copper recovery is significantly lower, at around 50%. The copper-rich leach residue can either be treated in a fourth pressurized leach stage or recycled to the smelter (Habashi,1997).

Cobalt is recovered from the 1st stage leach solution by contacting the sulphate solution with a nickel (III) hydroxide slurry thus precipitating insoluble cobalt (III) hydroxide. The precipitate is refined to produce cobalt metal and salts using the pentamidine process (Habashi,1997).

Atmospheric acid leaching offers several benefits, including lower capital and operational costs compared to high-pressure leaching methods. It also eliminates the need for specialized high-pressure equipment, making it a simpler and safer alternative for certain operations. However, the process is not without its challenges. One major limitation is the relatively low recovery rate for copper, which may necessitate additional treatment stages or recycling to improve efficiency.

The process is also less effective for high sulphur feeds as they are prone to forming passivation layers, which can inhibit leaching kinetics (Free,2013).

Acid Pressure leaching

Sherritt Gordon developed the acid pressure leaching process in the 1960s, which was later adopted by most of the major platinum miners in South Africa. Pressurized leaching is typically performed inside reactors at 135-160°C and oxygen partial pressures of 140-350 kPa. This process is favoured by the platinum producers because of the exceptionally high recoveries (>99.9%) of base metals and sulphur, which yields high-grade PGM leach residue/concentrate for the downstream platinum refinery. The plant flowsheet varies widely across the different mines. Some operations utilize two stages of continuous pressurized leaching at 135-150°C, whilst the smaller refineries start with a low-temperature atmospheric leach followed by a single stage of pressurized leaching at 160°C (Habashi, 1997).

These pressure-leaching processes offer the advantage of self-generating most of the sulphuric acid used in the process which is continuously recycled from the electrowinning units to the leaching autoclaves. As a result, the net acid consumption is minimal. An added benefit is that iron is removed by precipitating as ferric hydrous oxide, which is disposed of in the residue. The low iron content in the leach liquor makes direct electrowinning of copper feasible, eliminating the need for a liquid-liquid extraction plant and reducing associated costs (Paynter, 1973).

Chloride Leaching

The Cymet process is one of the several chloride-based methods developed for sulphide dissolution. A key advantage of chloride processes is their ability to operate under atmospheric. Leaching typically occurs at 75–80°C in a ferric chloride solution or anolyte.

The leach slurry underscores a second stage of leaching in the anode compartment of an electrolytic dissolution cell. Copper is then recovered as a powder in the cathode compartment and removed as a slurry, which is subsequently sent for electrorefining (Paynter, 1973).

Leach residues are processed in an autoclave at approximately 135°C for two hours to produce sulfur globules. These globules, once cooled, are screened off, with the screen underflow subjected to flotation. The resulting concentrate is recycled for leaching, while the tailings are discarded. The spent copper catholyte undergoes further copper removal through cementation with metallic iron. The purified ferrous chloride solution is directed to electrolytic iron cells, where high-purity iron is plated onto starter sheets, and ferric chloride is regenerated at the anodes. The process achieves an overall copper extraction rate exceeding 98%. Operating and capital costs are reportedly slightly lower than those of conventional smelting. With credits for by-products like iron and sulfur, the Cymet process becomes significantly more economical (Paynter, 1973).

The Cymet process takes advantage of copper's ability to exist in the cuprous state in chloride media, reducing electrowinning power consumption to about half of that required in sulphate media. However, a drawback is the production of copper powder, necessitating further electrorefining and increasing capital costs. The major limitation lies in the technological challenges of operating the slurry electrolytic cell, which may not be necessary given that direct ferric chloride leaching achieves comparable copper recoveries (Paynter, 1973).

Bacteria Assisted Leaching

Microbe-assisted leaching has been demonstrated on some low-grade copper ores and industrial waste. A particular subset of autotrophic bacteria can be used to speed up the oxidation of copper and iron sulphides. The common species used include *Thiobacillus thiooxidans*, for oxidation of sulphide to sulphate and *Thiobacillus ferrooxidans*, for oxidation of iron (II) to iron (III).

Bacterial leaching of copper sulphide ores is generally performed at 25-40°C, pH 1.5-3.5 (sulfuric), at a defined metal ion concentration, under sufficient oxygen and limited exposure to sunlight. Bioleaching as it is commonly known has increased in popularity due to its greener credentials and low energy demands (Habashi, 1997) .

The Talvivaara polymetallic deposit in, Finland, is a prominent example of heap bioleaching applied to the treatment of sulphide ore (Masloboev *et al.*, 2018). The ore consists of low-grade black schist, containing pentlandite, pyrrhotite, chalcopyrite, sphalerite and pyrite as the primary sulphide minerals (Riekkola-Vanhanen, 2013). The bioleaching process occurs in two stages: initially, the ore is heaped onto a primary pad and leached for 13–14 months (Masloboev *et al.*, 2018). Afterward, the partially leached ore is transferred and restacked onto a secondary heap pad for further leaching to extract residual metals that were not adequately contacted by the lixiviant during the primary stage. Metals are recovered from the leach solution by precipitation using hydrogen sulphide and pH control. The pH of the bulk solution is a critical parameter in bacterial leaching. At Talvivaara the pH value must be kept above 1.5 to prevent silicate precipitation while maximizing metal dissolution operations (Riekkola-Vanhanen, 2013).

After 500 days, the extraction efficiencies were 92% for Ni, 82% for Zn, 14% for Co, and only 2% for Cu. The low copper recovery was attributed to the electrochemical properties of the minerals. Sulphide minerals exhibit semiconductor behaviour, which leads to galvanic interactions when electrical contact occurs between different mineral phases. During the dissolution of a mixture containing various sulphides, minerals with the highest rest potentials act as cathodes, receiving galvanic protection. This delays their leaching until minerals with lower rest potentials are dissolved. Chalcopyrite and pyrite have higher electrochemical potentials compared to pyrrhotite, pentlandite, and sphalerite, further explaining the hindered leaching of copper (Saari and Riekkola-Vanhanen, 2012)

The Talvivaara Mining Company Plc. declared bankruptcy in 2015 and, after several transitions, is now owned by the state-run company Terrafame Oy. The bankruptcy was attributed to market pressures, challenges with their bioleaching technology, and significant environmental issues. The mine caused extensive environmental damage, including the leakage of toxic metals into nearby water systems (Sairinen, Tiainen and Mononen, 2017).

2.4 Deep Eutectic Solvent Leaching

2.4.1 Introduction

The premise for an idealised green solvent is that it needs to be harmless to people and the environment, whilst simultaneously being sustainable from a manufacturing and utility perspective. There are at least five qualifying criteria that green solvents need to meet: non-toxic, abundant, biodegradable, recyclable, non-flammable and inexpensive. So far, candidates that meet most of these criteria are very few and include supercritical fluids, water, ionic liquids (ILs), and perfluorinated solvents. ILs have been in the spotlight because of their high thermal stability and low vapour pressure, however, they need to be reconsidered due to their reported high toxicity and low biodegradability. Supercritical fluids on the hand are nontoxic, inert, and highly recyclable. However, they are generally considered poor solvents for most compounds and are limited by their requirement for complex high temperature (energy) and high-pressure reactors. Water is probably the greenest solvent known to man; however, it is limited by its narrow temperature range (0-100°C) and poor solubility for some inorganic compounds (García Álvarez, 2014).

The desire to overcome the numerous limitations posed by conventional green solvents has pushed researchers to explore new generations of solvents (García Álvarez, 2014). In this context, recent ground-breaking research has demonstrated the potential of DESs as exceptional green and renewable solvents.

DESs have been studied extensively for application in a wide range of areas such as electrochemistry, catalysis, material chemistry and more importantly extractive metallurgy (Binnemans and Jones, 2017).

2.4.2 Description and Formulation of Deep Eutectic Solvents

A scan of the literature indicates several names have been proposed to describe blends of two or more compounds which can form hydrogen bond interactions with one another resulting in a eutectic mixture, that is liquid melting between room temperature and 70ºC, with a specific melting point lower than the individual compounds. The popular names used to describe such mixtures include Deep Eutectic Solvents (DESs), Deep Eutectic Ionic Liquids (DEILs), Low Melting Mixtures (LMMs) and Low Transition Temperature Mixtures (LTTMs). The term Deep Eutectic Solvent was conceived by Abbott et al. (2003) to describe the creation of a eutectic mixture (melting point 12ºC) formed by mixing two solids i) choline chloride (melting point 133ºC), and ii) urea (melting point 302ºC) in a molar ratio of 1:2. If we consider the extensive number of affordable, nontoxic, renewable and biodegradable components that can be used to form eutectic mixtures, the feasibility of creating novel green DESs is almost limitless (**see Figure 2-1).**

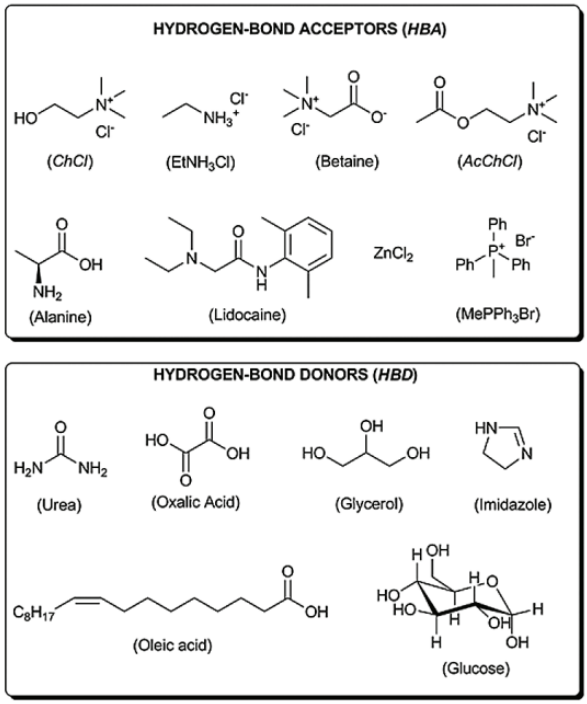


Figure 2-1 Examples of hydrogen bond donors and hydrogen -bond donors typically used for DESs synthesis (García Álvarez, 2014)

The exact mechanism of how eutectic mixtures are formed is not yet clear with some authors proposing cluster formation whilst others suggest mechanical mixing of components (García Álvarez, 2014). Nonetheless, the consensus is that to form DESs we need, a hydrogen bond acceptor (HBA), typically a quaternary ammonium salt and a hydrogen bond donor to complex with the halide ion of the salt. These DESs can be described by the general formula $[R^1\ R^2\ R^3\ R^4\ N^+\ X^-]\cdot[Y]$, which can be used to classify them into three distinct categories (type I-III) (see **Figure 2-2**). A fourth type of DES was proposed by Abbott et al. (2003) which is attained by combining various metal chlorides (e.g., $ZnCl_2$) with different HBDs (urea or glycerol).

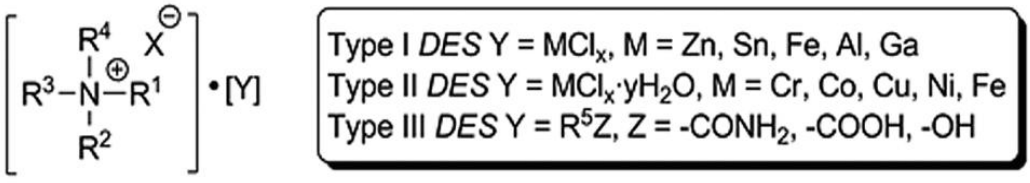


Figure 2-2 Basic formula for quaternary ammonium salt-based DES (García Álvarez, 2014)

Choline Chloride (ChCl) also known as vitamin B_4 is probably the most widely used ammonium salt for the formulation of DESs . Its appeal stems from the fact that it is readily available, nontoxic, and inexpensive. ChCl is produced on a massive scale globally as animal feed and for many other applications. It is biodegradable and can be produced sustainably from biomass (García Álvarez, 2014). If combined with various low-cost and non-toxic hydrogen-bond donors ChCl can form:

1. edible" solvents (using for example saccharinate, lactate, and hexanoate as HBDs)
2. natural deep eutectic solvents (NADESs) (using urea, renewable polyols and carboxylic acids or even water as HBDs) (García Álvarez, 2014)

ChCl-based DESs are often likened to conventional ionic liquids (ILs) but they are very different, as DESs offer numerous advantages over conventional ILs. They are much more affordable, simpler to synthesize, and non-toxic in contrast to ionic liquids (García Álvarez, 2014). However, their application in metal extraction faces some challenges, some of which include high viscosities and limited availability of material property data for engineering applications (Binnemans and Jones, 2023). Nonetheless these issues are the subject of ongoing research. According to the Dimensions database analytics 79 articles, 7 book chapters and 5 patents were published in the field of solvometallurgy for the year 2024.

2.4.3 Properties of DESs

One of the key challenges in expanding the applications of DESs is investigating their fundamental physicochemical properties, as these characteristics play a crucial role in determining their effectiveness as reaction media. Little is known about the physicochemical properties of DESs; however, they have been correlated to the character of the interactions of hydrogen bonding within the solvent and the

relative proportion of the constituent compounds. Thus, the strength of the hydrogen bonds is directly related to solvent properties like density, melting point, viscosity, stability, and polarity. The density of most DESs based on ChCl generally varies from 1.12 to 2.4 $g \cdot cm^{-1}$, which is comparable to conventional ILs but much higher than the density of many organic solvents and water. The density of DESs has been shown to decrease significantly if the ratio of the HBA (e.g., ChCl) is increased relative to the HBD. This effect of the ratio of components on density has been described in terms of "free volume. The density was also observed to decrease linearly with increasing temperature. A eutectic mixture of 1ChCl:2Urea has a density of 1.25 gcm^{-1} whilst 1ChCl:2Ethylene Glycol measures 1.12 gcm^{-1}, which indicates the effect of hydrogen bond interactions. Viscosity is also an important parameter in using DESs as green media, as it describes the resistance of a liquid to flow. Its implications go beyond just reaction considerations but also affect mixing, pumping and filtration operations. Hence the relatively high viscosity of DESs is an issue that also needs to be addressed" (García Álvarez, 2014).

2.4.4 Ionometallurgy

The discovery that metals and their salts showed high solubility and electrical conductivity in DESs ignited interest in their application for metal processing, giving rise to their consideration as prospective greener alternatives for ore processing, recovery of metals in solution, and electrorefining (Hansen *et al.*, 2021). The word ionometallurgy was first used by Abbott *et al.*, (2011) to describe the use of ILs and DESs in extractive metallurgy and to differentiate these liquids from the broader category of solvometallurgical solvents. These liquids allow the control of metal speciation in solution due to the high concentration of anionic ligands, consequently, the solvent formulation can be tailored to regulate other properties like the redox potential of metal species. ILs more importantly offer the separation properties of molten salts minus the high working temperatures (Abbott, Frisch and Ryder, 2008).

DESs have been used in the extraction of many metals, such as gold and various metal sulphides, rare earth carbonates, zinc and tin from smelter dust (Abbott *et al.*, 2009, 2017; Jenkin *et al.*, 2016; Entezari-Zarandi and Larachi, 2019; Zürner and Frisch, 2019). However, literature on the direct leaching of base metal sulphides in DESs is limited, whilst the identified studies primarily focus on electrochemical leaching and electrodeposition of metal oxides (see **Table 2-1**).

Table 2-1 Synopsis of base metal oxides/sulphides processed in various DESs with references.

Mineral	Solvent	Reference
CoO	ChCl: malonic acid/Urea	(Abbott and McKenzie, 2006)
Co_3O_4	ChCl: *p*-toluenesulfonic acid	(Rodriguez Rodriguez, Machiels and Binnemans, 2019)
Cu_2O	ChCl-ethylene glycol	(Abbott and McKenzie, 2006)
CuO	ChCl: oxalic acid/ phenyl-propionic acid	(Abbott *et al.*, 2004)
	EG: maleic acid/citric acid	(Chen *et al.*, 2019)
NiO	ChCl: U	(Abbott *et al.*, 2005)
	ChCl-malonic acid	(Abbott *et al.*, 2006a)
Ni_2O_3	ChCl-U (1:2)	(Huang and Zhang, 2018)
$CuFeS_2$	Ethaline and Iodine	(Jenkin *et al.*, 2016)
CuS, Cu_2S, $CuFeS_2$	ChCl: EG/urea/oxalic acid	(Anggara *et al.*, 2019)
$CuFeS_2$	ChCl: EG	(Carlesi *et al.*, 2022)
Ni-Cu matte	ChCl: U	(Rao *et al.*, 2019)
Cu Slag	ChCl: U	(Topçu, Rüşen and Küçük, 2021)

Leaching of Metal Oxides in DESs

A comparative study of three ChCl-based eutectic mixtures (malonic acid, urea, and ethylene glycol) and aqueous solvents (NaCl and HCl) was carried out on 17 metal oxides at 50°C for 2 days respectively. The malonic acid-based DES (maline) demonstrated significantly higher solubilities in contrast to the other two eutectic mixtures and brine solutions. Nonetheless, HCl outperformed all the other solvents by several orders of magnitude in terms of metal solubilisation. The oxides of Co and Cu showed significant solubility in the maline whilst NiO solubility was negligible. The authors also presented results for the dissolution of a few metal oxides in 1ChCl:2urea eutectic at 70°C. It was apparent that the dissolution of metal oxides showed strong temperature dependency specifically for Cu_2O and ZnO.

It was assumed that the maline and HCl demonstrated superior solubility for metal oxides due to the effect of protons acting as oxygen acceptors which changed the formed complex(Abbott et al., 2006). Fast atom bombardment mass spectrometry (FAB-MS) measurements showed that when ZnO was dissolved in the 1ChCl:2urea DES, the complex $[ZnClO(urea)]^-$ was formed (the oxygen remained attached to Zinc). However, the oxides of Cu and Zn formed mostly chlorometalate species of the form MCl_x^{-1} when the malonic acid-based eutectics were used. This substantiates the claim that protons act as oxygen acceptors (Abbott *et al.*, 2006).

Since demonstrating that certain metal oxides can dissolve in these novel solvents, it was critical to show that metals can effectively be recovered from solution. Electrowinning is one way to recover the dissolved metals considering the ChCl: urea eutectics have conductivities ranging between 1-12 mS cm^{-1}. Abbott *et al.*, (2005) previously conducted a study where they selectively extracted metals from mixed oxide matrixes (electric arc furnace waste) using ChCl:2Urea eutectic. The waste material was leached in the solvent for 2 days at 60°C. The final leach solution was analysed and found to contain just zinc and lead in the ratio of 6:1. This investigation showed ZnO can selectively be leached from other oxides. The eutectic solution underwent electrolysis for 1 hour, using a current density of 10 $mAcm^{-2}$, resulting in the electro-deposition of metallic zinc contaminated with trace amounts of lead and chloride.

A combination of choline chloride and the HBD p-toluenesulfonic acid monohydrate (ptsa) has previously been used to form new eutectic mixtures. The solubility of metal oxides in choline chloride-based DESs is highly influenced by the chemistry of the selected HBD, hence p-toluenesulfonic acid was specifically chosen for its high acidity. The solubilities of various metal oxides in ptsa/ChCl eutectic mixtures were determined experimentally by mixing an excess of the metal oxide with 2 mL of the DES for 1 day at 50°C. The influence of the component molar ratios (i.e., 2:1, 1:1, and 1:2) on the solubility of the metal oxides was also examined.

The metal oxides dissolved significantly more in the 1ptsa:2ChCl eutectic than in any other previously reported DESs. It appears that for most metal oxides increasing the ChCl content promoted higher solubilities (Rodriguez Rodriguez, Machiels and Binnemans, 2019).

Leaching of Metal Sulphides in DES

Although certain copper ores can effectively be treated using hydrometallurgy, processing chalcopyrite, the primary copper mineral, in aqueous solutions presents difficulties due to surface passivation. This passivation, typically caused by the formation of sulfur or polysulfide layers, necessitates harsh leaching conditions. However, the passivation of the chalcopyrite surface may be less of an issue when using non-aqueous solvents like DESs (Anggara *et al.*, 2019).

Studies have shown that the primary copper minerals chalcocite, covellite, and chalcopyrite can be electro-leached in eutectic mixtures of choline chloride (ChCl) and urea (U), ethylene glycol (EG), or oxalic acid dihydrate (Ox). The dissolution of chalcopyrite in DESs results in copper existing in mixed oxidation states (Cu(I) and Cu(II)), whereas other copper sulphides, such as covellite and chalcocite, predominantly yield Cu(II) species. The presence of chloride ions in DESs contributes to the formation of copper chloride complexes (e.g., $[CuCl_4]^{2-}$), enhancing dissolution efficiency. Notably, copper was successfully leached and electrowon in all tests, with no evidence of surface passivation. Furthermore, the oxidation of sulphide resulted in the formation of sulphate (SO_4^{-2}) in solution, avoiding the undesirable evolution of H_2S and SO_2 gases (Anggara *et al.*, 2019).

In another study, the leaching of chalcopyrite concentrate with ethaline at atmospheric pressure and moderate temperatures was reported to dissolve copper and iron in a non-redox reaction pathway and the solvent pH remained constant. The iron and copper formed stable chloride complexes with no indication of passivation. The chemical equilibrium of the chloride complex was said to retard the extent of leaching.

The rate-limiting step of the kinetics was believed to be the interdiffusion of ions within the extraction media. The dissolution mechanism is thought to involve chloride adsorption at active sites on the mineral surface, underscoring the critical role of surface states in the dissolution of chalcopyrite particles. If surface states indeed play a significant role, as suggested by the chloride ion adsorption, surface activation could potentially enhance leaching performance in choline chloride-based DESs (Carlesi *et al.*, 2022). However, this area remains underexplored. The only related study identified investigated the effect of mechanical activation on the dissolution behaviour of yttrium carbonate in a eutectic mixture of choline chloride, urea, and malonic acid (Li *et al.*, 2022). This highlighted the need for further research into similar mechanisms in chalcopyrite dissolution.

Jenkin et al. (2016) demonstrated the feasibility of leaching a variety of minerals from gold ore samples utilizing iodine (I_2) as an oxidant infused into a eutectic mixture of 1ChCl:2EG (i.e., ethaline). The gold ore samples consisted of the minerals, electrum, chalcopyrite, galena, pyrite, native tellurium and tellurobismuthite. Samples were cast into polished blocks which were then dissolved by a technique of etching which involved suspending them in the solvent at either 45°C or 50°C. The samples were then washed with water to remove excess solvent and air dried before measuring etch depth on individual minerals. Their findings indicated total dissolution of electrum after just 10 min whilst galena and chalcopyrite also dissolved but to a lesser extent. Pyrite failed to dissolve and was only partially tarnished in some areas. The native tellurium and tellurobismuthite both dissolved. Preliminary data indicated that chemically resistant phases, such as pyrite, can be dissolved in DESs by electrolysis.

The electrochemical dissolution of a Ni-Cu matte precursor sample has previously been conducted in a choline chloride-based DESs. The process involved sintering the matte with potassium chloride (KCl) at 450°C to form a chlorinated Ni-Cu matte which was then dissolved in 1ChCl:2U eutectic mixture (reline).

The metallic chloride electrolyte was then electrodeposited onto a Cu substrate as Ni-Cu alloy films. The chlorination step was inserted because the XRD identified matte phases (pentlandite, magnetite, NiFe alloy, pyrite, and chalcopyrite) which have poor solubilities in reline, hence these minerals needed to be converted to oxides or chlorides. The recovery of nickel and copper from the matte was estimated to be around 50% and 74%, respectively (Rao *et al.*, 2019).

Mining waste products such as copper slag are some of the most essential secondary sources of base metals that need to be assessed for the contained metallic values, with the quantity of waste generated exceeding 30 million tons annually. Topçu, Rüşen and Küçük (2021) investigated the feasibility of extracting copper and zinc from a copper converter slag using reline (1ChCl:2U) as a solvent. The leaching conditions involved contacting the slag with reline at a temperature of 25-95°C, duration (2-72h) and pulp density (1/10–1/40 g/mL). The optimal leaching conditions, which yielded 89.9% Cu, and 65.3% Zn recovery were established at 48 h, 95°C, 1/20 gmL^{-1} pulp density and 600 rpm stirring rate. The following leaching reactions were proposed for the extraction of Cu and Zn,

$$\boldsymbol{CuO + Ch^{+} + Cl^{-} \rightarrow [CuClO.urea]^{-} + Ch^{+}} \quad \textbf{(2.1)}$$

$$\boldsymbol{ZnO + Ch^{+} + Cl^{-} \rightarrow [ZnClO.urea]^{-} + Ch^{+}} \quad \textbf{(2.2)}$$

2.5 Kinetics of Leaching Reactions

The knowledge of thermodynamics and kinetics is fundamental and plays a critical role in many scientific and engineering disciplines such as biotechnology, chemical engineering, and extractive metallurgy (Coker, 2001). Thermodynamics is commonly employed to anticipate and propose the directions, energy changes, end products, and equilibrium states of chemical reactions (Faraji *et al.*, 2022). When thermodynamics is exclusively considered, it is assumed that time is limitless, and the focus is primarily put on properties associated with the initial and final states of

a system (House, 2007). As a result, the specific pathway or sequence of events during a reaction is not considered, limiting the understanding of the process in its entirety. However, the consideration of time is vital in all processes, and without taking into account kinetics, a genuine comprehension of diverse chemical and physical phenomena would be lacking (Habashi, 1999).

Kinetics can be seen as a valuable tool for examining the rate at which chemical reactions occur and gaining insights into how various processes are influenced or impacted (Fogler, 2016). Kinetics is closely linked to profitability and engineering design, and it finds extensive applications in various areas. These applications include estimating the amount and volume of the reactants, designing appropriate reactors, controlling the reaction parameters, optimizing the process, and scaling it up for industrial implementation (Faraji et al., 2022).

Leaching is classified as a solid-liquid reaction, which falls under the broader category of heterogenous reactions (Faraji et al., 2022). It is often the first and most important stage in many hydrometallurgical process flowsheets. Hence it is critical to figure out the mechanisms and mathematical models for the kinetics of leaching. The widely used approach for studying the kinetics of leaching involves the application of models introduced by Levenspiel, (1999) specifically tailored for fluid-particle reactions. These models offer simplified analytical solutions for complex heterogeneous reactions. In broad terms, the kinetics of leaching encompasses two main aspects: particle reaction and transport phenomena, as well as reactor-level reaction and transport phenomena.

2.5.1 Models and Mechanisms

Heterogeneous reactions typically involve multiple sequential steps, and the overall rate of the reactions is predominantly controlled by the slowest step in the sequence. During the leaching process, depicted in **Figure 2-3**, the lixiviant(s) must undergo diffusion via a liquid film to arrive at the surface of the solid particle. If there is a surface obstacle, such as previously formed solid reaction products, the lixiviants might have to permeate through this solid barrier as well.

Ultimately, the lixiviants react on the surface of the unreacted core of the particle, dissolving the desired elements and forming new products (Faraji et al., 2022).

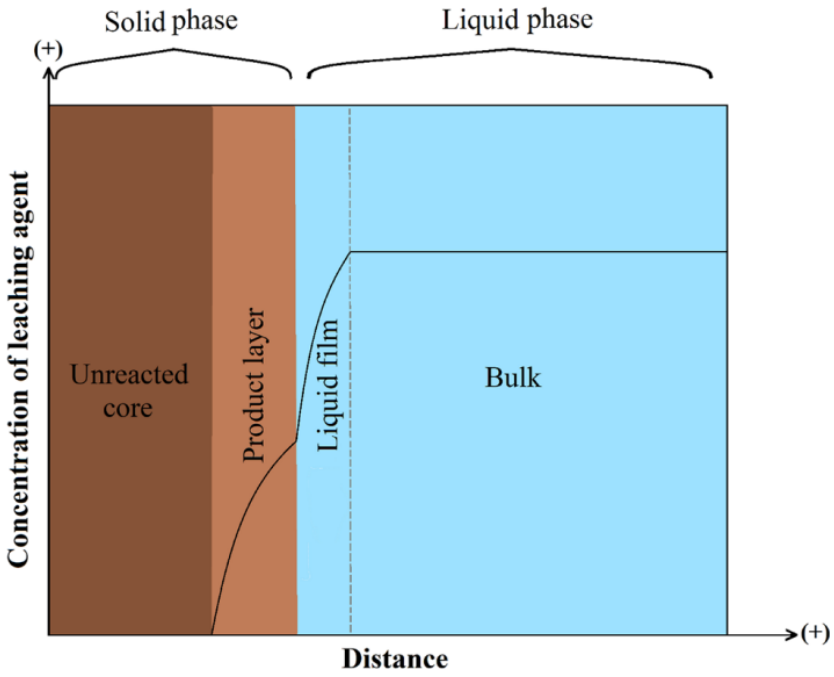


Figure 2-3 Graphic representation of leaching steps

These leaching steps are usually represented mathematically using either the progressive conversion model (PCM) or the shrinking core model (SCM) (Faraji *et al.*, 2022). The PCM is used to deal with highly porous particles, which permit the liquid phase to diffuse through the solids easily. Hence, the reaction occurs across the whole volume of the solid particles and the grade of the unreacted metallic minerals stays constant throughout the porous matrix. The key assumption in the SCM is that the reaction initiates from the surface of the particle and progresses inward until the reaction front reaches the core of the particle. Three main scenarios can be used to describe a leaching process depending on the leaching conditions and nature of the products formed (Levenspiel, 1999).

1. It is presumed that the reaction produces a thick solid layer that coats the unreacted

2. The reaction product does not adhere to the unreacted core, or it gets dissolved in the liquid, resulting in the absence of a solid product layer on the surface of the unreacted core. Consequently, the particle undergoes leaching, gradually decreasing in volume until it ultimately vanishes
3. As the leaching process progresses, the particle reduces in size, and simultaneously a solid product layer forms, covering the particle's surface

While there are various models utilized by researchers, these specific scenarios are widely recognized as the primary models for describing leaching kinetics in hydrometallurgical systems. Hence, the leaching mechanisms have been classified into four categories of “constant particle size, shrinking core model-constant size, shrinking core–shrinking particle and shrinking particle” (Faraji et al., 2022).

The shrinking core model (SCM) was chosen for this study because its assumptions align closely with the behaviour of the system under investigation. The leaching system consists of low-porosity sulphide ore particles and high viscosity lixiviants where the reaction is likely to be controlled by surface phenomena and diffusion through product layers. Furthermore, the SCM has been extensively validated in the literature for hydrometallurgical systems and a few solvometallurgical applications, making it a reliable and appropriate choice for modelling the leaching kinetics in this work.

Shrinking Core Model

The progression of leaching following the shrinking core model in constant particle size is illustrated in **Figure 2-4** (Faraji et al., 2022)

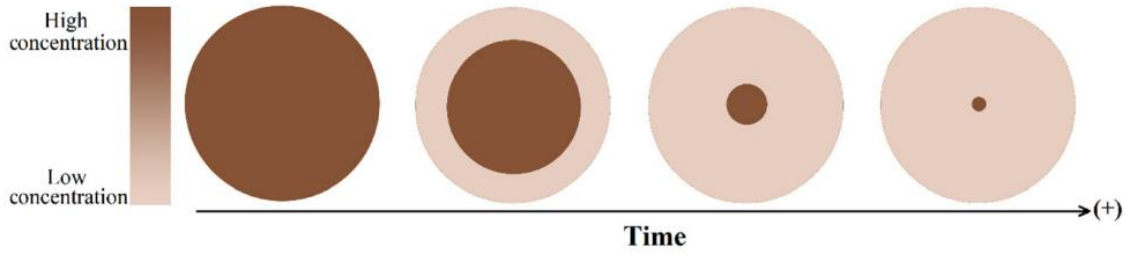


Figure 2-4 Leaching of particles based on the Shrinking-Core-Model – Constant Size *(Faraji et al., 2022)*

The leaching process can be divided into several sequential steps, which include "the diffusion of the leaching agent through the liquid film surrounding the particle, the diffusion of the leaching agent through the solid product layer, and the reaction occurring on the surface of the unreacted core". If a soluble product is formed, it must diffuse via the product layer and liquid film to reach the bulk of the liquid. Overall, the leaching kinetics are governed by three primary mechanisms: diffusion through the liquid film, diffusion through the product layer, and the chemical reaction. If any of the previously stated steps significantly lags the other two, it becomes the rate-determining step of the leaching process. To derive relevant mathematical functions for this model it is generally assumed that; as the leaching process progresses, the shape and size of the particles remain unchanged, while the concentration of the lixiviant in the bulk solution does not change, the reaction occurring on the surface of the core follows first-order kinetics, and the diffusion coefficient of the liquid through the product layer remains constant. Equations associated with each regime for spherical particles in the SCM-constant size are given below (Levenspiel, 1999).

Liquid film diffusion regime:

$$\frac{t}{\tau_F} = X \qquad \textbf{2.3}$$

Solid product layer diffusion regime:

$$\frac{t}{\tau_P} = 1 - 3(1 - X)^{\frac{2}{3}} + 2(1 - X) \qquad \textbf{2.4}$$

Chemical reaction regime:

$$\frac{t}{\tau_R} = 1 - (1 - X)^{\frac{1}{3}} \qquad \textbf{2.5}$$

Where *t* represents the leaching time; X is the fractional conversion of the reactive chemical component in the solid; τ_F, τ_P *and* τ_R denote the completion times for leaching in the liquid film diffusion, solid product layer diffusion and chemical reaction regimes, respectively. Details of how these equations are derived are provided by Faraji et al., (2022).

Researchers often choose the SCM simply because it is popular, which means sometimes the wrong model is chosen (Lekakh *et al.*, 2008). Therefore, it is important to always analyse the structure of the samples before and after leaching, to establish porosity and the presence or absence of a solid product layer to validate the choice of model. The emergence of DESs as alternative green lixiviants has introduced new considerations for the leaching process. DESs are said to exhibit low volatility, tuneable viscosity, and remarkable solvating properties (Binnemans and Jones, 2017). These unique properties of DESs are likely to affect the transport phenomena and reaction kinetics, requiring careful assessment of their applicability to existing models.

Kinetics in DES systems may differ significantly due to their higher viscosity (Haghbakhsh, Duarte and Raeissi, 2021) compared to aqueous solutions, which could slow the diffusion of lixiviants through the liquid film or solid product layer. Additionally, DESs can form specific complexes with metal ions (e.g., $CuCl_2^-$, $CuCl_3^{-2}$) which might influence the leaching reaction's chemical pathway and rate (Carlesi *et al.*, 2022). However, some studies have shown that certain DES-based leaching systems demonstrate mixed control mechanisms, where diffusion and surface reactions contribute simultaneously (Jafari et al., 2022; Ebrahimi et al., 2023).

The shrinking core model fitted the experimental data well in such studies. The shrinking core model, therefore, serves as a useful starting point for modelling DES leaching.

2.5.2 Influence of Leaching Variables

Typically, the rate of a reaction can be affected by several factors including temperature, pressure, catalysts, properties of the reactants, their concentrations, the way they interact and the ore mineralogy. Out of all the factors mentioned, the most crucial parameters for the process are often the lixiviant type, temperature, particle size, agitation, and pulp density. These variables play a significant role in determining the effectiveness and efficiency of the leaching process (Faraji *et al.*, 2022).

Influence of lixiviant

The type and concentration of the lixiviant(s) are key factors that directly and indirectly affect the leaching rate, requiring careful selection and optimization for effective leaching processes. The influence of the lixiviant can be variable depending on factors like the leaching mechanism (e.g., complexolysis, acidolysis and redoxolysis), the anion group of the leaching agent (e.g.,SO_4^{2-}, Cl^- and NO_3^-), and the dosage and the type of redox agent. Variations in the redox potential can lead to the creation or elimination of a passive layer, which can serve as an obstacle for diffusion and charge transfer processes (Córdoba *et al*, 2008). In the case of leaching metals from sulphides like chalcopyrite, a passive covering layer of elemental sulphur is formed, which inhibits the leaching process, thus oxidizing agents can be added to aid in removing this layer. The use of ethaline in combination with common oxidants (I_2, $CuCl_2$, $FeCl_3$. H_2O_2 and O_2) to enhance leaching efficiencies of a sulphide flotation concentrate has previously been reported (Xie *et al.*, 2023; Bidari *et al.*, 2024).

The effect of the lixiviant type was investigated in the leaching of rare earth metals from carbonate salts and bastnäsite minerals using ChCl DESs based on malonic acid, urea, and citric acid. The findings of the study showed DESs based on malonic acid achieved higher extraction rates of REEs as compared to those based on urea and citric. This disparity in leaching efficiencies was explained by variability in proton availability for complexation between the different hydrogen bond donors (Entezari-Zarandi and Larachi, 2019).

Influence of Temperature

The kinetics of leaching are affected by temperature in various ways. Temperature can speed up the diffusion and reaction rates, impact the solubility of reactants or products and alter the direction of reversible chemical reactions (Faraji *et al.*, 2022). The relationship between temperature and kinetics is often represented by the Arrhenius equation

$$k = k_0 exp\left(-\frac{E_a}{RT}\right) \qquad \textbf{2.6}$$

where k is the reaction rate constant, k_0 is the pre-exponential factor, E_a is the activation energy, T is the absolute temperature, and R is the universal gas constant (Missen, 1999).

Temperature can either have a major or minor effect on the reaction rate based on the magnitude of the activation energy. Chemical reactions typically have high activation energies, meaning a small increase in temperature results in a significant increase in the reaction rate. Diffusion processes on the other hand are physical processes where particles or molecules move due to concentration gradients. Diffusion has a much lower activation energy than chemical reactions, so its rate changes less dramatically with temperature. This ultimately explains why diffusion is rate-limiting at higher temperatures since it becomes significantly slower than the chemical reaction.

Jafari *et al.*, (2022) showed that temperature significantly affected the recovery of critical battery metals under a variety of DESs. The investigation aimed to recycle spent Li-ion batteries using ternary and binary DESs. Kinetic modelling using SCM, and activation energy calculations indicated a mixed control reaction mechanism (diffusion and chemical reaction).

Influence of Particle Size

Particle size is inversely proportional to the rate of leaching, and its effect also varies depending on which leaching mechanism is in control. The influence of particle size on leaching is greatest when diffusion is the limiting step and least when the chemical regime dominates kinetics (Levenspiel, 1999). The reaction rate is faster for smaller particles because more surface area is available for interaction with the solvent and the product layer is thinner. The particle size distribution (PSD) and its coefficient of variation (CV) also need to be considered as they can affect the leaching kinetics. It can be assumed that as leaching progresses, a point is reached when smaller particles are entirely dissolved while the bigger ones remain un-leached. Therefore, when the CV is small, PSD has a negligible effect on the leaching rate, while if it is large (CV >0.3), the effect of PSD needs to be reflected in the kinetic model. Details of the equations derived for estimating the fraction of unreacted particles and adjustments to the SCM are provided elsewhere (Gbor and Jia, 2004).

Mechanical activation is an important technique that has been used to improve the extraction efficiency of hydrometallurgical processes. It can induce deagglomeration and the creation of active surfaces, including changes in the physical and chemical properties of the particles, as well as a decrease in the particle size, and the formation of new phases that are more susceptible to leaching. The leaching behaviour of a rare earth (yttrium) carbonate was studied both before and after undergoing mechanical activation in choline chloride–urea–malonic acid DESs. In the absence of mechanical activation, the yttrium dissolution reached approximately 49%.

However, after 60 minutes of mechanical activation, the leaching efficiency increased significantly to 85%, primarily due to the reduction in particle size and the enhanced contact area facilitating the reaction. The dissolution process was governed by a combination of chemical reaction and diffusion through the solid product layer (Li et al., 2022). These results compare favourably with the leaching of activated surfaces in normal acidic solutions. The use of mechanical activation led to a significant increase in the leaching of REEs from phosphor-gypsum from 15% to about 70% in sulfuric acid media (Xie *et al.*, 2023). Nonetheless this leaching efficiency was lower than what was reported in DES leaching studies.

Influence of Agitation

Generally, if agitation is increased, the leaching rate rises to a threshold, after which it may begin to decline. Ideal mixing improves diffusion and surface reactions by thinning the liquid film layer surrounding the particles. In contrast, harsh mixing affects fluid flow by the generation of bubbles and a vortex, which limits the diffusion of reactants onto the particle surface. It is important to note that the influence of mixing on leaching kinetics can differ depending on the nature of the lixiviant. The kinetics of some solvent systems will be unaffected by higher mixing rates while others will show a positive or negative correlation.

Adebayo, Ipinmoroti and Ajayi (2003) investigated the leach kinetics of chalcopyrite in H_2O_2 and H_2SO_4 media. They observed that an increase in stirring rate negatively impacted the leach rate, likely due to the accelerated decomposition of H_2O_2. This decomposition promotes the formation of molecular O_2, leading to bubble adsorption on the surface of the mineral powder, which hinders contact between the sample and the peroxide. The dissolution rate in a chalcopyrite leaching system with H_2SO_4 and $K_2Cr_2O_7$ increased as the stirring rate rose to 400 rpm but decreased significantly beyond that point (Adebayo, Ipinmoroti and Ajayi, 2003).

The influence of stirring speed on zinc dissolution from zinc oxide dust in ChCl−urea−EG DESs was examined by Zhu *et al.* (2019). The findings revealed that zinc extraction efficiency improved as the stirring speed increased from 200 to 600 rpm but remained unaffected at speeds above 600 rpm, indicating mass transfer control at lower speeds.

Influence of the solid-to-liquid ratio (pulp density)

The volume of a leaching agent is an important parameter that can be manipulated to accelerate the leaching rate if used in sufficient quantities. The solid-to-liquid ratio (S/L) represents the molar proportion of the reactive chemical component in the solid phase to the leaching agent in the liquid phase. This ratio is typically represented as kilograms of solids per Liter of liquid (or grams per millilitre). The equations presented thus far were derived under the assumption that the lixiviant is present in large excess, ensuring its concentration remains constant throughout the entire leaching process. However, this assumption does not hold if the S/L is high, as the concentration of the leaching agent will change. In this scenario, adjustments should be made to the relationship between recoveries and time to consider the changing concentration of the leaching agent. The time-conversion relationship generalisation used to consider the effect of the S/L ratio on the leaching rate is provided below in the case of chemical reaction control (SCM). Other scenarios for liquid film and product diffusion control are provided by Faraji et al., (2022).

$$\frac{t}{\tau_R} = \int_0^X \frac{dX}{3(1-X)^{\frac{2}{3}}(1-\alpha X)} \qquad \textbf{2.7}$$

Where t is the leaching time; X is the fractional conversion of the reactive chemical component in the solid; τ_R is the time of completion of leaching in the chemical reaction regimes (Faraji et al, 2022).

The stoichiometric ratio "α" is defined as the number of moles of leaching agent required to completely dissolve metal in the mineral (solid) to the actual number of moles of leaching agent present in the liquid. A stoichiometric mixture of solid and liquid is represented by α = 1. When α is less than 1, it signifies an excess of the leaching agent, with the extreme case being α = 0. It is important to note that most research findings indicate S/L has a negative correlation with the leaching rate. This relationship exists because increasing the number of solid particles per unit quantity of solvent leads to higher viscosity, a decrease in diffusion coefficient and poor convection, resulting in low metal recoveries (Faraji *et al.*, 2022).

The influence of solid to liquid on the leaching efficiency of Cu and Zn from converter slag using a ChCl-2urea mixture was investigated by, varying the S/L between, 2.5% (1/40 g/mL) and 10% (1/10 g/mL). It was established that copper extraction improved at lower S/L values (see **Figure 2-5**). The most copper recovery achieved was 89.16% at an S/L of 1/40 g/mL (Topçu, Rüşen and Küçük, 2021).

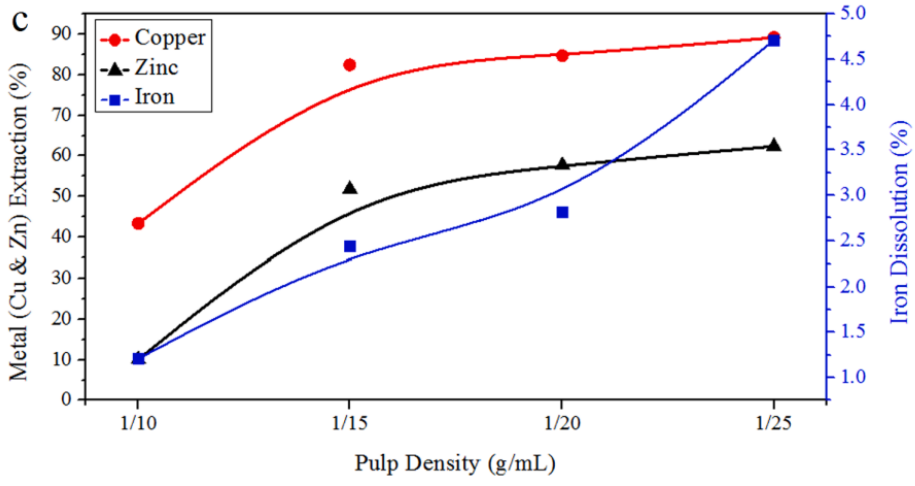


Figure 2-5 Effect of solids to liquid ratio (pulp density) on the extraction of base metals from converter slag *(Topçu, Rüşen and Küçük, 2021)*

2.6 Summary

This study is aimed at establishing the potential of ionometallurgical leaching of Ni-Cu sulphide concentrates using choline chloride-based DESs containing urea, malonic acid, and ethylene glycol as hydrogen bond donors. Ionometallurgical extraction is a process in which ILs and DESs are used to aid in the recovery of metals from ores and concentrates. The literature review contained in this chapter has shown the limitations and difficulty involved in the processing of base metal sulphides using conventional methods. The extraction of copper, nickel and cobalt from ore concentrates has traditionally been achieved by pyrometallurgical means, which has serious drawbacks. For instance, pyrometallurgy is highly energy-intensive and causes pollution to the environment, due to the release of noxious gases that require costly equipment/processes to treat. Hydrometallurgy, a relatively more benign and chemically selective approach has been used to circumvent some of the issues posed by pyrometallurgy. However, it also has some drawbacks, in particular, the toxicity of solvents used and the lack of chemical selectivity when treating low-grade and polymetallic ore material. Solvometallurgy/ionometallurgy has been touted as a complementary new approach to addressing the shortcomings of both pyrometallurgy and hydrometallurgy. The technology readiness level of this new technology is still very low and requires further research effort before its industrial application can be realised.

CHAPTER THREE

MATERIALS AND METHODS

3.1 Introduction

The chapter outlines the process of preparation of the materials and provides a detailed description of the experimental methods and analytical techniques used in the study. Furthermore, the data analysis methods employed are discussed. Finally, a summary is presented to encapsulate the key points covered in the chapter.

3.2 Materials

3.2.1 Copper-Nickel Sulphide Ore Concentrate

The copper-nickel sulphide flotation ore concentrate used in this study was provided by the liquidator of BCL Pty Ltd, Botswana in 2019 and has been stored at the BITRI laboratory since then. The samples were stored in zip-lock bags in a freezer to minimize oxidation. The stored material agglomerated over time, hence became unsuitable for direct analytical or experimental tests. Therefore, sample preparation work entailed sample reduction (>200 kg batch) through riffling (1 kg subsamples), size classification through sieve analysis and homogenization through milling.

Subsampling

Sampling methods are primarily concerned with the gathering of reliable data. The collected samples are tested for some characteristics such as metal grade or particle size, and the data is used to guide process improvements. The reliability of sample data depends on taking precautions to avoid errors associated with the collection of the bulk sample and preparation of a suitable subsample for analysis. The fundamental principle guiding the sampling technique is that every particle should have an equal chance of being sampled.

The most common methods for reducing samples in laboratory settings include cone and quartering, riffling and rotary splitters . Sample reduction is achieved by dividing the bulk material into two or more subsamples and repeating the process until the required mass needed for analysis is acquired (Holdich, 2020). For this study an initial head sample weighing 40 kg was reduced to 1 kg subsamples using a laboratory riffler and the reduced sample was used for sieve analysis.

Sieve Analysis

Sieve analysis is a procedure used to determine the particle size distribution (PSD) of a given material by letting the material pass through a stack of sieves of gradually decreasing mesh size and weighing the quantity of material that is retained by each sieve as a percentage of the total mass. Sieving is performed on wet or dry materials on a vibrating platform to expose all the particles to the pores (Wills and Finch, 2016). Dry sieving was used for this study since it is faster, requires less equipment and it preserves the chemical and physical structures of the particles that may be soluble in water. A sieve test was performed on a 1kg subsample with a stack of 16 sieves that ranged from 25 mm to 160 μm. The top and bottom sieves were selected based on the criteria that the mass retained by the coarsest and finest sieve should not exceed 5% of the total weight. The test was initiated by pouring the whole mass onto the coarsest sieve and vibrating the sieve stack for 20 minutes, allowing the material to percolate down the stack. The mass retained on each sieve was weighed and the data tabulated as shown in **Table A1**, **Appendix A**. The data from **Table A1** can be used to establish several metrics such as the median particle size or diameter *i.e.*, d_{50}. The sieve analysis data, sieve size *vs* % passing was plotted on a semi-logarithmic plot (see **Figure A1**). The d_{50} from the graph was approximately 2.75 mm, estimated using the trendline interpolation function in excel. This indicated the material was coarse and required further milling.

Milling and Classification

The 1 kg subsample was milled with a vibrating cup mill. Milling was carried out at 1200 rpm for 5 minutes, that was repeated several times until the desired particle size was achieved *i.e.*, 100% passing 100 μm. The milled sample was classified into different size fractions using sieves (100+90 μm, -90+80 μm, -80+71 μm, -71+38 μm and -38 μm). The milled samples were used for chemical and mineralogical analysis, whereas the different size fractions were used for leaching experiments.

Head grade Analysis

Prior to experimentation, the percent (%) metal (Ni, Cu, Co*, etc)* content in the sulphide ore concentrate was calculated as a percentage of the total mass of the concentrate (see example in **Appendix B**). The % metal content in the concentrate was determined by the Agilent 4200 Microwave-Plasma Atomic Emission Spectrophotometer (MP-AES) after digestion of ore in a two-acid solution prepared by combining concentrated nitric acid (∼65%) with concentrated hydrochloric acid (∼37%). The two acid digestions ($2HNO_3$:1HCl) are used for samples with high organic or sulphide content. For samples with no organic or low in sulphide content, aqua regia (3HCl: $1HNO_3$) is often used.

Approximately 0.5g of a homogenized sample was weighed out and transferred into a 250 mL glass beaker equipped with a watch glass. Then 12 mL of the two-acid solution was added to the sample beaker and was allowed to digest on a hot plate for 3 hours at a temperature of 110˚C. The digestion mixture was allowed to evaporate to near dryness and diluted with 20 mL of 2% (*v/v*) nitric acid. The solution was filtered into a 250 mL volumetric flask and diluted to the mark with deionised water. This digestion procedure was carried out in four replicates. The four solutions were then taken for analysis using MP-AES.

3.2.2 Reagents

All the reagents utilized in the study were of high purity (reagent plus ≥ 98.5%) and sourced from Merck in South Africa, unless specified otherwise. They were used in their original form without additional purification.

Table 3-1 List of chemicals used in the study

Reagent	Form	Purity	Molecular Weight (g/mol)
Urea	Pellets	≥99.5%	60.06
Malonic Acid	Powder	99%	104.06
Choline Chloride	Powder	≥98%	139.62
Hydrochloric acid	Liquid	≥37%	36.46
Nitric acid	Liquid	65%	63.01
Ethylene Glycol	Liquid	99.8%	62.07

3.2.3 Synthesis of DESs

Guidelines on the preparation of DESs were adopted from El Achkar, Greige-Gerges and Fourmentin, (2021). The quaternary ammonium salt choline chloride [HOC_2H_4N $(CH_3)_3Cl$] (ChCl) was mixed with various molar ratios of hydrogen bond donors (HBDs) *i.e.*, ethylene glycol (EG), urea (U), and malonic acid (MA) to form eutectic mixtures. The choline chloride was obtained in powder form and was dried in a vacuum oven at 80°C for 24 hours prior to use. The precursors were mixed in a Schott bottle equipped with a magnetic stirrer and heated on a hot plate at 60-80°C until the mixture formed a clear and homogeneous liquid. The resulting liquid was then stored in a desiccator in the presence of silica gel or used immediately for the experiment. The DESs formed included the binary and ternary mixtures of ethaline (1ChCl:2EG), reline (1ChCl:2U: nEG), and maline (1ChCl:1MA: nEG), with "n" ranging from 0 to 3 moles.

3.3 Experimental Methods

3.3.1 Design of Experiments

The aim of the study was two-fold. The first part was to conduct screening experiments to identify significant factors and select the most effective solvent(s). Secondly, optimization of the important factor levels was conducted to maximize metal recovery by leaching. The design of experiments (DOE) methodology was employed to achieve the above-mentioned goals. One of the main benefits of employing DOE is its ability to offer a structured approach for selection of the most suitable experimental objectives. Consequently, when DOE is applied, it becomes possible to gather more valuable and accurate information about the system under study since it assesses the combined impact of all factors (Montgomery, 2017).

Screening of factors (**Chapter 5**) was carried out initially to establish the effect of the studied factors on the responses (nickel, copper, and cobalt recovery), and to identify their appropriate ranges. A half and quarter basic fractional factorial designs with a resolution of three (2_{III}^{4-1} and 2_{III}^{5-2}) were used to determine the significant factors. The experimental results were analysed with DOE software, to establish statistically the significance of the factors. The software performs multivariate data analysis, which involves statistical techniques like Principal Component Analysis (PCA) and Partial Least Squares (PLS) regression. Various tools and graphical representations can also be used to visualize the relationships between factors and responses (Analytics, 2017).

Once a preferred solvent was identified using ANOVA, the fractional factorial design was expanded into a full factorial design to estimate high order interactions. A full factorial design was chosen over a conventional fold over design since the latter has limited resolution as it can estimate some two-way interactions but might miss important information about higher-order interactions (three-factor or four-

factor) that could be significant. In addition, the number of calculated experimental runs was equal for both designs.

Based on the identified influential factors, the next step was to build predictive models that explain the relationships involving the factors and responses. Optimization studies were then performed to discover the best factor settings that maximize or minimize the desired responses.

The response surface methodology (RSM) was used in the optimization study. The design process for the RSM entailed: (1) design and execution of a sequence of experimental runs for the acceptable and reliable measurement of the response (nickel, copper, and cobalt recovery) (2) development of a predictive model, (3) identifying the best group of experimental variables and, (4) representation of the effects of process variables using 3-D plots (Analytics, 2017). The optimization experiments were designed using an I-optimal design.

3.3.2 Factor Settings

Tables 3-2 to **3-4** show the experimental designs indicating factor level settings, used in the solvent and factor screening leaching studies.

Table 3-2 Ethaline factor level settings

Factor	**Lower level (-)**	**High level (+)**
Temperature (℃)	25	60
Percent Solids (w/v %)	2	10
Stirring rate (rpm)	300	600
Time (h)	1	4

Table 3-3 Reline factor level settings

Factor	**Lower level (-)**	**High level (+)**
Temperature (˚C)	25	60
Percent Solids (*w/v* %)	2	10
Stirring rate (rpm)	300	600
Time (hours)	1	4
Diluent (moles EG)	0	3

Table 3-4 Maline factor level settings

Factor	**Lower level (-)**	**High level (+)**
Temperature (˚C)	25	60
Percent Solids (*w/v* %)	2	10
Stirring rate (rpm)	300	600
Time (hours)	1	4
Diluent (moles EG)	0	3

3.3.3 Apparatus and Experimentation

All ore concentrate samples were dried at 80˚C in an oven until non-variation in weight was observed, then allowed to settle to room temperature and added to a Schott bottle that contained the DES preheated to the desired temperature. The slurry mixture was maintained at a set agitation rate on a temperature-programmable heating-stirring plate. The agitation rate was set to maintain the solid-liquid suspension and avoid aggregation or settlement of the solids. It is common practice to create a water-free or inert atmosphere when working with DESs, due to their hygroscopic nature. During this study, no effort was made to avoid contact between the eutectic liquid surface and laboratory air. The leaching apparatus employed in this study is shown in **Figure 3-1**.

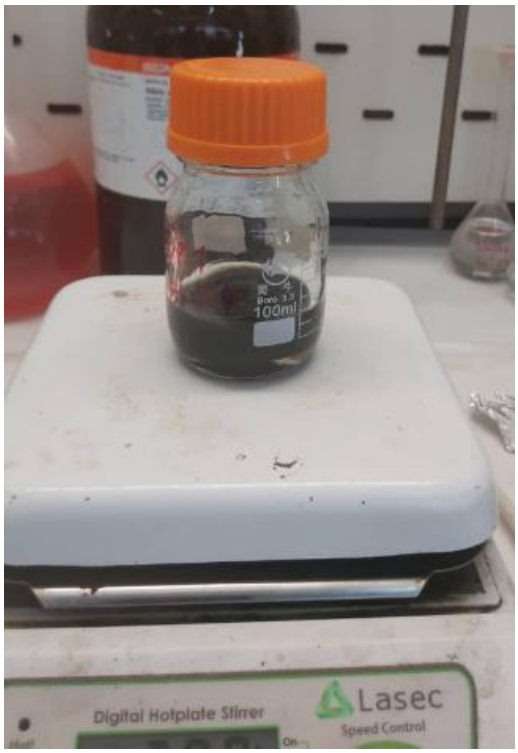


Figure 3-1 Leaching test setup

3.4 Analytical Techniques: Chemical Analysis

The chemical analysis entailed the use of three techniques.

1. Pyrosulphate fusion, with an X-ray Fluorescence (XRF) finish method for base metals
2. Two-acid digestion with a Microwave Plasma Atomic Emission Spectrometry (MP-AES) finish for base metals
3. Sodium Peroxide Fusion with an Inductively Coupled Plasma Optical Emission Spectrometry (ICP-OES) finish for multi elements

3.4.1 Sample Digestion

Sample digestion is the process of converting a solid sample into a dissolved state by transforming the elements of interest into soluble salts in solution. This allows for easier chemical analysis and a better understanding of the sample's composition. A major challenge in the preparation of most solid or geologic samples is that they

are not water soluble thus, require digestion through various methods such as acid digestion, fusion, and ashing (Hu and Qi, 2014). Acid digestion is typically carried out using a variety of strong mineral acids such as nitric acid (HNO_3), hydrochloric acid (HCl) and aqua regia (1HNO_3:3 HCl). The latter is suitable for samples with no organic compounds or low in sulphides, however the samples used in this study were high in sulphides. A two-acid digestion (2HNO_3:1HCl) protocol was developed and used for digestion of the current test samples (see **Appendix A**).

3.4.2 Atomic Emission Spectroscopy

Atomic spectroscopy relates to several analytical methods that are employed to determine the elemental makeup of a sample by analysing its electromagnetic or mass spectrum (Agilent Technologies, 2021). Inductively coupled plasma optical emission spectroscopy (ICP-OES) and microwave plasma atomic emission spectroscopy (MP-AES) are examples of several techniques that identify an element in a sample by its electromagnetic spectrum. The dissolved metal concentration in the digested samples was quantified by an Agilent 4200 MP-AES, equipped with an autosampler, see **Figure 3-2.** All solutions were prepared with ultra-pure de-ionized water (18.2 MΩ·cm resistivity). Calibration standards of 20 to 100 ppm were prepared for all elements from a 1000 ppm multi-element standard. All samples were diluted to the correct concentration range and were measured in triplicates (see **table A2**).



Figure 3-2 The Agilent 4200 Microwave-Plasma Atomic Emission Spectrometer.

MP-AES is an atomic emission technique that works on the principle that excited atoms emit unique wavelength patterns of light akin to a fingerprint when they return to their ground state electron configuration. The source of the atomic emission in this instance is a high temperature (5000 K) microwave induced plasma. This emission is pointed towards an optical system that is made up of a quick scanning monochromator and a charge coupled device (CCD) detector. The measured spectra are ultimately used to quantify the concentration of individual elements in a sample by comparing their emissions to a calibration curve (Agilent Technologies, 2021). The working principle for ICP-OES is similar to MP-AES the main difference is only the plasma generation source. In ICP-OES, plasma is generated by passing argon gas through an oscillating radio frequency (RF) field. The RF field accelerates electrons which collide with argon atoms, producing more ions and free electrons in a chain reaction.

3.4.3 X-Ray Fluorescence Spectroscopy

The operational concept of XRF spectroscopy relies on irradiating sample atoms with high-energy X-rays, leading to the release of characteristic photons with a specific energy closely associated with the atomic number Z of each element, as

described by Moseley's law, see equation 3.1 (Streli, Wobrauschek and Kregsamer, 2016; Haschke, Flock, and Haller, 2021).

$$E = C_1 \cdot (Z - C_2)^2 \qquad \textbf{3.1}$$

with

E = energy difference between the electron levels

Z = atomic number of the atom

C_1, C_2 = constants

By measuring the energy (or wavelength) of the emitted photons (fluorescent X-rays), we can identify the elements present in a sample (qualitative analysis). The number of X-rays of a specific energy indicate how much of that element is present (quantitative analysis). In addition to its precise and swift ability to analyse multiple elements, one notable characteristic of XRF is its non-destructive nature, allowing analysis to be conducted without altering or damaging the sample. XRF analysis requires a spectrometer comprising an excitation source (X-ray tube), a sample, and a detection system. The detection system is available in two options, wavelength-dispersive or energy-dispersive configurations (Streli, Wobrauschek and Kregsamer, 2016).

In this study, XRF analysis was performed using the Bruker S8 TIGER WDXRF spectrometer, which is equipped with a rhodium (Rh) tube capable of generating energy levels up to 60 keV. The analysis was conducted in a helium (He) atmosphere using pulverized samples, and data interpretation was carried out with SPECTRA standardless software.

3.5 Mineral Analysis

3.5.1 X-ray Diffraction

XRD is a powerful tool used to study crystalline and powdered materials. It reveals both the types of compounds present and their quantity. X-ray diffraction data was

obtained using Malvern PANalytical's Empyrean diffractometer with monochromated CuKα radiation ((λ = 1.5406 Å) operated at an accelerating voltage of 40 kV, a current of 40 mA, a step size of 0.033°, and a scanning rate of $0.1°s^{-1}$ over a 2θ range from 3° to 80°. Angle calibration was performed with a synthetic sintered silicon standard. Identification and quantification of crystal phases was done using XRD analysis software Highscore Plus version 4.8 with PDF 2 database and Rietveld analysis

X-ray diffraction takes place when an electromagnetic wave with a wavelength around 1 angstrom interacts with a structured arrangement of atoms, such as in a molecular or ionic crystal. Upon interaction with the electron cloud of an atom, the incident electromagnetic wave acts as a source for the generation of a secondary wave of the same wavelength. This scattered wave emanates from each atom in the material. The presence of a three-dimensional, regular atomic arrangement in crystalline materials leads to a phenomenon of interference between these secondary waves. This interference can be either constructive or destructive, solely dependent on the relative spatial arrangement of the atoms within the crystal lattice. Constructive interference leads to diffracted rays being dispersed solely along specific directions. The orientation and strength of these diffracted rays are determined by the crystal's symmetry, the atomic number, and spatial arrangement of atoms within the crystal lattice. This set of diffracted rays carries valuable information regarding the three-dimensional atomic configuration of the crystal. Based on Bragg's explanation of X-ray diffraction, we can conceptualize a crystal as comprising infinite planes hosting atoms, with orientations determined by the crystal's unit cell parameters. Each group of these planes will exhibit diffraction in accordance with Bragg's law (see **Equation 3.2**),

$$n\lambda = 2dsin\theta \qquad \textbf{3.2}$$

where the integer 'n' signifies the order of the plane, 'λ' denotes the wavelength of the incident X-ray radiation, 'd' represents the interplanar spacing, and 'θ'

corresponds to the angle of incidence between the X-ray wave and the diffracting atomic plane. In practice, XRD analysis requires three components; an X-ray emitter which is typically monochromatic, a goniometer for orientating the sample in accordance with Bragg's law and a detector for collecting the diffracted rays (Cassetta, 2015).

3.5.2 AutoSEM Analyses – by TIMA-X

The mineralogical characterization was conducted with a Tescan scanning electron microscope (SEM). The Tescan is an automated mineralogy instrument that employs TIMA-X software to perform rapid quantitative analysis of samples. TIMA-X integrates Backscattered Electrons (BSE) and Energy Dispersive X-Ray/Spectroscopy (EDX/EDS) analyses to identify minerals and generate mineral images. The images are then processed to ascertain mineral concentrations, elemental distributions, and various mineral texture characteristics, including grain size, associations, liberation, and locking parameters.

Polished blocks with transverse cuts, as illustrated in **Figure 3-3**, underwent automated SEM analysis using the Tescan TIMA-X system. The analysis encompassed bulk mineralogical composition analysis employing TIMA line scan analysis (TLS/TLA).

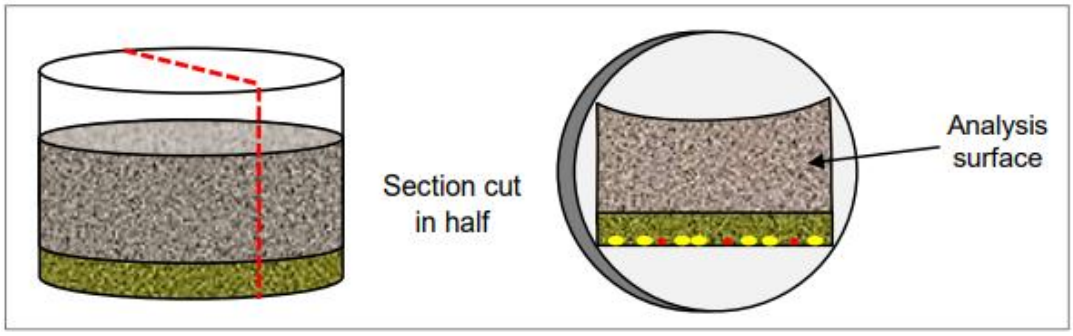


Figure 3-3 A diagram representing a transverse-cut polished block.

3.6 Data Analysis

The data was acquired as detailed in the preceding sections of this chapter. The collected data was utilised to establish relationships between base metal recovery and the experimental variables (e.g., temperature, time, and percent solids etc). A deeper analysis of these relationships and the findings will be presented in the chapters that follow. The base metal recovery after leaching the sulphide ore concentrate was determined by comparing the amount of metal dissolved in the solvent to the initial amount of metal present in the concentrate. Some of the data in chapter 4 and 5 were analysed statistically.

3.7 Summary

The focus of this chapter was on the laboratory procedures employed in the study. Hence, we highlighted the following activities involved in the experimental phase:

- Preparation of ore concentrate samples (milling, sieving, and size classification)
- Preparation of DESs
- The selection of an experimental design approach (DOE)
- Apparatus and experimental setup
- Chemical and mineral characterisation techniques
- Data analysis and interpretation

CHAPTER FOUR

CHARACTERIZATION OF SULPHIDE ORE CONCENTRATE

4.1 Introduction

Characterization is a critical step in the processing of mineral resources as it provides detailed insights into the chemical, and mineralogical properties of the material. For the copper-nickel flotation concentrate sourced from BCL Mine in Botswana, characterization plays an essential role in understanding the concentrate's composition and anticipating its behaviour during processing. Various researchers have reported on the composition of BCL ore, as discussed in **Chapter 2**. These studies provide valuable baseline data on the mineralogical and chemical makeup of the ore, highlighting the presence of key sulphide minerals such as pentlandite, chalcopyrite, and pyrrhotite, along with significant amounts of gangue material. However, variations in ore composition due to geological heterogeneity, operational changes at the mine, and potential alterations during the flotation process necessitate an independent and updated investigation. Furthermore, the copper-nickel flotation concentrate used in this study was stored for several years following the closure of BCL Mine before it was sampled for analysis. Prolonged storage of the concentrate introduces the possibility of changes in its physical and chemical properties due to factors such as oxidation, moisture absorption, and other environmental interactions. These changes may significantly impact the mineralogical composition, surface chemistry, and overall reactivity of the concentrate during subsequent processing.

4.2 Results and Discussions

4.2.1 Chemical Analysis Results

The results of the chemical assays carried out on the concentrate sample are presented in **Table 4-1**. The chemical analysis sub-samples were pulverised for the determination of:

- 'Base Metals' (determined by pyrosulphate fusion and XRF finish method).
- 'Multi elements' (determined by Sodium Peroxide Fusion and ICP-OES finish method)

Table 4-1 Elemental analysis of the copper-nickel concentrates (wt.%)

Ni	Cu	Co	Fe	S	Cr	Al	K	Mg	Si
7.35	2.83	0.39	30.93	>10.00	0.28	0.54	0.3	2.32	4.2

The XRF results revealed that the Cu-Ni sulphide flotation concentrates predominantly consisted of high concentration levels of iron at 30.93%. The second most abundant base metal was nickel at 7.35% followed by copper at 2.83%.

4.2.2 Auto SEM: Bulk Mineralogy Analysis

The mineralogical composition of the concentrate is shown in **Table 4-2**. The bulk mineralogical analysis (BMA) results were determined using Auto-SEM (TIMA). Most of the mineralogical make-up of the sample was ~41% Ni-bearing minerals, ~8% Cu-bearing minerals, ~33% sulphur (S) -bearing minerals, ~11% silicate minerals, ~2% oxide minerals, as well as mineral phases that are "Fe-sulphide/oxide mixed" (~5%).

Table 4-2 Mineralogical Composition of the Samples, as Determined by Auto-SEM

Mineral	**Mineral Abundance (Mass%)**
Pentlandite	39.8
Maufite	1.2
Ni bearing minerals	**41.3**
Chalcopyrite	3.8
Bornite	3.1
Cubanite	0.8
Cu bearing minerals	**7.7**
Pyrrhotite	28.9
Pyrite	4.3
Fe sulfides	**33.2**
Hematite/Magnetite	1.7
Fe-sulfide/oxide mix phase	5.4
Silicate minerals	10.6
Total	**100.0**

4.2.3 Ni and Cu Deportment

BMA results showed that the Ni-bearing minerals, making up ~41 mass %, were pentlandite, maufite, violarite, Ni-bearing pyrite and a Ni-bearing spinel phase. The distribution of Ni, normalised to 100%, is shown in **Table 4-3**.

Table 4-3 Distribution of Ni in Ni-bearing Minerals

Ni-bearing minerals	Distibution (%) of Ni / Mineral
Pentlandite	99.4
Maufite	0.1
Violarite	0.5
Pyrite (Ni)	0.0
Spinel (Ni)	0.0
Total	**100.0**

Similarly, BMA results showed that the Cu-bearing minerals, making up ~8 mass %, were chalcopyrite, bornite and cubanite. The distribution of Cu throughout these minerals, normalised to 100%, is shown in **Table 4-4**.

Table 4-4 Distribution of Cu in Cu-bearing Minerals

Cu-bearing minerals	Distibution (%) of Cu / Mineral
Chalcopyrite	58.7
Bornite	35.7
Cubanite	5.6
Total	**100.0**

4.2.4 Grain Size Distribution of Ni and Cu Bearing Minerals

A mineral grain refers to a unit composed of a single mineral type. Multiple grains can combine to form a particle. When a grain is fully liberated, it is considered synonymous with a particle. A particle usually refers to a fragment of a rock or ore, the size of which is dependent on crushing and milling conditions. **Figure 4-1** shows a schematic representation of grain vs particle.

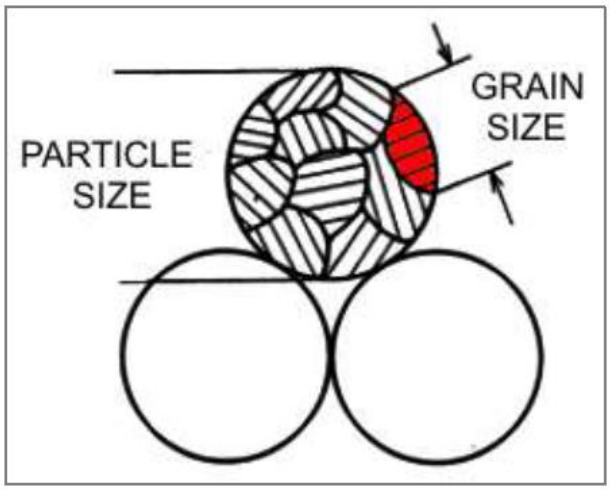


Figure 4-1 Explanation of grain versus particle (BITRI, 2023)

Table 4-5 indicates the particle size ranges at which 80% of each mineral in each sample are finer, i.e., the size below which 80% of the mineral grains will pass through a given sieve aperture. The GSD of grains were considered in isolation (see definition of 'grain' above); the data is given as the mass percent of mineral grains which fall into each size class. Since the analyses were not performed on sized material, there may be stereological bias resulting in underestimating grain size distributions. The GSD data for the minerals of interest is given in **Appendix A.**

Table 4-5 Size (ranges) at which 80% of mineral grains will pass

Sample	Mineral	80 % passing
Ni-Minerals	Pentlandite	30-40 µm
	Maufite	30-40 µm
	Violarite	25-35 µm
	Pyrite-Ni	5-15 µm
	Spinel-Ni	15-25 µm
Cu-Minerals	Chalcopyrite	70-90 µm
	Bornite	40-60 µm
	Cubanite	10-30 µm

4.2.5 Liberation Analysis

Liberation characteristics, which are schematically represented in (**Figure 4-2**), are the classification of minerals of interest (Ni and Cu bearing minerals, in this instance) into the following three categories:

1. Fully liberated: More than 80 % area of the particle is the mineral of interest.
2. Middlings: Between 30 and 80 % area of the particle is the mineral of interest. This can be further divided into Lo middling (>30% ≤50%) and Hi middling (>50% ≤80%).
3. Locked: Less than 30 % area of the particle is the mineral of interest.

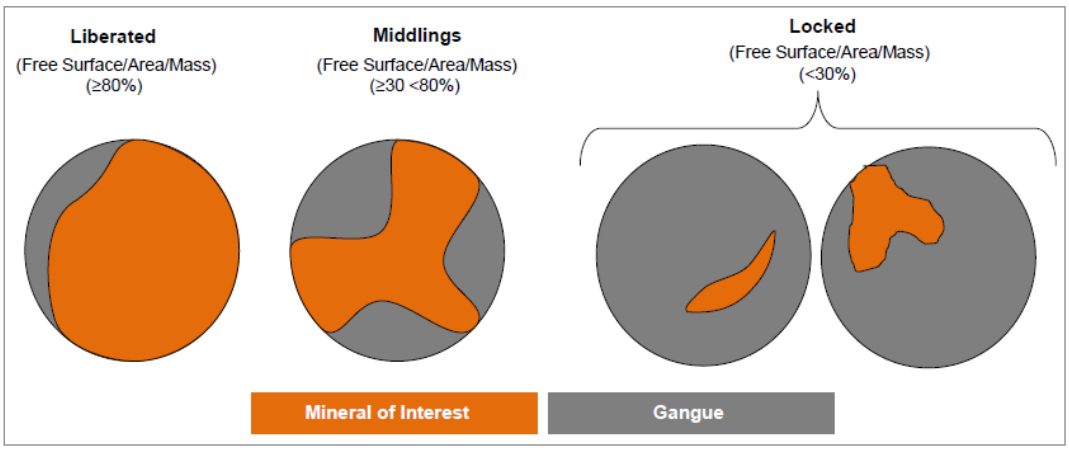
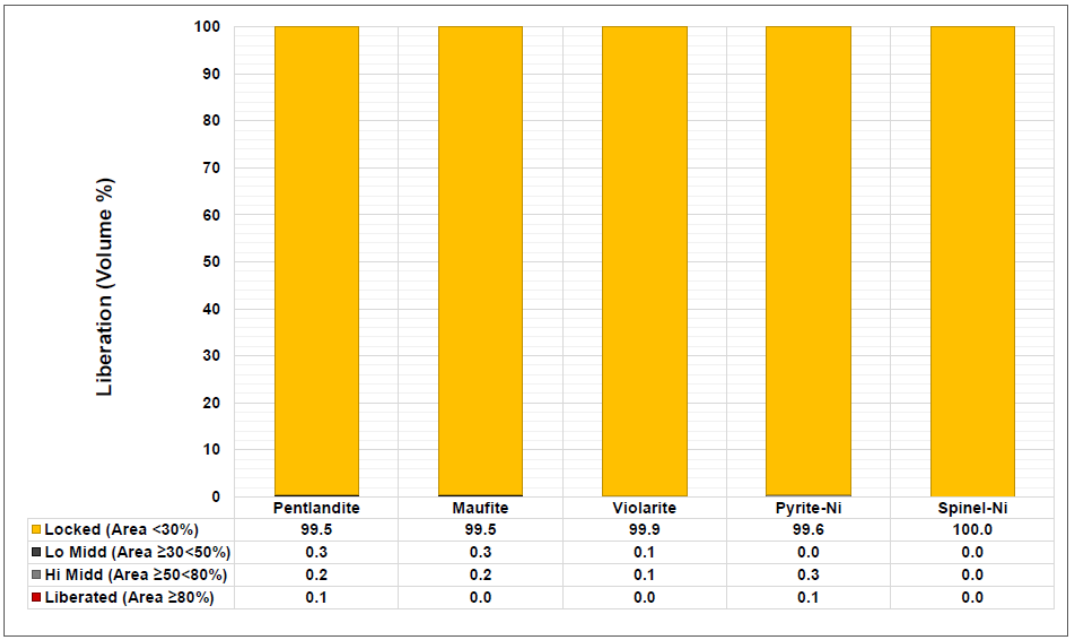


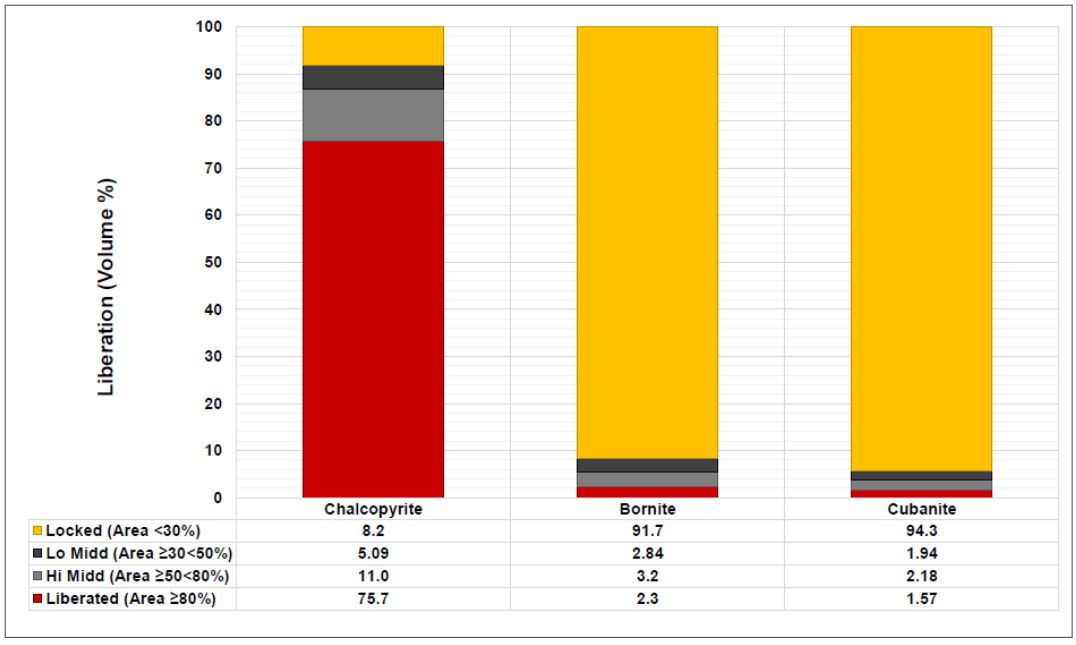
Figure 4-2 A schematic representation showing how a grain of interest can occur in varying degrees of liberation

The liberation characteristics data (for the significant Cu and Ni bearing minerals), classified as "fully liberated" (≥80% surface/area), "middling" (≥30% <80%) and "locked" (<30%), are graphically displayed in **Figure 4-3** and **Figure 4-4**. All of the Ni-bearing mineral grains were found to be locked (<30% liberation). For the Cu-bearing minerals, bornite and cubanite mineral grains were mostly locked, while the chalcopyrite was high (Hi) middlings (>75% liberated).



	Pentlandite	Maufite	Violarite	Pyrite-Ni	Spinel-Ni
Locked (Area <30%)	99.5	99.5	99.9	99.6	100.0
Lo Midd (Area ≥30<50%)	0.3	0.3	0.1	0.0	0.0
Hi Midd (Area ≥50<80%)	0.2	0.2	0.1	0.3	0.0
Liberated (Area ≥80%)	0.1	0.0	0.0	0.1	0.0

Figure 4-3 Liberation of Ni-bearing Minerals



	Chalcopyrite	Bornite	Cubanite
Locked (Area <30%)	8.2	91.7	94.3
Lo Midd (Area ≥30<50%)	5.09	2.84	1.94
Hi Midd (Area ≥50<80%)	11.0	3.2	2.18
Liberated (Area ≥80%)	75.7	2.3	1.57

Figure 4-4 Liberation of Cu-bearing Minerals

4.2.6 Associations of Minerals

The mineral association data is presented in **Table 4-6**. The major mineral associations for pentlandite are pyrite (8%), spinel (6.8%) and mixed iron sulphide/oxide phases (11.4%). Chalcopyrite was strongly associated with pentlandite (12.6%), bornite (27.7%), cubanite (5.4%) and pyrrhotite (5.2%). Bornite was also strongly associated with pentlandite (21.7%), chalcopyrite (17%), cubanite (7.2%) and pyrrhotite (5.5%)

Table 4-6 Association of Minerals Present in Sample)

Mineral in Sample	Mass (%) of Association							
	Pentlandite	Maufite	Violarite	Pyrite-(Ni)	Spinel-(Ni)	Chalcopyrite	Bornite	Cubanite
Pentlandite		49.3	59.4	56.9	50.5	12.6	21.7	34.3
Maufite	3.5		0.8	2.5	0.7	0.7	1.1	1.1
Violarite	0.9	0.0		0.0	0.0	0.0	0.0	0.0
Pyrite (Ni)	0.2	0.0	0.0		0.0	0.0	0.0	0.0
Spinel (Ni)	0.0	0.0	0.0	0.0		0.0	0.0	0.0
Chalcopyrite	1.1	0.9	0.2	0.5	0.0		17.0	8.9
Bornite	1.9	1.6	0.9	1.9	2.5	27.7		11.9
Cubanite	1.4	0.4	0.3	0.8	0.0	5.4	7.2	
Amphibole	0.9	1.3	0.0	0.0	0.0	0.1	0.2	0.2
Clinopyroxenes	2.1	7.1	0.1	0.7	0.0	0.4	0.8	0.7
Ferrosilite	4.9	4.2	1.0	2.8	0.0	1.0	2.2	1.6
Plagioclase	0.0	2.9	0.0	0.0	0.0	0.0	0.0	0.0
Hem/Mag*	1.2	0.3	0.2	0.6	0.0	0.6	0.6	1.3
Pyrite	8.0	0.5	0.4	6.2	0.0	0.3	0.5	0.6
Quartz	0.1	0.5	0.0	0.0	0.0	0.0	0.0	0.0
Carbonates	0.0	0.1	0.0	0.0	0.0	0.1	0.0	0.0
Pyrrhotite	11.1	2.6	2.0	5.9	0.0	5.2	5.5	11.6
Spinel	6.8	5.8	2.9	2.3	43.3	2.0	3.1	4.8
Other	0.7	6.0	0.1	2.6	3.0	0.4	0.4	0.5
Pyrrhotite - Hem/Mag* (mix)	7.5	1.7	2.4	3.1	0.0	2.0	3.1	7.0
Pyrite - Hem/Mag* (mix)	3.9	1.3	0.6	1.1	0.0	1.0	1.7	4.0
Free particles	**43.7**	**13.5**	**28.6**	**11.9**	**0.0**	**40.4**	**34.8**	**11.3**
Total	100.0	100.0	100.0	100.0	100.0	100.0	100.0	100.0

* Hem/Mag – Hematite/Magnetite

4.3 Summary

The chemical and mineralogical characterisation of the Ni, Cu concentrate sample revealed the following salient data and conclusions:

- Chemical composition of the sample, was dominated by four elements Ni (~7%), Cu (~3%), Fe (~31%) and S (>10%)
- Bulk mineralogical composition of the sample by mass % consisted of 41%Ni-bearing minerals, 8% CuS-bearing minerals, 33% other S-bearing minerals, 2% oxide minerals, 5% Fe-sulphide/oxide (mix) phase and 11% silicate minerals
- Composition of Ni-bearing minerals showed that 99.4% of the nickel was distributed in pentlandite mineral.
- Composition of Cu-bearing minerals showed distribution % of Cu was spread across chalcopyrite (59%), bornite (36%) and cubanite (6%)
- The liberation data showed that all the Ni-bearing mineral grains were locked (<30% liberation). For the Cu-bearing minerals, bornite and cubanite mineral grains were mostly locked, while the chalcopyrite was high (Hi) middlings (>75% liberated).

CHAPTER FIVE

SCREENING OF SIGNIFICANT FACTORS AND SOLVENT ALTERNATIVES

5.1 Introduction

This chapter focuses on identifying critical factors that influence the extraction of base metals from sulphide ore concentrate and evaluating a trio of DESs that promise to enhance performance, sustainability and cost efficiency. Screening significant factors is a crucial step in experimental design, allowing researchers to focus on variables with the most substantial impact while minimizing resources spent on less influential ones (Montgomery, 2017; Ochromowicz and Leśniewicz, 2018). Similarly, exploring solvent alternatives is vital for aligning process development with environmental and economic objectives, particularly in contexts where green chemistry principles or regulatory considerations are important. The solvents selected for this study were based on mixtures of choline chloride with the hydrogen bond donors, ethylene glycol, urea and malonic acid respectively.

The approach adopted involves a systematic evaluation of factors and solvents using statistical tools based on factorial designs. These methods enable the identification of both main effects and interactions among variables, offering a comprehensive understanding of the system's behaviour. Factorial designs are particularly valuable for their efficiency in testing multiple variables simultaneously, significantly reducing the experimental burden (Montgomery, 2017).

Leaching variables are numerous, encompassing solute and solvent properties as well as thermodynamic parameters. However, for this study, only five key factors were selected for investigation: temperature, leaching time, stirring rate, pulp density (solids loading), and the addition of a diluent to reduce viscosity.

The effects of these factors, along with their interactions, were analysed using a two-level, four and five factor fractional factorial design of experiments (2^{4-1} and 2^{5-2}) and a full factorial design of experiments (2^4). The percentage (%) of metal leached or recovered was used as the measured response. The detailed experimental methodology employed in this chapter is outlined in **Chapter 3**.

The chapter is structured to provide insights into the methodology, results, and implications of the screening process. Key outcomes include a refined list of significant factors and a solvent that meets the desired performance criteria. These findings serve as a foundation for subsequent optimization and process development steps.

By combining statistical rigor with a focus on sustainability and efficiency, this chapter aims to contribute valuable insights toward process innovation and improvement.

5.2 Experimental Factor Levels

A statistical design of experiments (DOE) approach was utilized to investigate the leaching behaviour of copper-nickel sulphide concentrate, employing a 2^{4-1} and 2^{5-2} fractional factorial design, and a 2^4 full factorial design. The selection of factors and their respective levels was informed by insights gained from an extensive literature review and some preliminary experimental findings, ensuring a focused and systematic exploration of the process variables.

Experimental design factors were categorized into controlled and constant factors. The controlled factors, outlined in **Table 5-1**, were selected for detailed investigation. In contrast, constant factors, such as particle size, were maintained at fixed levels—in this case, +38 µm -75 µm to minimize variability. While these constant factors might influence the response, they were deemed outside the primary scope of interest for this study.

The factors were investigated using their coded values of -1 and +1, with the corresponding physical values. The coded levels of the controlled variables, as described by Box et al., (1978), were calculated using the following formula:

$$\boldsymbol{coded\ value} = \frac{X - X_O}{05(X_2 - X_1)} \quad \textbf{(5.1)}$$

Where, X is the actual value of the factor, X_o is the centre point or mean of the factor range, X_1 is the lowest value of the factor and X_2 is the highest value of the factor

Table 5-1 Experimental factors and their level settings

Factor	**Lower level (-1)**	**High level (+1)**
Temperature ℃	25	60
Pulp density (%w/v)	2	10
Stirring rate (rpm)	300	600
Diluent (nEG: HBD) *	0	3
Leaching time (hours)	1	4

* n represents the mole of ethylene glycol per mole of a specific hydrogen bond donor

5.3 Methodology for Data Analysis

The experimental results were statistically analysed using several techniques, including the half normal probability plot of effects, Pareto chart, Analysis of Variance (ANOVA), diagnostic plots (residuals analysis), and model graphs. These methods provided a comprehensive evaluation of factor significance and model fit.

5.3.1 Half-Normal Probability Plot of Effects

A half-normal probability plot of estimated factor effects is a graphical tool used for analysing the results of two-level factorial designs (Montgomery, 2017). It helps identify the most significant factors or interactions affecting the response by

separating these from random noise. The plot represents the ordered absolute values of the factor effects plotted against the expected cumulative probabilities of the absolute effects (based on a normal distribution). The plot helps differentiate between significant effects (factors or interactions with large magnitudes) that deviate from randomness and insignificant effects (pure noise) that align with the normal distribution. Insignificant effects form a straight line on the plot, as they are assumed to follow a normal distribution. Significant effects deviate from this straight line and appear as outliers towards the upper-right corner of the plot (Box, Hunter and Hunter, 2005).

The half normal plot has some clear advantages. It is easy to identify significant factors visually making the half normal plot suitable for initial screening in factorial designs. It assumes errors are normally distributed making it appropriate for well controlled experiments. However, the assumption of normality is also a limitation as it might not always hold in some cases. Furthermore, the interpretation of deviation from the "straight line" is subjective hence can lead to inconsistencies in analysis of results. To mitigate the limitations of half normal plots the analysis can be combined with statistical tests like ANOVA or supplemented with Pareto charts.

5.3.2 Pareto Chart

Pareto charts visually rank the effects of factors and interactions on the response variable in descending order of magnitude (Antony, 2023). This helps identify the most significant factors. The Pareto chart is based on an algorithm that produces a statistically based acceptance limit of significance represented by vertical bar graphs. The bars are ordered by effect size with the longest bars representing the largest effects. Statistical significance threshold lines, such as t-values or Bonferroni limits, may be added to identify significant effects. Pareto charts complement half-normal plots by clearly showing effect sizes and significance visually (Whitcomb and Oehlert, 2007).

5.3.3 Analysis of Variance (ANOVA)

Analysis of Variance (ANOVA) is a statistical method used to assess the significance of factors (main effects) and their interactions on the response variable (Montgomery, 2017). ANOVA focuses on four key concepts which are partitioning variance, null hypothesis testing, F-statistic and degrees of freedom (df). ANOVA divides or partitions the total variability in the response into components attributable to factors (main effects), interactions and error (residual or random noise). For each factor or interaction, ANOVA tests the null hypothesis that its effect is zero ($H_{0:}$ Effect = 0). A small p-value (e.g., <0.05) indicates a significant effect. ANOVA uses the F-statistic to compare the variance explained by each factor to the residual variance. The F-statistic is given by:

$$F = \frac{Mean\ square\ of\ the\ effect}{Mean\ square\ of\ the\ error} \quad \textbf{(5.2)}$$

A high F-value indicates that the factor has a significant impact on the response. Each factor or interaction has associated degrees of freedom based on the number of levels in the design. The error term's degrees of freedom depend on replicates and total experimental runs (Antony, 2023)

5.3.4 Diagnostic Plots (Residual analysis)

Diagnostic plots are used to validate model assumptions and evaluate the adequacy of the experimental model (Heckert *et al.*, 2002). Residuals are the differences between observed and predicted responses and analysing them helps identify potential problems with the model. There are several diagnostic plots employed in model verification. The normal probability plot of residuals is used to check if residuals follow a normal distribution, which is an assumption for ANOVA. Residuals are plotted against expected values under normality and points should lie approximately on a straight line.

Deviations indicate non-normality, suggesting a need for data transformation. Residuals vs. Fitted Values is another diagnostic plot, which is used to evaluate the assumption of constant variance (homoscedasticity). Residuals are plotted against predicted values. Residuals should scatter randomly around zero without forming patterns. Patterns (e.g., funnel-shaped) suggest heteroscedasticity. Residuals vs. Runs plot is used to identify systematic effects or trends linked to experimental runs or factor levels. Random scatter in the plot indicates no lurking variables. Patterns may suggest time-dependent effects or overlooked factors. Other diagnostic plots include histogram of residuals and cook's distance or leverage plots (Montgomery, 2017).

If diagnostics reveal issues, remedies can include adding interaction or quadratic terms to the model, transforming response variables and revisiting experimental design for missing factors or confounding.

5.3.5 Model Graphs

Model graphs are visual tools used to represent the effects of factors and their interactions on the response variable (Antony, 2023). These graphs help in interpreting results, validating the model, and communicating findings effectively.

There are several types of model graphs. Main effects plots show the effect of changing one factor from its low level to its high level on the response. The mean response is plotted for each level of the factor, often as a straight line connecting the two means. A steep slope indicates a strong main effect. A flat line suggests the factor has little or no effect. The interaction plot visualizes interactions between two factors, revealing whether the effect of one factor depends on the level of another. Lines are plotted for one factor at each level of another factor. Non-parallel lines suggest an interaction. Parallel lines indicate no significant interaction.

Contour and Surface plots represent the relationship between factors and the response over a continuous range. Contour plots use lines of constant response, while surface plots use 3D representations. These plots are useful for visualizing optimal settings or curvature in the response surface. Other model graphs include cube plot, residual vs predicted plot and interaction profiles (Heckert *et al.*, 2002).

5.4 Screening Experiments

5.4.1 Fractional Factorial Design

The fractional factorial design provided an initial screening of factors affecting metal recovery using the three solvents, ethaline, reline, and maline. This approach was chosen to efficiently identify significant main effects and interactions while minimizing the number of experimental runs.

5.4.1.1 Ethaline

The fractional factorial design results (**Table 5-2)** for ethaline revealed that nickel recovery ranged from 47.86% to 54.98%, the highest among the three solvents studied. This highlights ethaline's potential for efficient and selective nickel extraction.

Table 5-2 Base metal recovery results for the 2_{IV}^{4-1} fractional factorial design (leaching in ethaline). A (temperature), B (pulp density), C (stirring rate) and *D (leaching time*)

Run	A	B	C	D	Ni Recovery	Co Recovery	Cu Recovery
	℃	% w/v	rpm	hours	%	%	%
1	25	10	300	4	49.2	12.23	2.3
2	25	2	300	1	53.11	12.97	4.08
3	60	10	300	1	48.63	12.22	2.74
4	60	2	300	4	52.65	14.16	5.25
5	25	2	600	4	47.86	13.55	4.65
6	25	10	600	1	49.23	12.3	1.77
7	60	10	600	4	48.63	12.3	3.9
8	60	2	600	1	54.98	14.77	5.06

Statistical analyses, including the half-normal probability plot and Pareto chart (**Figures 5-1 and 5-2**), suggested that leaching time (D), pulp density (B), and their interaction (AB) might influence nickel recovery. However, none of these factors crossed the statistical significance thresholds (Bonferroni and t-value limits), and the model was ultimately deemed non-significant.

No further efforts were made to analyse the nickel data as these results indicate a need to modify the experimental design. To address the limitations of fractional designs, a higher-resolution design was later implemented (see **Section 5.4.2**), allowing for better separation of effects.

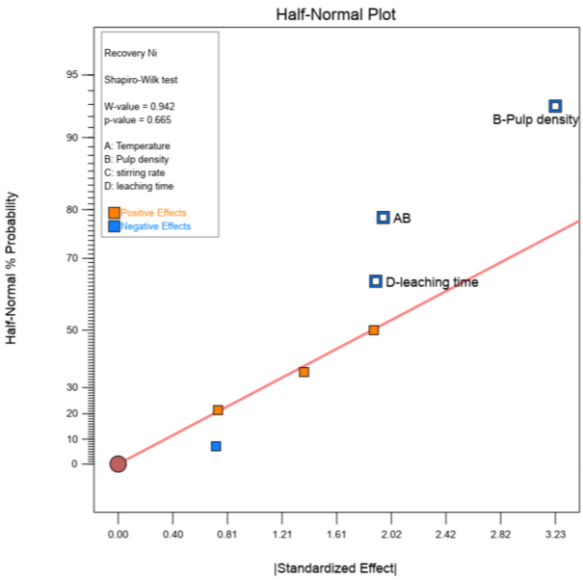


Figure5-1 Half Normal plot of estimated factor effects of Ni recovery using ethaline

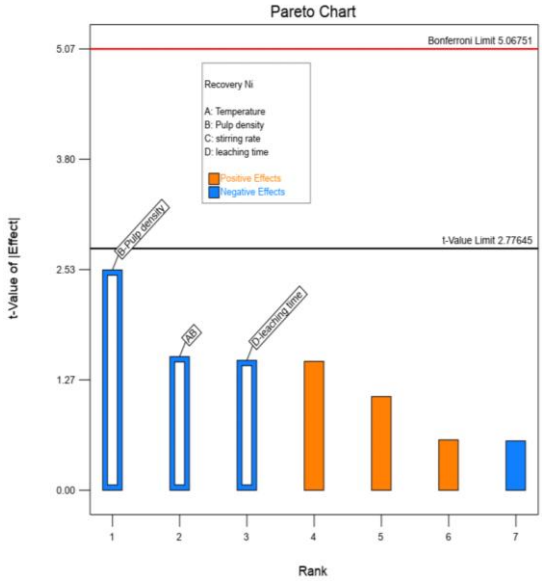


Figure5-2 Pareto chart for ranking of main and interactive effects (Ni recovery)

The cobalt and copper recovery data from **Table 5-2** was also analysed using half normal plots, Pareto charts, ANOVA and residuals, the results are summarised in **Table 5-3**.

Table 5-3 Summary of estimated main and interaction effects and diagnosis for ethaline

Model	ANOVA	Terms	Diagnostics	Min %	Max %
Ni	Not significant	-	-	47.86	54.98
Cu	Significant	A, B	Outlier	1.77	5.25
Co	Significant	A, B, AB	Good	12.22	14.77

Pulp density was identified as a significant main effect for Co recovery as confirmed by a t-value that significantly exceeded the Bonferroni limit, see **Figure 5-3**. Higher pulp densities reduced cobalt recovery. Temperature showed a marginal impact, and the interaction between these two factors (AB) was also statistically significant.

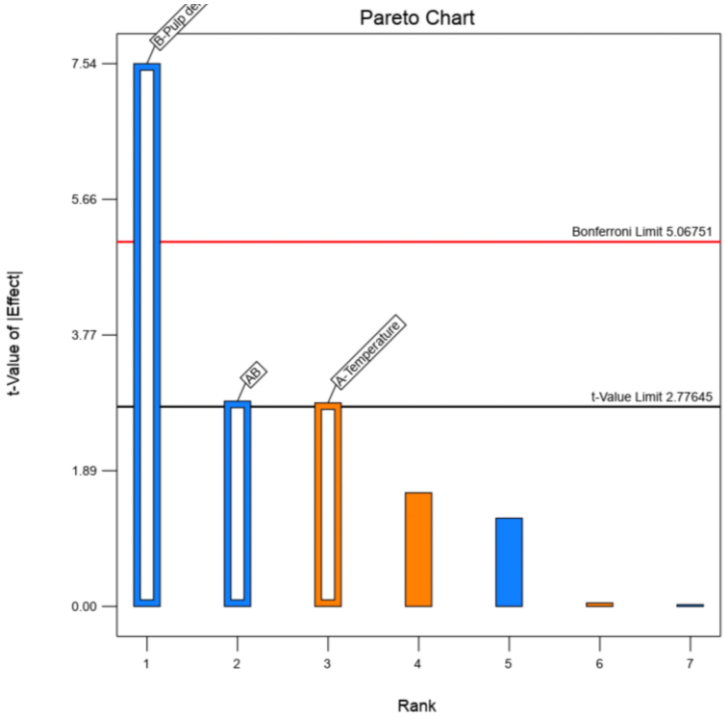


Figure 5-3 Pareto chart for ranking of main and interactive effects (Co recovery)

The ANOVA confirmed the model's validity (see **Table 5-4)**, with good residual diagnostics suggesting reliability. The results highlight the need to control pulp density to improve cobalt extraction.

These findings align with prior studies, which suggest that lower pulp density increases metal recovery (Topçu, Rüşen and Küçük, 2021; Ebrahimi et al., 2023).

Table 5-4 ANOVA for the selected Co recovery model

Source	**Sum of Squares**	**df**	**Mean Square**	**F-value**	**p-value**	
Model	6.57	3	2.19	24.35	0.0050	significant
A-Temperature	0.7200	1	0.7200	8.00	0.0474	
B-Pulp density	5.12	1	5.12	56.90	0.0017	
AB	0.7320	1	0.7320	8.14	0.0463	
Residual	0.3599	4	0.0900			
Cor Total	6.93	7				

Temperature (A) and pulp density (B) were identified as significant main effects for copper recovery as their standardized effect values crossed the Pareto threshold limits see **Table 5-3**. Both factors crossed the t-value limit but only pulp density crossed the Bonferroni limit indicating it had the highest influence on copper recovery. The ANOVA for the copper recovery model indicated a significant model (p value = 0.0027) however the normal plot of residuals, see **Figure 5-4**, showed the presence of an outlier. The point that lies to the far right of the straight line corresponds to run number 7.

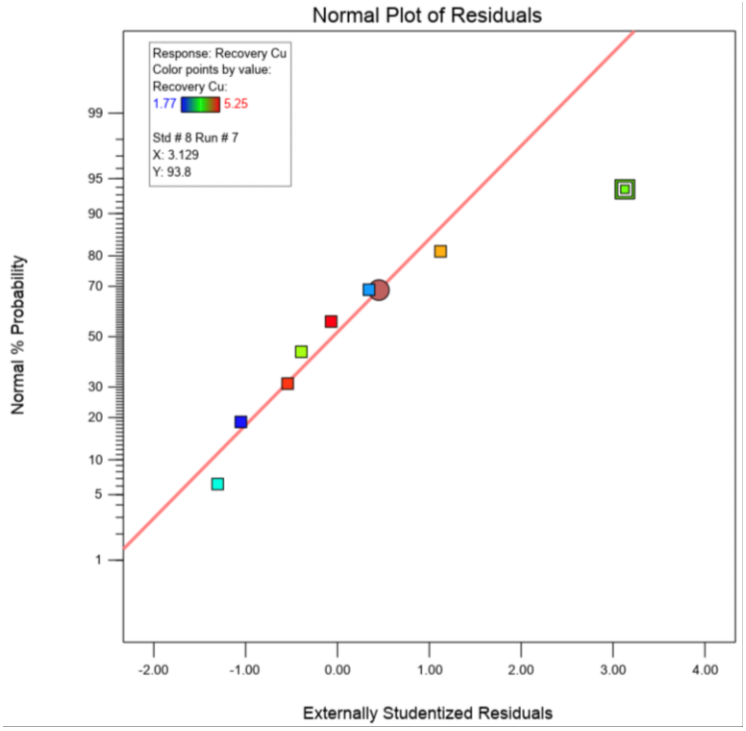


Figure 5-4 Normal plot of residuals for Cu recovery

5.4.1.2 Reline

The results for reline Table **5-5** revealed nickel recovery values ranging from 33.56% to 54.76%, with cobalt and copper recoveries ranging from 9.56% to 16.05% and 0.25% to 5.29%, respectively.

Table 5-5 Base metal recovery results for the 2^{5-2}_{III} fractional factorial design (maline). A (temperature), B (pulp density), C (stirring rate), D (leaching time) and E (Diluent)

Run	A	B	C	D	E	Recovery Ni	Recovery Co	Recovery Cu
	℃	% w/v	rpm	hours	moles	%	%	%
1	25	2	300	4	3	50.23	14.48	2.55
2	60	2	300	1	0	42.9	12.59	5.29
3	25	2	600	4	0	54.76	16.05	2.17
4	60	2	600	1	3	46.66	13.6	0.39
5	25	10	300	1	3	47.06	13.6	0.33
6	60	10	300	4	0	46.77	13.97	1
7	60	10	600	4	3	33.56	9.56	0.25
8	25	10	600	1	0	46.46	13.6	0.65

Statistical analyses, including half-normal plots and Pareto charts, indicated that none of the studied factors or their interactions significantly influenced metal recovery (see **Table 5-6**). This lack of significance highlights a limitation of the fractional factorial design used, particularly its low resolution and susceptibility to confounding effects. It is generally assumed that even with a low-resolution design, main effects and some interactions can still be identified provided higher order interactions are negligible. However, sometimes neglected interactions (assumed negligible) can turn out to be significant. This limitation of partial factorial design is addressed in **section 5.4.2** using a high resolution full factorial design.

Table 5-6 Summary of estimated main and interaction effects and model diagnosis for reline

Model	ANOVA	Terms	Diagnostic	Min %	Max %
Ni	Not significant	-	-	33.56	54.76
Co	Not significant	-	-	9.56	16.05
Cu	Not significant	-	-	0.25	5.29

5.4.1.3 Maline

The effects of different factors on metal recovery, as determined by the fractional factorial design for leaching in ethaline, are presented in **Table 5-7**. This tables shows the metal recovery values for various combinations of the studied factors.

Table 5-7 Base metal recovery results for the 2_{III}^{5-2} fractional factorial design (leaching in maline). A (temperature), B (pulp density), C (stirring rate), D (leaching time) and E (Diluent)

Run	A	B	C	D	E	Ni Recovery	Co Recovery	Cu Recovery
	℃	% w/v	rpm	hours	(nEG:MA)	%	%	%
1	25	2	600	4	0	50.35	13.43	6.98
2	25	10	600	1	0	46.87	12.97	5
3	60	10	300	4	0	49.27	13.9	15.02
4	60	2	600	1	3	51	14.59	19.61
5	25	2	300	4	3	53.15	13.37	7.21
6	60	10	600	4	3	51.09	13.67	7.87
7	60	2	300	1	0	53.76	14.39	15.1
8	25	10	300	1	3	43.76	12.88	4.33

The nickel, cobalt and copper recovery data from **Table 5-7** was analysed using half normal plots, Pareto charts, ANOVA and residuals, the results are summarised in **Table 5-8**.

Temperature and pulp density were identified as significant by the half-normal plot for nickel and cobalt recovery. However, the Pareto chart and ANOVA showed that temperature was an insignificant model term for nickel recovery. Furthermore, the selected Ni recovery model was non-significant based on ANOVA with a p-value of 0.0522 > 0.05. The Co recovery model was statistically significant (p = 0.0001) and overall residual analysis was also good.

Temperature was identified as the most significant factor ($p < 0.05$) in maline, where copper recovery increased significantly at higher temperatures. Copper recovery was generally low, ranging from 4.33% to 19.61%, however maline outperformed the other solvents in terms of recovery. The ANOVA indicated the selected factorial model for copper recovery was significant however model diagnostics showed presence of outliers corresponding to run 6. Addressing outliers through increased replicates, better process control, or data transformation is critical to improving model reliability.

Table 5-8 Summary of estimated main and interaction effects and model diagnosis for maline

Model	ANOVA	Terms	Diagnostic	Min %	Max %
Ni	Not significant	A, B	-	43.76	53.76
Co	Significant	A, B	Good	12.88	14.59
Cu	Significant	A	Outlier	4.33	19.61

5.4.1.4 Comparison of Solvents

Across all solvents, nickel recovery ranged from 33.56% to 54.98%, with ethaline showing the highest recovery, while maline was better for Cu recovery (19.61%).

However, the maximum nickel recovered did not differ significantly across the three solvents. The relatively high recovery of copper in maline suggests opportunities for sequential or targeted leaching stages, which could maximize overall process efficiency.

Cobalt recovery was low, ranging from 9.56% to 16.05% across all solvents. Cobalt recovery, like nickel recovery, showed minimal variation across solvents, suggesting that solvent choice has less impact on cobalt extraction. The limited improvement in cobalt recovery across solvents suggests that further optimization or alternative approaches, such as sequential leaching, may be necessary.

The lack of variation in recovery trends suggests that leaching efficiency alone is not a sufficient criterion for solvent selection. Instead, it should be combined with consideration of unique solvent properties, such as viscosity. Among the three solvents evaluated, ethaline exhibits the lowest viscosity, ranging from 87.449 mPa·s to 14.913 mPa·s over a temperature range of 20–60°C (Haghbakhsh, Duarte and Raeissi, 2021). In comparison, maline's viscosity falls between 1650.56 mPa·s and 132.75 mPa·s within the same temperature range (Jangir, Nain and Kuperkar, 2021), while reline's viscosity ranges from 1371.97 mPa·s to 68.65 mPa·s (Yadav and Pandey, 2014).

Ethaline's superior nickel recovery and practical handling advantages (low viscosity) make it a strong candidate for further optimization. Thus section 5.4.2 and chapter 6 focused exclusively on this solvent.

5.4.2 Full Factorial Design

While fractional factorial designs provided valuable initial insights into factor significance and solvent performance, their limitations underscore the importance of complementing them with higher-resolution designs for greater accuracy. Ethaline emerged as the most promising solvent for nickel recovery, laying the

groundwork for subsequent optimization steps (discussed in **chapter 6**).

The effects of different factors on metal recovery, as determined by the full factorial design, are presented in **Table 5-9**. This table shows the metal recovery values for various combinations of the studied factors.

Table 5-9 Base metal recovery results for the 2_V^4fractional factorial design (leaching in ethaline). A (temperature), B (pulp density), C (stirring rate) and D (leaching time

Std	Run	A	B	C	D	Ni recovery	Cu recovery	Co recovery
		℃	% (w/v)	rpm	hours	%	%	%
12	1	60	10	300	4	43.82	3.72	11.59
10	2	60	2	300	4	52.65	5.25	14.16
13	3	25	2	600	4	47.86	4.65	13.55
15	4	25	10	600	4	46.3	2.78	11.7
8	5	60	10	600	1	44.4	4.04	11.68
6	6	60	2	600	1	54.98	5.06	14.77
14	7	60	2	600	4	54.44	4.28	14.37
11	8	25	10	300	4	49.2	2.3	12.23
16	9	60	10	600	4	48.63	3.9	12.3
1	10	25	2	300	1	53.11	4.08	12.97
4	11	60	10	300	1	48.63	2.74	12.22
2	12	60	2	300	1	51.24	2.93	14.23
7	13	25	10	600	1	49.23	1.77	12.3
5	14	25	2	600	1	56.34	3.72	15.58
9	15	25	2	300	4	55.55	4.32	15.63
3	16	25	10	300	1	45.47	2.36	11.76

By analysing the recovery values for nickel, copper, and cobalt under similar conditions, several key observations can be made. Ethaline demonstrated the highest influence on nickel recovery, achieving rates between 43.82% and 56.34%. In contrast, cobalt recovery was relatively low, ranging from 11.59% to 15.63%, while copper recovery was minimal, between 1.77% and 5.25%. Furthermore, a comparison between the fractional factorial design and the full factorial design reveals an increase in the maximum recoverable nickel, improving from 54.98% to 56.34%.

The correlation between mineral liberation (**chapter 4**) and metal recovery is not straightforward. Although nickel-bearing pentlandite was largely locked (<30% liberation), nickel still exhibited the highest recovery among the studied metals. In

contrast, chalcopyrite was relatively well liberated (~75%) yet displayed the lowest copper recovery. This discrepancy can be attributed to the refractory nature of chalcopyrite, which is known to exhibit slow leaching kinetics and to form passivating surface layers that hinder further dissolution (Li et al. 2013).

This preliminary analysis indicates that ethaline is highly selective towards nickel recovery hence copper and cobalt may need to be recovered through subsequent leaching stages. The following sections and chapter will, therefore, mainly focus on analysis of the nickel recovery model.

5.4.2.1 Selection of Effects (factorials)

The analysis of the factorial design entailed the identification and separation of the significant factor effects from the insignificant effects and pure error. The Half-Normal plot (see **Figure 5-5**) was used to select effects for the model in combination with the Pareto plot.

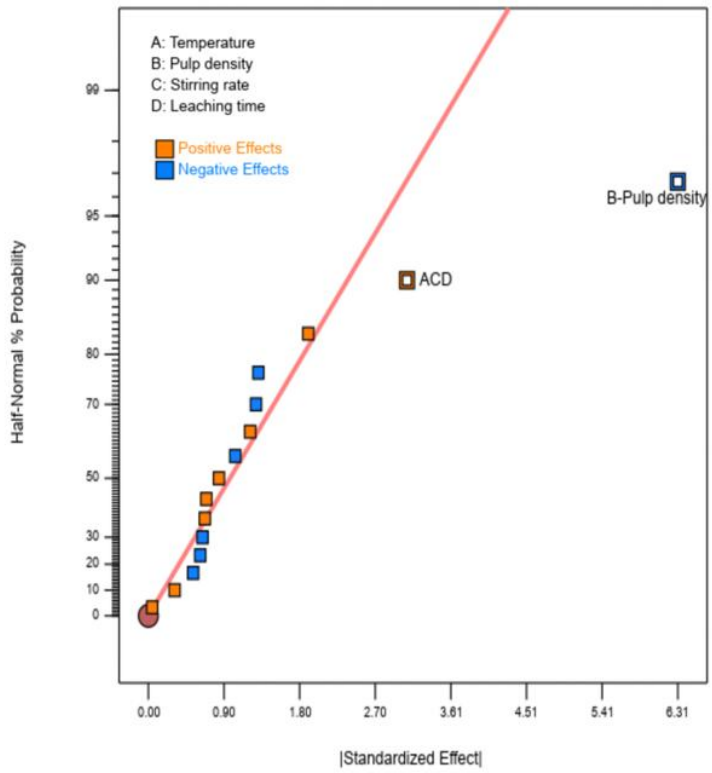


Figure 5-5 Half normal plot for Ni recovery

From **Figure 5-5** it can be seen that pulp density and the three-way interaction (ACD) are significant effects hence these were selected as model terms. Effects that were below the t-value limit on the pareto plot were selected automatically by the program to support hierarchy i.e. all lower order terms that comprise higher order terms must also be included in the model, see **Figure 5-6**.

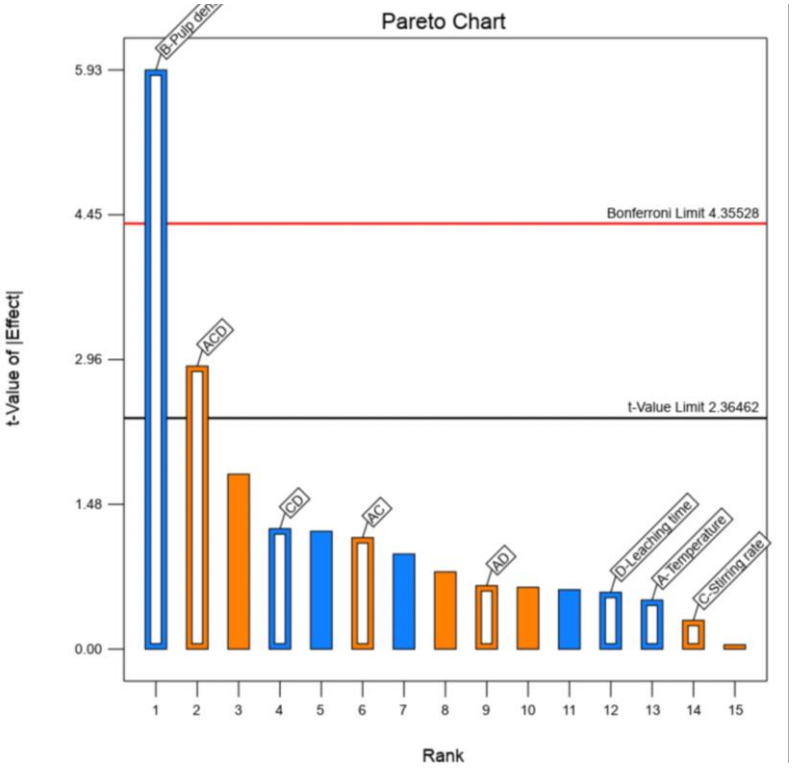


Figure 5-6 Pareto chart for ranking of effects on Ni recovery

5.4.2.2 ANOVA

The Analysis of Variance (ANOVA) was used for the descriptive statistics and statistical tests. Low p-values were used to identify important model terms. The ANOVA indicated that the selected model was statistically significant as shown by an F- value of 5.93 and p-value of 0.0149, see **Table 5-10**. This implies there is only a 1.49% chance an F-value this large could occur due to noise. The individual terms were tested independently for significance and only pulp density and ACD passed the test with p-values of 0.0006 and 0.0231 respectively.

Table 5-10 ANOVA for the selected Ni recovery model

Source	Sum of Squares	df	Mean Square	F-value	p-value	
Model	215.11	8	26.89	5.93	0.0149	significant
A-Temperature	1.14	1	1.14	0.2513	0.6316	
B-Pulp density	159.33	1	159.33	35.13	0.0006	
C-Stirring rate	0.3938	1	0.3938	0.0868	0.7768	
D-Leaching time	1.53	1	1.53	0.3377	0.5794	
AC	5.89	1	5.89	1.30	0.2918	
AD	1.91	1	1.91	0.4214	0.5369	
CD	6.88	1	6.88	1.52	0.2579	
ACD	38.04	1	38.04	8.39	0.0231	
Residual	31.75	7	4.54			
Cor Total	246.86	15				

The fit statistics (see **Table 5-11**) showed that the difference between the Predicted R-squared and Adjusted R-squared was greater than 0.2 indicating possible issues with the model. This could be due to a large block effect or errors in the data. Model reduction, response transformation and outliers were explored to improve the fit statistics. Nonetheless, the model also showed Adequate Precision (i.e. >4) with a signal-to-noise ratio of 7.523, suggesting the model could be used to navigate the design space.

Table 5-11 Fit statistics for Ni recovery

Std. Dev.	2.13		**R^2**	0.8714
Mean	50.12		**Adjusted R^2**	0.7244
C.V. %	4.25		**Predicted R^2**	0.3281
			Adeq Precision	7.5231

The coefficient estimate showed a negative correlation between pulp density and Ni recovery with an expected change in response per unit change in factor value of -3.16. The model equation in coded terms is provided below (**Equation 5.3**) and can be used to make predictions about the response for given levels of each factor**.**

$$Ni\ recovery = 50.12-0.2669A-3.16B+0.1569C- 0.3094D + 0.6069AC + 0.3456AD-0.6556CD+1.54ACD \quad \textbf{(5.3)}$$

5.4.2.3 Model Validation (Diagnostic Plots)

Externally studentized residual plots were used to check the regression assumptions and find issues with the model analysis (**Figure 5-7**). Studentizing the residuals maps all the different normal distributions (associated with raw residuals) to a single standard normal distribution.

No outlying abnormalities were found with the data as all residuals formed a straight line. The **Residuals vs Predicted** plot was used to test the assumption of constant variance. The plot shows a random scatter i.e., a constant range of residuals across the graph. The **Residuals vs Run** plot was used to check for lurking variables that may have influenced the response during the experiment. The plot shows a random scatter hence no lurking variables were detected. The **Box-Cox** plot was used to calculate the best power law transformation, in this case, none was required as the data followed a normal distribution.

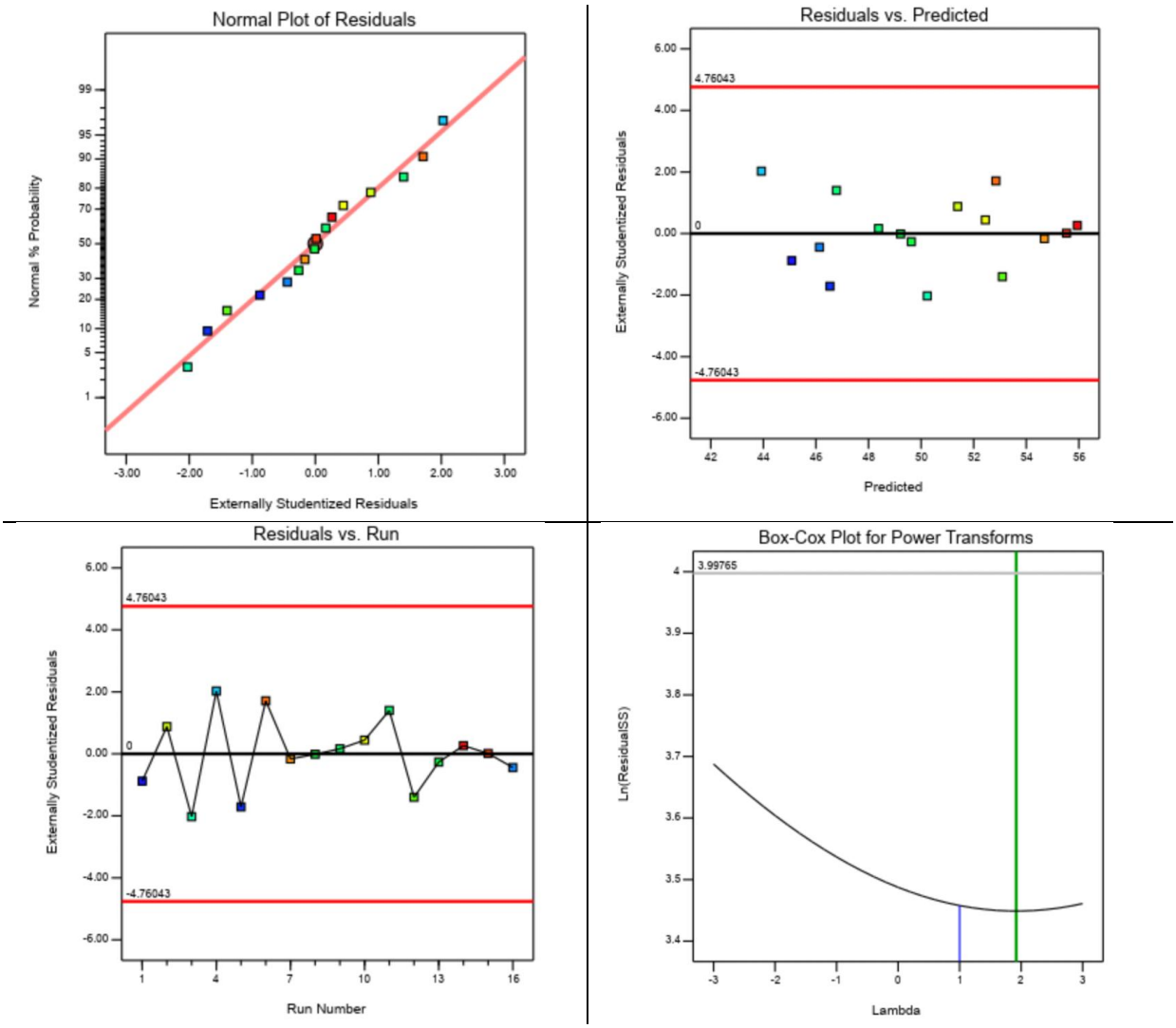


Figure 5-7 Diagnostic plots, top left (Normal plot of residuals), top right (Residuals vs Predicted), bottom left (Residuals vs Run) and bottom right (Box-Cox Plot)

5.4.2.4 Model graphs

Interpretation of the selected model was carried out using the one factor, interaction and cube model graphs. The one-factor graph was used to check the main effects for factors that are not part of an interaction. Since pulp density was the only main effect that was identified its one factor graph is provided in **Figure 5-8**. This graph shows the linear effect of changing the levels of pulp density with respect to the predicted responses at the high and low factor settings.

The I-beams around the predictions are the result of 95% least significant difference (LSD) calculations. The LSD I-beams are approximate tests to check if the predictions at the displayed factor combinations are significantly different. From **Figure 5-8** it is clear the LSD I-beams do not overlap which indicates a significant difference between the two points. The practical implication of this graph is that in order to improve Ni recovery pulp density must be minimized.

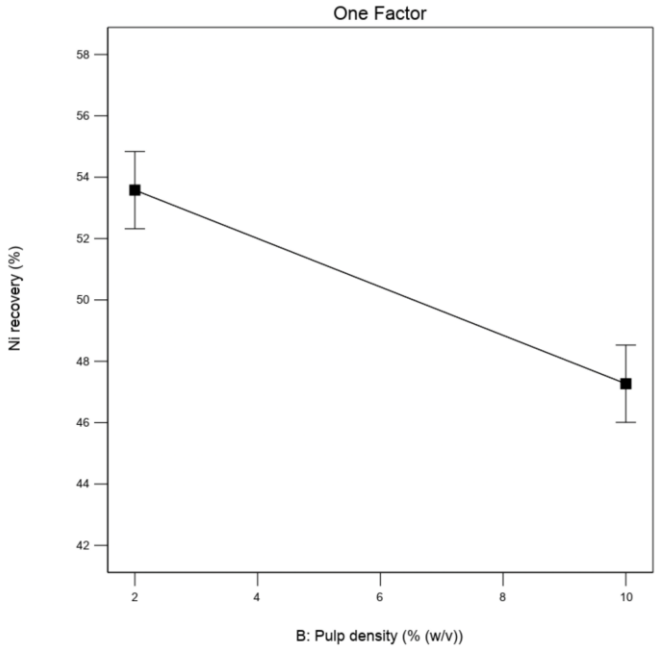


Figure 5-8 An interaction plot of pulp density vs Ni recovery

The interaction graph was used to display two-factor interactions. The Ni recovery was pre-optimized by adjusting the factor settings for the non-axis factors from their default settings (i.e., midpoint levels). A higher Ni recovery (55.94%) was predicted by shifting settings to the highest stirring rate, lowest temperature and leaching time (i.e., 600rpm, 25℃ and 1hour), see **Figure 5-9**.

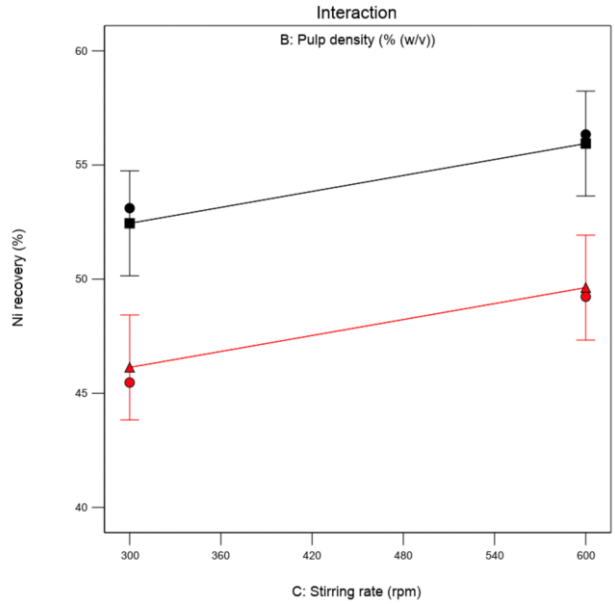


Figure 5-9 Two-way interaction plot for Ni recovery vs stirring rate and pulp density: red graph (B=10% w/v) and black graph (B=2% w/v)

The cube plot was useful for viewing the relationship among three factors, see **Figure 5-10**. All values shown are predicted values. The factors of interest as shown are A, C and D. Theoretical maximum Ni recovery of 55.9406% occurs at settings of C+, A- and D-.

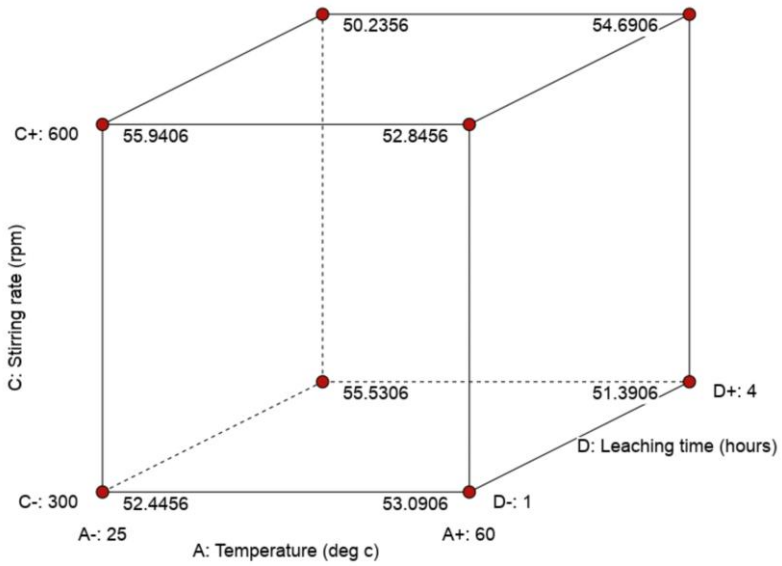


Figure 5-10 Cube plot for Ni recovery

5.5 Summary

Chapter 5 explored the screening of critical factors and alternative solvents for the leaching of base metals from copper-nickel sulphide concentrates using DESs. Three solvents; ethaline, reline, and maline were evaluated for their performance through fractional and full factorial designs. Five variables; temperature, pulp density, stirring rate, leaching time, and diluent ratio—were analysed for their impact on metal recovery.

Key findings indicate that ethaline achieved the highest nickel recovery (up to 56.34%) with selective leaching properties, while cobalt and copper recoveries remained low to moderate across all solvents. Pulp density emerged as the most significant factor influencing nickel recovery. Statistical analyses, including ANOVA and diagnostic plots, validated the recovery models, though limitations such as model fit and outliers were identified. High-resolution full factorial designs provided improved clarity on significant factors and interactions.

The results highlight ethaline's potential for efficient and selective nickel recovery, establishing a foundation for subsequent optimization (**Chapter 6**) and greener metallurgical processes.

CHAPTER SIX

PARAMETER OPTIMIZATION

6.1 Introduction

Optimization theory is probably one of the oldest branches in mathematics and has played a pivotal role in the development of calculus and geometry (Lange, 2013). Today it is widely applied across various engineering and scientific fields, reflecting its foundational role in problem-solving. Optimization lies at the heart of any decision-making problem, whether in engineering or economics (Chong, 2013). Decision-making entails selecting the best option from a set of alternatives, guided by the goal of making an optimal choice. The quality of these alternatives is quantified through an objective function or performance index, which serves as a measurable criterion. Optimization, therefore, focuses on maximizing or minimizing a specific desirability function to achieve the best possible outcome (Coleman, Branch and Grace, 1999).

This study aimed to determine experimental conditions that maximize the recovery of nickel while minimising co-dissolution of copper, cobalt and iron, using a custom response surface design. Response surface methodology (RSM), first introduced by Box & Wilson, (1951) was originally developed to optimize manufacturing processes in the chemical industry. It focused on enhancing chemical reactions to achieve high yields and purity while reducing costs through sequential experimentation (Dean *et al.*, 2017). Beyond its initial application, RSM is widely used to model and optimize any response that is influenced by one or more quantitative factors. It employs a combination of mathematical and statistical techniques to establish a functional relationship between a target response and associated control or input variables (Khuri and Mukhopadhyay, 2010).

This chapter builds upon the insights gained from the factor screening experiments detailed in the previous chapter to optimize the leaching process conditions for nickel recovery. Pulp density, identified as a statistically significant factor during the screening, was chosen for optimization, while the non-significant factors, stirring rate, leaching time, and temperature were kept constant. Additionally, the recoveries of Co, Cu, and Fe were monitored to evaluate their impact on nickel recovery.

6.2 Model Derivation

The data presented in **Table 6-1** were obtained by conducting experiments based on the integral (I-optimal) response surface design. The I-optimal design chooses runs that minimize the integral of the prediction variance across the entire experimental space. The table presents the observed response values, specifically Ni, Co, Cu and Fe recoveries for different levels of pulp density.

Table 6-1 Base metal recovery results for the I-optimal design

Run	Pulp density (% w/v)	Ni recovery %	Co recovery %	Cu recovery %	Fe Recovery %
1	2	50.95	13.53	15.37	3.43
2	0.5	58.16	17.5	8.14	4.3
3	1.7375	51.06	13.61	8.49	3.43
4	1.495	53.3	14.24	7.66	3.6
5	1.25	53.26	14.45	6.25	3.66
6	2	52.61	13.66	5.96	3.6
7	0.875	53.05	14.41	6.43	3.7
8	2	51.17	13.13	5.54	3.49
9	0.6875	55.81	15.48	6.4	4.01
10	1.25	52.08	13.76	6.02	3.55
11	0.5	59.06	16.37	5.7	4.35
12	1.0625	50.06	13.13	5.45	3.52
13	1.25	49.69	12.71	5.47	3.48

A summary of the response information is provided in **Table 6-2**. The highest Ni recovery of 59.06% was achieved at a low pulp density of 0.5% (Run 11). As pulp density increased, Ni recovery generally decreased, with values dropping to around 50–52% at higher pulp densities, such as 2%. Cobalt recovery followed a similar trend, with the highest recoveries observed at lower pulp densities i.e.,17.5% and 16.37% Co recovery at 0.5% pulp density in Runs 2 and 11 respectively. In contrast, copper (Cu) recovery peaked at 15.37% at a pulp density of 2% (Run 1), although this appears to be an outlier, as replicate runs (6 and 8) reported much lower recoveries of around 6%. Iron recovery remained consistently low across all runs, ranging from 3.43% to 4.35%, showing minimal sensitivity to changes in pulp density.

Table 6-2 Response information

Response	Units	Observations	Minimum	Maximum	Mean	Std. Dev.	Ratio
Ni recovery	%	13.00	49.69	59.06	53.10	2.93	1.19
Co recovery	%	13.00	12.71	17.5	14.31	1.38	1.38
Cu recovery	%	13.00	5.45	15.37	7.14	2.67	2.82
Fe Recovery	%	13.00	3.43	4.35	3.70	0.3154	1.27

The results from **Table 6-1** were used to fit a quadratic response model and estimate the regression coefficients. The model equation in coded and actual terms is provided below in **Equations 6.1** and **6.2** respectively. The coded equation is useful for identifying the relative impact of factors by comparing their coefficients. The equation in terms of actual terms can be used to make predictions about the response for given levels of pulp density.

$$\hat{y} = 51.47 - 3.12x + 3.54x^2 \quad \textbf{(6.1)}$$

$$Ni\ recovery = 66.48450 - 19.86747 * Pulp\ density + 6.28452 * Pulp\ density^2 \quad \textbf{(6.2)}$$

where "x" is the pulp density and $\hat{y}$ is the Ni recovery.

6.3 Evaluating the Validity of the Model

The validity of the fitted quadratic model was evaluated through analysis of variance (ANOVA), as presented in **Table 6-3**.

Table 6-3 ANOVA for Ni recovery model

Source	Sum of Squares	Degrees of Freedom (df)	Mean Square	F-value	p-value	
Model	80.98	2	40.49	18.23	0.0005	significant
x-Pulp density	61.00	1	61.00	27.46	0.0004	
x^2	29.70	1	29.70	13.37	0.0044	
Residual	22.21	10	2.22			
Lack of Fit	13.57	5	2.71	1.57	0.3166	not significant
Pure Error	8.65	5	1.73			
Cor Total	103.20	12				

The ANOVA was used for the descriptive statistics and statistical tests to evaluate the model. Terms with low p-values (i.e., $p < 0.05$) were identified as significant contributors to the model. Curvature was assessed using the squared term x2 which indicated significant nonlinearity (p of 0.0044 $\ll$ 0.05 and F=13.37). This suggests there is only a 0.44% probability that an F-value this large could result from random noise. Additionally, the lack of fit was not significant ($p = 0.3166 >> 0.05$), which is which is desirable as it indicates the model appropriately fits the data.

The coefficient table (**Table 6-4**) provides detailed information about the model coefficients, including confidence intervals (CI) and variance inflation factors (VIF), which measure factor collinearity. According to a general rule of thumb, VIF values below 10 are considered acceptable. In this case, the VIF is approximately 1, indicating that the factors are orthogonal and exhibit minimal collinearity.

Table 6-4 Coefficients in Terms of Coded Factors

Factor	Coefficient Estimate	df	Standard Error	95% CI Low	95% CI High	VIF
Intercept	51.47	1	0.6288	50.07	52.87	
x-Pulp density	-3.12	1	0.5949	-4.44	-1.79	1.02
x^2	3.54	1	0.9667	1.38	5.69	1.02

Table 6-5 presents the fit statistics for the fitted model alongside those for alternative models, enabling a comparative evaluation. The selected model was evaluated using various metrics, including R^2 and *PRESS*. The standard deviation for the quadratic model appears satisfactory, with the objective being to minimize this value.

Table 6-5 Model Summary statistics (Ni Recovery)

Source	Std. Dev.	R^2	Adjusted R^2	Predicted R^2	PRESS	
Linear	2.17	0.4969	0.4512	0.2956	72.69	
Quadratic	**1.49**	**0.7847**	**0.7417**	**0.6687**	**34.19**	**Selected**
Cubic	1.32	0.8488	0.7983	0.7167	29.24	
Quartic	1.40	0.8488	0.7732	0.5152	50.03	
Fifth	1.20	0.9025	0.8328	0.6924	31.74	
Sixth	1.26	0.9082	0.8163	-1.5967	267.97	

The next three columns in the table are different versions of the R^2 statistic, all of which should be maximized. Although the raw R^2 seems to favour the higher-order polynomials (e.g., cubic, quartic), these additional terms were shown to be insignificant based on the sequential model sum of squares (*SMSS*).

There is reasonable agreement between *Adjusted* R^2 and *Predicted* R^2 for the quadratic model i.e., within 0.073 difference of each other. The final column lists the PRESS (Predicted Residual Sum of the Squares) a measure which must be minimized. While Predicted R^2 already accounts for *PRESS*, this metric still serves as a useful overall indicator for model comparison.

PRESS is particularly valuable for assessing the model's relative precision in forecasting future outcomes.

6.4 Statistical Properties of the Model

The next step after selection of a statistically significant model was to diagnose the residuals for abnormalities. A residual represents the difference between an observed value and its corresponding predicted value. Ideally residuals should be independent of each other and distributed according to a normal distribution with constant variance (Montgomery, 2017).

Figure 6-1 illustrates how observed values are processed through statistical analysis to filter out noise. The resulting model is then used to predict values, and the differences between these predicted values and the original observations produce the residuals. These residuals are analysed for patterns that might suggest the presence of factors other than noise. If the residuals appear to consist solely of noise (i.e., no discernible patterns or signals), the analysis is considered complete (Montgomery, 2017).

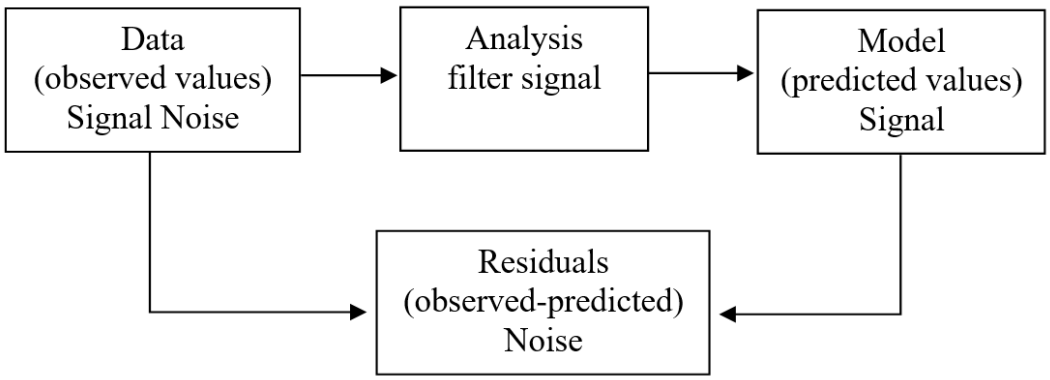


Figure 6-1 Derivation of residuals

6.5 Normal Plot of Residuals

A quick but effective tool for diagnosing residuals is the normal plot of residuals as shown in **Figure 6-2**. In this plot, the residuals align closely with the expected straight line, indicating conformity to a normal distribution.

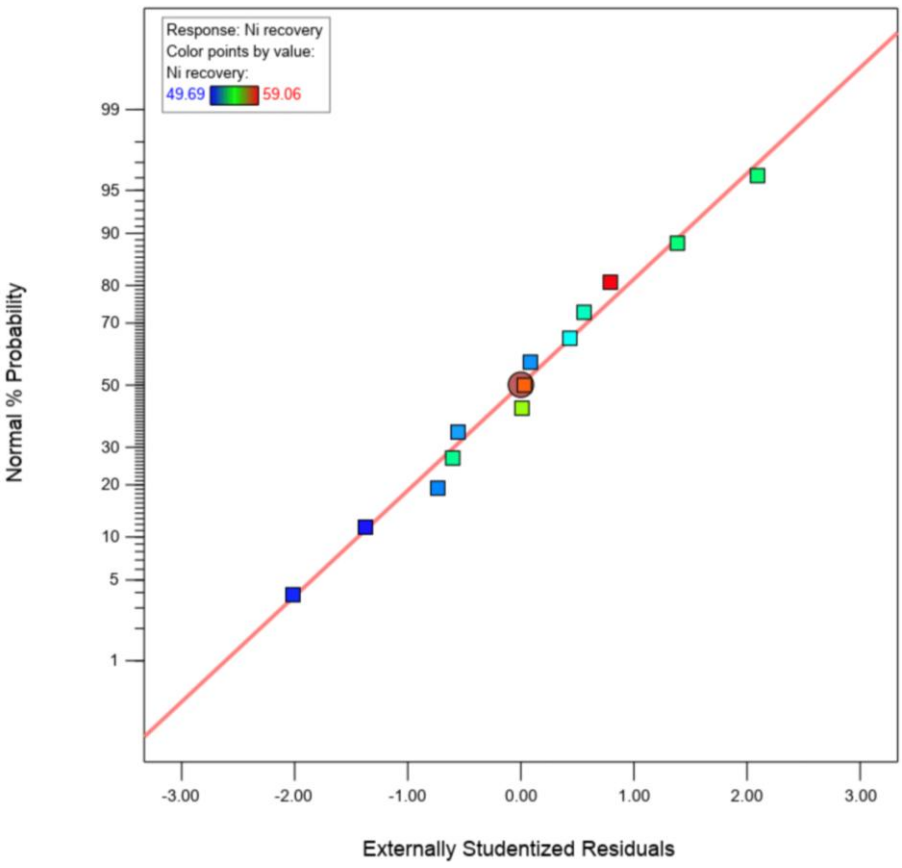


Figure 6-2 Normal plot of residuals for Ni recovery

6.6 Residuals vs Predicted

The Residuals vs Predicted plot (see **Figure 6-3**) was used to test the assumption of constant variance. The plot shows a random scatter, indicating a constant range of residuals across the graph. This confirms that the assumption of constant variance holds true.

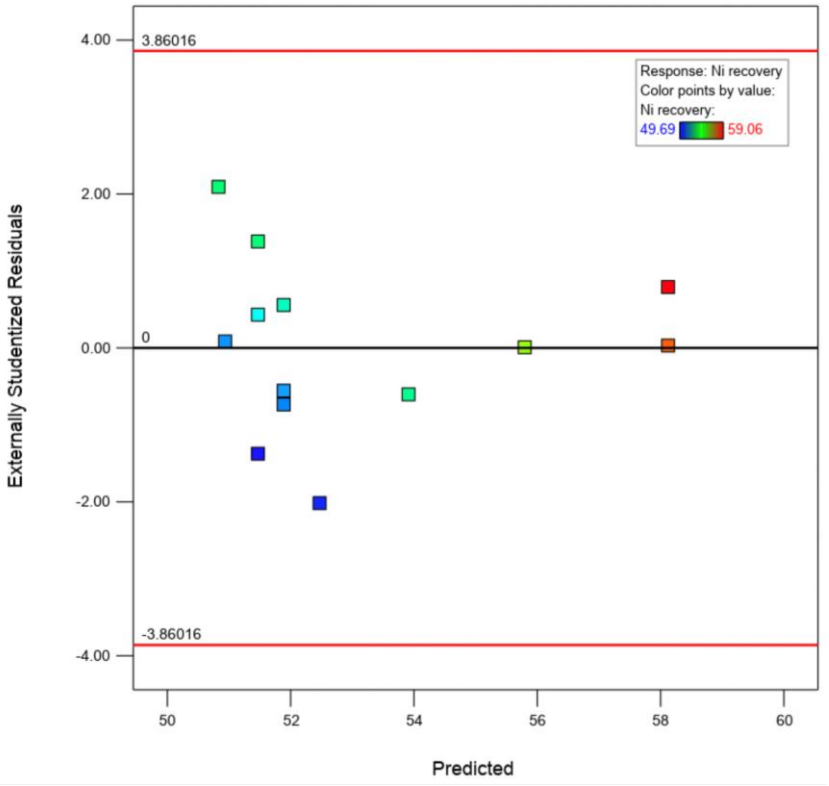


Figure 6-3 Residuals vs Predicted response

The diagnostic plots discussed thus far, combined with ANOVA were sufficient to determine model and abnormalities. Additional diagnostic plots were also generated to detect outliers and influential factor combinations. These included leverage plots, Residuals vs. Run plots, and Predicted vs. Actual plots. All these plots indicated satisfactory model statistics.

6.7 Model Graphs

The DOE data was used to generate a response surface plot to visualize how nickel recovery varied as a function of the pulp density (see **Figure 6-4**). The dotted lines on the plot represent the 95% confidence band on the mean prediction at any given pulp density, providing a measure of the prediction's reliability.

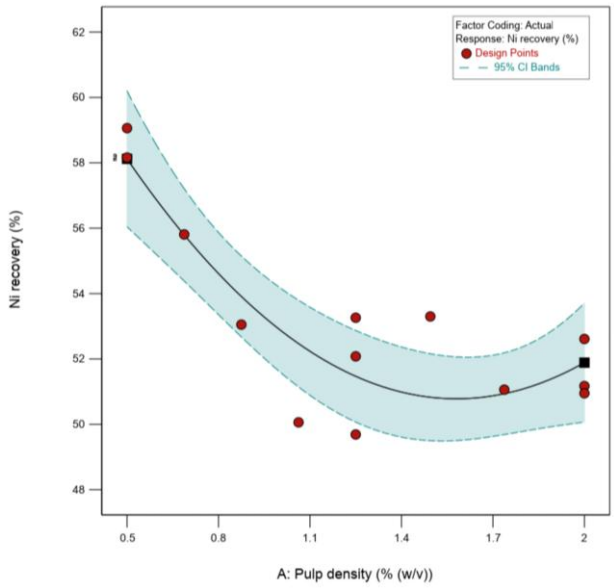


Figure 6-4 Response surface plot for Ni recovery

The Co and Fe recovery data were also analysed and successfully fitted to quadratic models, with the resulting response surface plots shown in **Figure 6-5** and **6-6**, respectively. However, the copper recovery data could not be modelled, as the test statistics and ANOVA showed that all the potential models and associated terms were statistically insignificant.

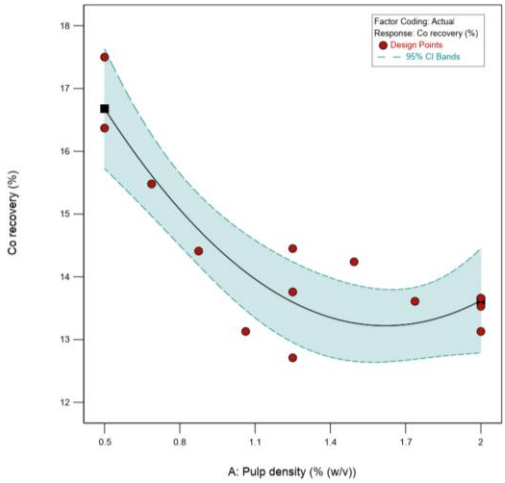


Figure 6-5 Response surface plot for Co recovery

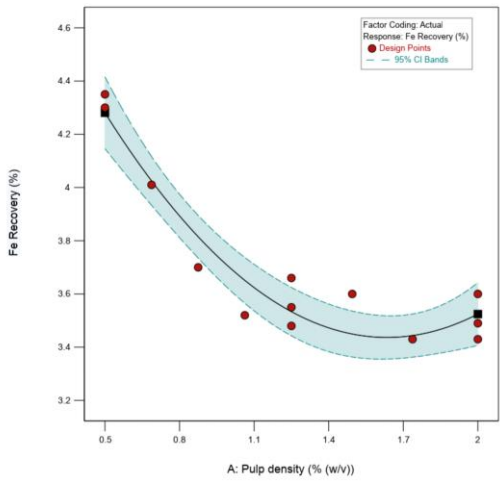


Figure 6-6 Response surface plot for Fe recovery

The experimental data fits the selected models reasonably well as shown in the

figures above. However, it was important to test if an even higher-order model could be applied to the data and if so, determine how it would improve the fit. The evaluation node was used to assess a cubic model and compare it to the quadratic Ni model.

6.8 Comparing Cubic to Quadratic model

The evaluation of the cubic model terms (**Table 6-6**) shows high *VIF* values (>10) for the linear (x) and cubic terms (x^3) and low power. These high *VIF* values are a cause for concern as they indicate coefficients are poorly estimated due to multicollinearity. Additionally, the R_i^2 values are notably high (ideal R_i^2 is close to 0.0), further suggesting strong correlations between terms. This multicollinearity undermines the reliability of the cubic model, resulting in a poor fit.

Table 6-6 Model terms for cubic model

Term	Standard Error*	VIF	R_i^2	Power
x	1.41	12.6671	0.9211	9.8 %
x^2	0.6491	1.01875	0.0184	78.3 %
x^3	1.56	12.6853	0.9212	8.9 %

Another useful plot for evaluating and comparing models is the Fraction of Design Space (FDS), see **Figures 6-7 and 6-8**.

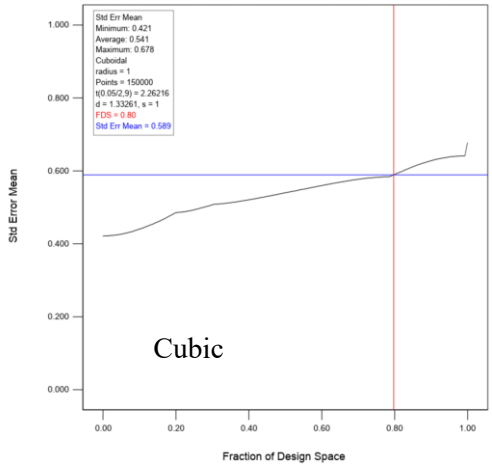


Figure 6-7 FDS plot for cubic model

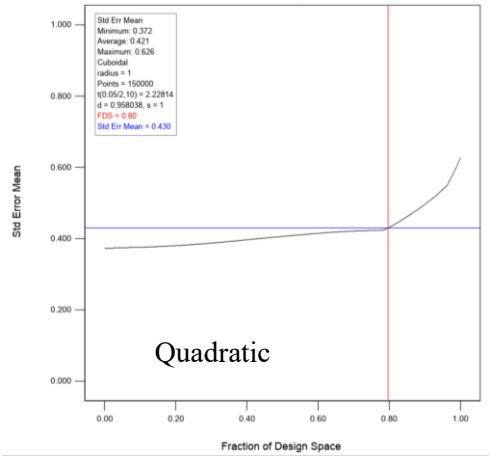


Figure 6-8 FDS plot for quadratic model

The FDS statistics are particularly useful if a design has multilinear constraints, which inflates the VIFs and R_i^2, rendering these metrics ineffective. The FDS graph calculates the volume of the design space where the prediction variance is less than or equal to a specified value. The ratio of this volume to the total volume of the design space is the fraction of design space. Generally, a lower and flatter FDS curve indicates a better model or design.

An FDS score of 0.8 is a commonly used benchmark for assessing experimental designs or models. It represents the point where 80% of the design space has a prediction variance below a specific threshold. Comparing the models (**Figures 6-7 and 6-8**), the cubic model exhibits a higher standard error mean (0.589) at the 0.8 FDS line compared to the quadratic model (0.430). This indicates that 80% of the design space is predicted with greater error using the cubic model, despite its increased complexity. As a result, the cubic term does not significantly enhance predictions and instead reduces accuracy in most of the design space.

6.9 Standard Error of Design

The Standard Error of Design (SED) plot for the quadratic model (see **Figure 6-9**) was used to visualize how the precision of the estimated nickel recovery changes as the levels of pulp density are varied. The SED varies moderately across the experimental runs from 0.373 up to 0.626. Pulp density levels between 0.85% and 1.7% (w/v) exhibit minimal variability, indicating the highest reliability in predictions within this range.

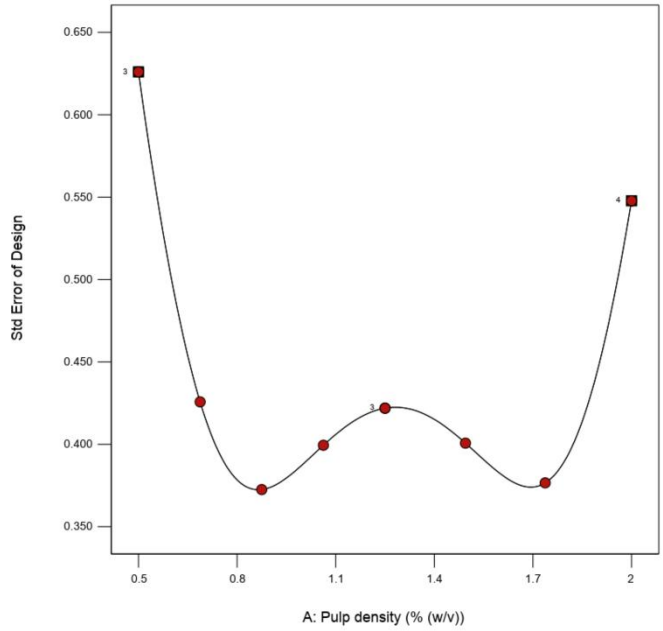


Figure 6-9 Standard error of design for quadratic model

6.10 Determination of Optimum Conditions

The previous sections were critical in evaluating the suitability of the fitted model for navigating the region specified by the design matrix coordinates. With the quadratic model deemed adequate, it can now be employed to identify the point of maximum nickel recovery. The generic quadratic response model for k factors is expressed as follows (Hottinger Bruel & Kjaer Inc, 2024).

$$\hat{y} = \hat{\beta} + \sum_{i=1}^{k} \hat{\beta}_i \, x_i + \sum_{i=1}^{k} \hat{\beta}_{ii} \, x_i^2 + \sum_{i=1}^{k} \sum_{j-1}^{i-1} \hat{\beta}_{ij} \, x_i x_j \qquad \textbf{(6.3)}$$

By taking partial derivatives of the response ($\partial\hat{y}/\partial x_1$, $\partial\hat{y}/\partial x_2$,… $\partial\hat{y}/\partial x_k$) and setting them to zero we can calculate a stationary point which also happens to be the optimal response value. At the stationary point, the response could either be maximized, minimized, or result in a saddle point (Hottinger Bruel & Kjaer Inc, 2024).

For two-factor experiments, these points can often be identified visually using contour plots. However, in experiments involving more than two factors and multiple responses, a general mathematical or numerical approach is required to locate the stationary point. Hence in this study numerical optimization was used for locating the point at which Nickel recovery was optimum.

6.11 Numerical Optimization

The leaching process has thus far been established to be selective towards nickel recovery. Therefore, optimization efforts were focused on maximizing nickel recovery while minimizing the co-dissolution of other elements. This is particularly important because the co-dissolution of metallic elements, especially iron (Fe), can complicate downstream purification processes. Numerical optimization was selected for finding the "sweet spot" that addresses these competing objectives. The potential optimization goals included maximizing, minimizing, targeting a specific value, maintaining within a range (for responses only), or setting an exact value (for factors only).

The Design-Expert software utilizes a statistical method rooted in chemical engineering process optimization, known as the "desirability function," to evaluate numerous responses. To identify the optimal combination of responses, the software employs an objective function, *D(x),* which uses a multiplicative mean instead of an additive one. Statisticians refer to this as the geometric mean. The desirability function is mathematically expressed as follows (Montgomery, 2017):

$$D = (d_1 \times d_2 \times \ldots \times d_n)^{1/n} = \left(\prod_{i=1}^{n} d_i\right)^{1/n} \quad \textbf{(6.4)}$$

The individual desirability (d_i), varying from 0 (least desirable) to 1 (most desirable), signifies the desirability of each specific response (i), while n denotes the total number of responses being optimized. This approach is straightforward: all criteria are converted into a common scale of desirability (d_i) to facilitate their combination into a single, easily optimized overall desirability value (D) (Montgomery, 2017).

The overall desirability can be visualized with contour plots or three-dimensional surface plots utilizing similar tools applied in response surface methodology (RSM) for single responses. By leveraging numerical optimization tools, we can look for the highest D, optimizing responses as well as factors. Typically, factors are allowed to vary freely within their experimental ranges.

An ideal outcome would result in $D = 1$, indicating all goals have been met. However, overly stringent desirability criteria may yield an overall desirability of zero. As a general guideline, it is advisable to set objectives only for the most important responses initially, gradually incorporate less significant responses, and finally start assigning goals to the factors.

The following steps and criteria were set to find the optimal solution for the leaching process

1. Maximize nickel recovery (see **Figure 6-10**)
2. Maximize nickel recovery and minimize iron or cobalt recovery

Copper recovery was excluded from the optimisation process as its data could not be accurately fitted by any model.

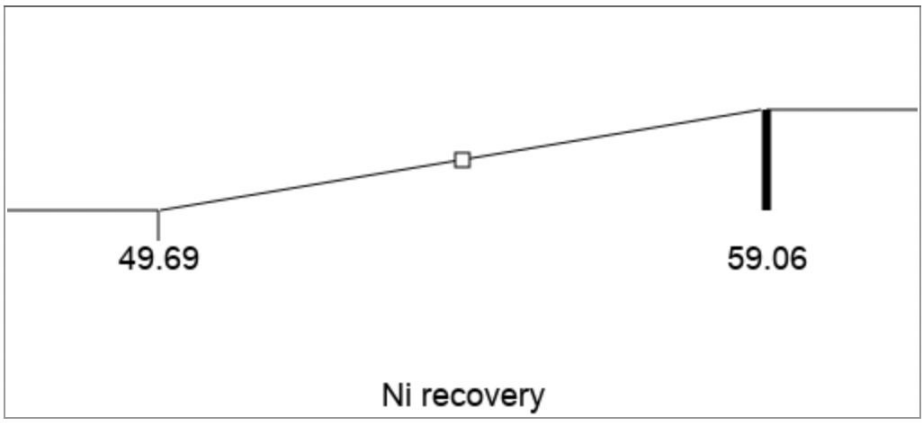


Figure 6-10 Goal is to maximize nickel recovery within the range

The program uses an algorithm called "simplex optimization" which works together with desirability functions for handling multiple responses from RSM experiments. Using this approach, the algorithm generated two solutions for criteria (1), achieving nickel recoveries of 51.8% and 58.12%, respectively. **Figures 6-11** and **6-12** illustrate the optimal solution, which resulted in a desirability score of 0.9.

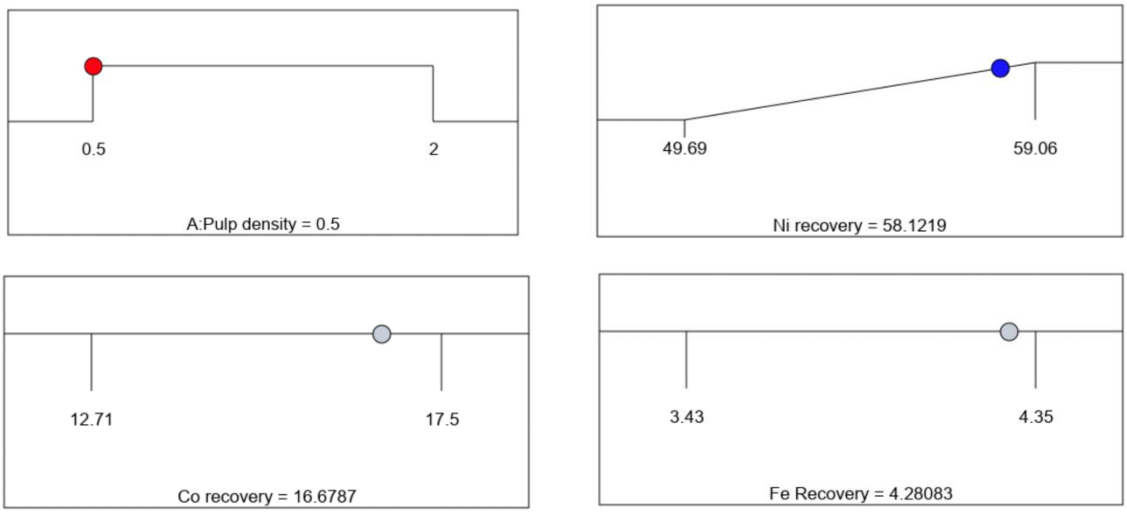


Figure 6-11 Solution to Ni recovery maximization via numerical optimization

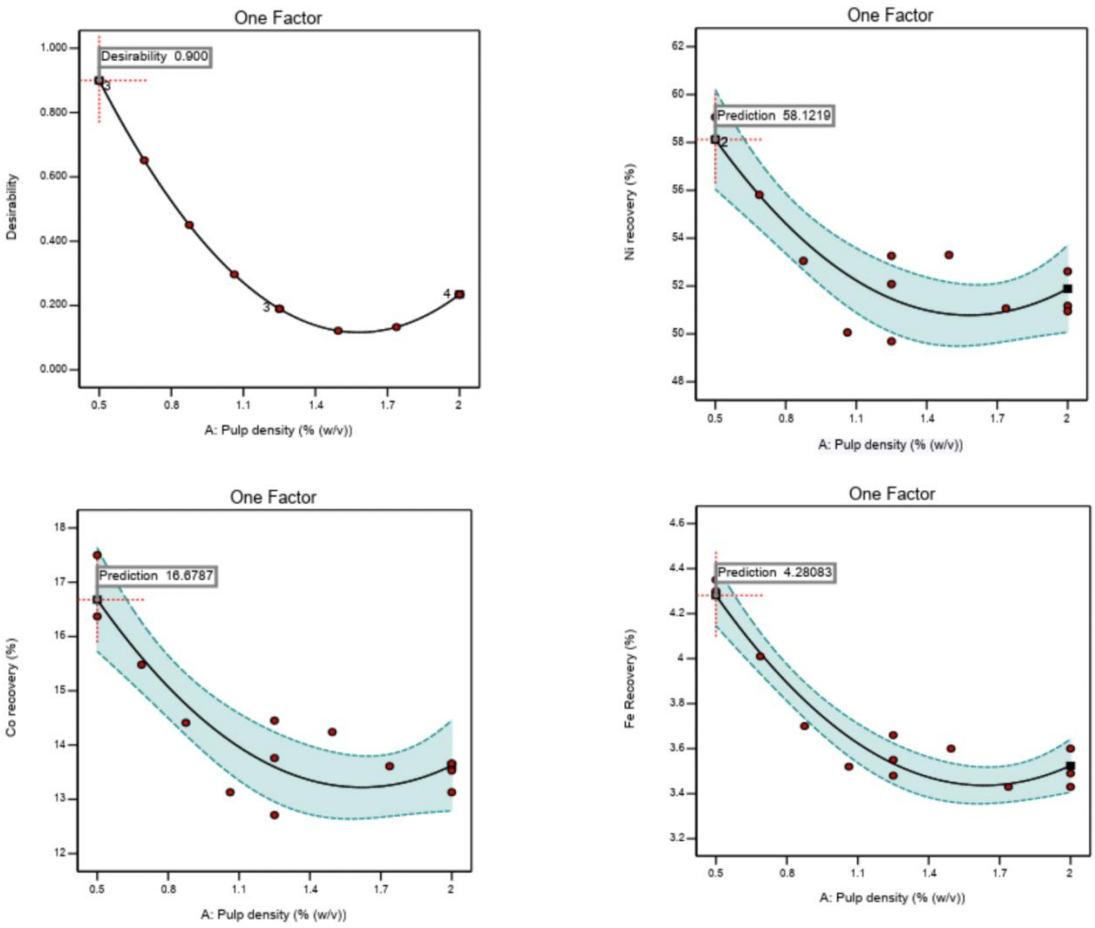


Figure 6-12 Numerical optimization graphs indicating the predicted responses and factor levels

The algorithm generated three solutions for criteria (2) with nickel recoveries of 54.19%, 54.10% and 51.89% respectively. The optimal solution with a desirability of 0.513 predicted recoveries of 54.19% Ni, 14.89% Co and 3.85% Fe at a pulp density 0.84%. However, minimizing iron and cobalt recovery comes at a cost of reduced nickel recovery, a trade-off that might require a cost-benefit analysis considering the relatively lower desirability score.

6.12 Response Prediction and Confirmation

To check the validity of the optimized settings predicted by the model in **section 6.6**, replicated experiments (n=2) were performed with the settings recommended

by the model. The conditions used in the confirmatory experiments were as follows; temperature (25°C), leaching time (1 hour), stirring rate (600 rpm) and pulp density (0.5 %w/v).

The nickel extraction under these conditions was 58.16% and 59.06% respectively which is consistent with the model prediction of 58.12%. From **Table 6-7** we can see that the experimental data mean for Ni recovery (58.61%) falls within the prediction interval range (PI) of 54.99% - 61.26%, which shows the model is confirmed.

Table 6-7 Confirmation of Ni recovery at optimum leaching conditions

Analysis	Predicted Mean%	Predicted Median%	Std Dev	n	SE Pred	95% PI low	Data Mean%	95% PI high
Ni recovery	58.1219	58.1219	1.49045	2	1.40759	54.986	58.61	61.2582
Co recovery	16.6787	16.6787	0.683212	2	0.645229	15.241	16.94	18.1164
Fe Recovery	4.28083	4.28083	0.0967354	2	0.091357	4.0773	4.325	4.48439

Practical Implications and Commercial Feasibility

The optimized extraction parameters identified in this study, while demonstrating significant improvements in extraction efficiency, require careful consideration of their practical implications for commercial application. Notably, the optimal pulp density of 0.5% presents a substantial challenge for scale-up.

Working with such a low pulp density on a commercial scale would necessitate processing extremely large volumes of liquid to recover a relatively small amount of target material. This would lead to significant increases in equipment size and associated capital costs. For instance, the required tankage, pumps, and filtration systems would need to be substantially larger than those used in conventional processes with higher pulp densities.

Furthermore, the energy consumption associated with handling and processing such large volumes of dilute solutions would be considerable, impacting operational costs and environmental sustainability. Pumping, mixing, and potentially heating these volumes would result in a high energy demand.

The high solvent usage associated with a 0.5% pulp density also raises concerns about waste treatment and environmental impact. Effective solvent recycling and treatment strategies would be crucial, adding to the overall cost of the process. In addition, the separation and concentration of the desired product from such a dilute solution would require advanced and potentially expensive separation technologies. To mitigate these challenges, potential alternative approaches should be explored. Modifying the extraction process to achieve comparable extraction efficiencies at higher pulp densities would be beneficial.

From an economic perspective, a thorough cost-benefit analysis is essential. The increased capital and operational costs associated with handling large volumes of dilute solutions must be weighed against the benefits of the enhanced extraction efficiency. Comparison with industry standards and benchmarks is crucial. Many industrial extraction processes operate at significantly higher pulp densities, reflecting the need for practical and cost-effective solutions. Therefore, the results of this study are most likely relevant to niche applications where high extraction rates are critical, even at the cost of increased operational complexity and cost.

6.13 Summary

This study successfully optimized the leaching process for recovering nickel from a base metal sulphide flotation concentrate using ethaline as a leaching solvent. A two-level custom I-optimal response surface design was employed to investigate the effect of pulp density, on metal recovery.

The results indicated that pulp density was a significant factor influencing metal recovery, with lower pulp densities generally leading to higher nickel recovery. Numerical optimization was utilized to determine the optimal conditions for maximizing nickel recovery while minimizing the co-dissolution of iron and cobalt. The optimal conditions identified were a pulp

density of 0.5%, resulting in a predicted nickel recovery of 58.12% with reasonably lower recoveries of cobalt (16.68%) and iron (4.28%), see **Table 6-8**.

Table 6-8 Final optimum leaching conditions

Pulp density Leaching time Stirring rate Temperature	0.5 %w/v 1 hour 600 rpm 25 ℃
Predicted Ni recovery	58.12 %
Confirmed Ni recovery	58.16 % and 59.06 %
Predictive model	$Ni\ recovery = 66.48450 - 19.86747 * Pulp\ density + 6.28452 * Pulp\ density^2$

CHAPTER SEVEN

KINETIC STUDY

7.1 Introduction

Kinetic studies play a pivotal role in understanding the mechanisms that govern chemical reaction processes, providing insights into the factors that influence reaction rates and control reaction progression. These studies are essential for identifying whether a reaction is limited by diffusion, chemical interaction, or other transport phenomena. Researchers often rely on mathematical tools, such as rate laws and concentration tracking, to interpret reaction behaviour and predict the dominant steps in a reaction pathway (Vallance, 2008).

In fluid-solid systems, mathematical models are frequently employed to analyse experimental data and uncover details about reaction mechanisms. One such widely used model is the Shrinking Core Model (SCM), which provides a framework for understanding reactions where solid particles react with a surrounding fluid (Dong, Mazzarino and Alexiadis, 2021). This model is particularly useful in the study of metal leaching from minerals and metal-rich materials, where the dissolution of the solid material is a key step in the process (Bruce *et al*, 2024). By assuming that the solid particle is spherical and undergoes an isothermal reaction with the fluid, the SCM simplifies the complex interactions between the fluid and the solid. Additionally, it assumes that the fluid's concentration remains constant or is present in excess, ensuring that the reaction rate is not limited by the availability of the leaching agent (Levenspiel, 1999). These assumptions make the SCM especially relevant to the current study, where ethaline, a novel eutectic mixture, was used as the lixiviant in leaching experiments.

The application of the SCM is closely tied to the concept of reaction control mechanisms, which are often characterized by the system’s activation energy.

Activation energy which is defined as the least amount of energy needed to initiate a reaction, serves as a diagnostic tool to distinguish between diffusion-controlled and chemically controlled processes. Typically, diffusion-controlled processes exhibit lower activation energies compared to those governed by chemical reactions. Understanding the activation energy for a given system not only reveals which steps are most sensitive to changes in temperature but also provides deeper insights into the dominant reaction pathways (Fogler, 2016). For this reason, determining activation energies was a key focus of this investigation.

This chapter presents the kinetic analysis of the leaching of nickel, copper, and cobalt from a sulphide concentrate using ethaline as the lixiviant. The primary objective was to develop conceptual kinetic models that explain the observed reaction behaviour and underlying mechanisms. These models were informed by kinetic experiments designed to systematically analyse reaction rates under controlled conditions. The parameter settings used in this investigation were carefully selected based on insights from literature and screening experiments. The results presented in this chapter aim to deepen our understanding of the leaching kinetics and provide a foundation for optimizing future leaching processes.

7.2 Extraction Profiles

The extraction profiles presented focus on the effect of temperature on metal dissolution, as it is a key parameter influencing reaction kinetics. The extent of metal dissolution was observed at five different temperatures (25℃, 40℃, 60℃, 90℃, and 100℃) over time by monitoring the metal concentration in solution. These concentrations were converted into recovery percentages and plotted against time (**Figures 7-1** to **7-3**). Prior screening and optimization studies confirmed that among other potential factors, only pulp density significantly affected metal recovery. Hence, for this study, pulp density and other factors were maintained constant to isolate the temperature effect, ensuring a focused analysis of its impact on dissolution behaviour.

7.2.1 Nickel Dissolution

Nickel recovery at different temperatures is shown in **Figure 7-1**. At 25°C, Ni recovery after 2 hours reached approximately 50%, then plateaued. Similar behaviour was observed at 40°C, with slightly higher recoveries (~50%). Increasing the temperature to 60°C did not improve results, instead recoveries were comparable to or slightly below those at 25°C.

Pentlandite leaching in conventional sulphate and chloride media follows an electrochemical process, where iron is preferentially removed, leaving behind a skeletal sulphur-rich passivating layer that slows down the oxidative dissolution of metal species. Lu et al., (2000) demonstrated that temperature increase enhanced pentlandite leaching in mixed sulphate-chloride solutions up to 85°C, beyond which the process became diffusion-controlled with minimal rate increase. In contrast, DES leaching at 90°C and 100°C (**Figure 7-1**) shows initial nickel recoveries of 54.97% and 46.19%, respectively, which subsequently declined sharply to 40% and 24%. This drop could be attributed to solvent instability or reprecipitation of nickel due to the breakdown of the solvent at elevated temperatures.

It has been reported that DESs may lose their special properties, such as enhanced solubility and transport, when exposed to temperatures above 80°C, resulting in slower dissolution or possible metal reprecipitation (Delgado-Mellado *et al.*, 2018). Further investigations into solvent composition and secondary reactions (e.g., nickel complex formation or adsorption onto solid residues) could provide deeper insights into these phenomena.

The lack of consistent improvement in recovery as temperature increases suggests a potential threshold beyond which temperature becomes detrimental, highlighting the need for careful thermal optimization during nickel leaching.

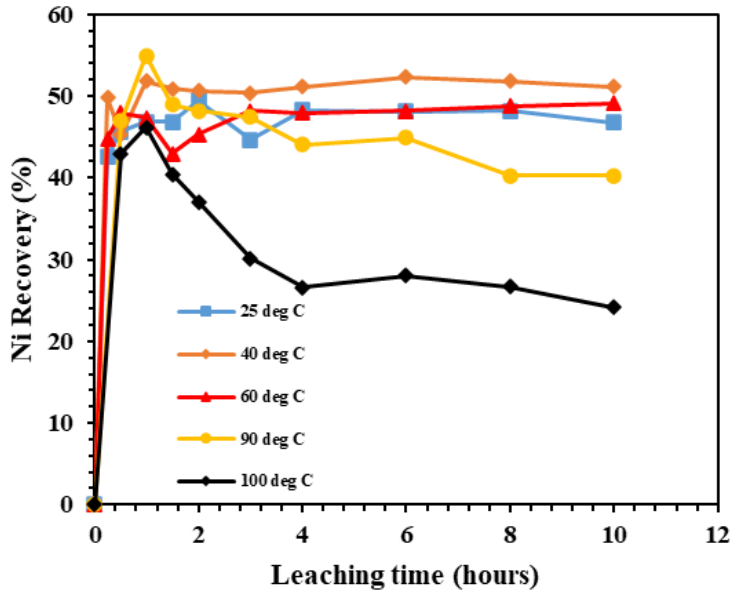


Figure 7-1 Nickel (pentlandite) dissolution from a Cu-Ni sulphide ore concentrate in terms of recovery at different temperatures

7.2.2 Cobalt Dissolution

Figure 7-2 illustrates cobalt recovery at different temperatures. Cobalt recovery was consistently low compared to nickel, peaking at 16%. Cobalt occured primarily in solid solution within pentlandite, making its recovery dependent on the efficiency of pentlandite dissolution (Mulaba -Bafubiandi and Medupe, 2007). This dependence on a specific host mineral may explain its limited recovery.

Similar to nickel, cobalt recovery peaked within the first 1–2 hours and plateaued thereafter. Interestingly, at elevated temperatures (90°C and 100°C), cobalt recovery did not exhibit a significant decline over time, suggesting greater thermal stability of the cobalt-bearing solvent system compared to that for nickel. If solvent decomposition were the primary cause of decline in nickel recovery, it would affect the overall recovery of all metals dissolved in the solvent. However, the stability of cobalt recovery at high temperatures suggests that solvent decomposition alone may not fully explain the observed decline in nickel recovery. Changes in solvent composition (e.g., using techniques like FTIR and TGA) at high temperatures need to be monitored to confirm these prior assumptions.

If nickel reprecipitation is the dominant mechanism, it could explain why cobalt remains stable while nickel declines. Checking for Ni precipitates on residual solids by XRD and SEM-EDS is recommended for future studies.

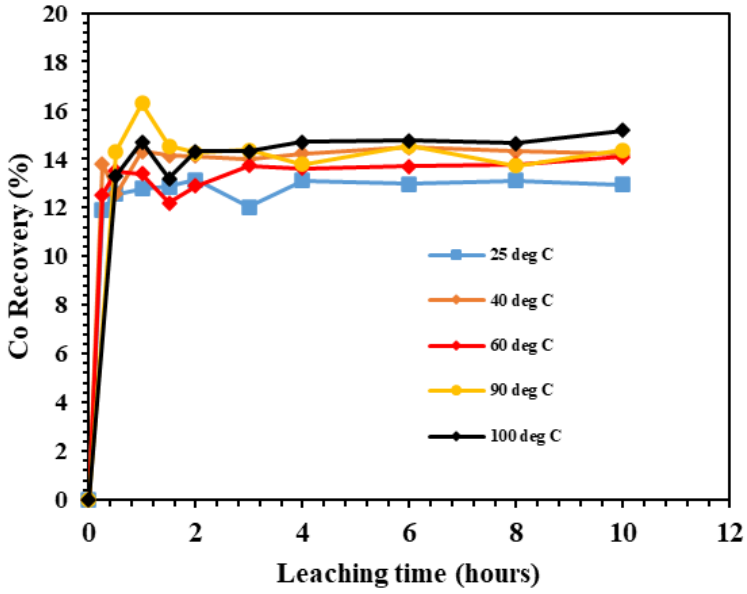


Figure 7-2 Cobalt (pentlandite inclusion) dissolution from a Cu-Ni sulphide ore concentrate in terms of recovery at different temperatures

7.2.3 Copper Dissolution

Copper recovery, depicted in **Figure 7-3**, was significantly lower than that of nickel and cobalt, peaking at 6.4%. At elevated temperatures (90°C and 100°C), copper was undetectable in solution, as indicated by the absence of isotherms in **Figure 7-3**. This under-ranging at high temperatures suggests that copper dissolution could be highly temperature-sensitive, potentially due to copper's low solubility in the DES or its precipitation at elevated temperatures.

Interestingly, copper's behaviour does not align with findings by Carlesi et al., (2022), who reported that copper recovery from chalcopyrite concentrates (72% chalcopyrite, 0.57% bornite,3.5% tennantite and 9.99% pyrite) in ethaline peaked near 16% at 90°C.

These authors also noted that copper recovery could exceed 60% when the solid-liquid ratio was significantly reduced. In the present study, the lower copper recovery and its absence at high temperatures suggest an opportunity to optimize conditions for selective recovery of nickel in the presence of copper. For example, by operating at higher temperatures we could produce copper-free nickel solutions, thereby simplifying downstream processing.

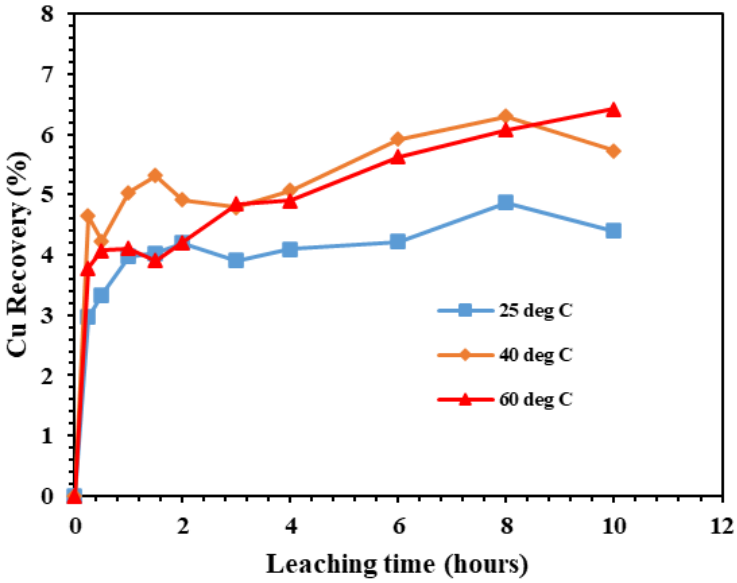


Figure 7-3 Copper (chalcopyrite) dissolution from a Cu-Ni sulphide ore concentrate in terms of recovery at different temperatures

The sections that follow focus on fitting the shrinking core model (SCM) to the leaching data.

7.3 SCM rate controlling mechanisms

The analysis of nickel (Ni) dissolution rates from sulphide concentrate was conducted using the SCM with the assumption that the concentrate comprises of homogeneous solid particles reacting isothermally with the lixiviant. The SCM was selected due to its common application in modelling heterogeneous reactions involving fluid-solid systems (Levenspiel, 1999).

7.3.1 Modelling Framework and Assumptions

The SCM describes dissolution processes using three potential rate-controlling mechanisms:

1. **Film Diffusion Control**: The rate is governed by mass transfer through a fluid film surrounding the particle.

$$x = kt \quad \textbf{7.1}$$

2. **Chemical Reaction Control**: The overall rate is governed by the reaction rate at the particle surface.

$$1 - (1 - x)^{1/3} = kt \quad \textbf{7.2}$$

3. **Product Layer (Ash) Diffusion Control**: The accumulation of insoluble products around the particle slows the reaction.

$$1 - 3(1 - x)^{2/3} + 2(1 - x) = kt \quad \textbf{7.3}$$

4. **Mixed Control**: A fourth equation is often used for situations where there is overlapping mechanisms i.e., surface reactions and mass transfer equally dominate.

$$1 - (1 - x)^{2/3} = kt \quad \textbf{7.4}$$

Here, x is the conversion (fraction of metal recovered), t is time (s), and k is the reaction rate constant (s^{-1}). These equations assume isothermal conditions, uniform particle size, and negligible effects of particle surface irregularities (Saldaña *et al.*, 2022). However, in real systems, deviations from these assumptions can affect the model's applicability.

7.3.2 Experimental Conditions

Kinetic experiments were conducted with ethaline (a 1:2 molar ratio of choline chloride: ethylene glycol) as the lixiviant, a stirring rate of 300 rpm, and a pulp density of 2% w/v. Dissolution rates of Ni, Cu, and Co were studied across three temperatures: 25°C, 40°C, and 60°C, to evaluate temperature dependence and establish the dominant rate-controlling mechanism.

7.3.3 Results and Analysis

To interpret the leaching kinetics, the shrinking core model was applied, considering the following possible rate-controlling steps: diffusion, surface reaction and mixed control. The experimental data was fitted to these models at different temperatures, to identify a possible dominant leaching mechanism for each metal. The coefficient of determination (R^2) values were used to assess the quality of model fitting. **Table 7-1** summarizes the R^2 values for each metal and model.

Table 7-1 R-squared values for SCM fits

Metal	Temperature (°C)	Film Diffusion (R^2)	Surface Reaction (R^2)	Product Layer Diffusion (R^2)	Mixed Control (R^2)
Nickel	25	0.1539	0.1516	0.1477	0.1528
	40	0.2305	0.2341	0.2934	0.2323
	60	0.4156	0.4229	0.4351	0.4193
Cobalt	25	0.2209	0.2211	0.2229	0.221
	40	0.221	0.2215	0.227	0.2212
	60	0.4793	0.4807	0.4949	0.48
Copper	25	0.5824	0.5832	0.6097	0.5828
	40	0.6797	0.68	0.6853	0.6799
	60	0.9702	0.9707	0.9803	0.9705

Cobalt Leaching Kinetics

The cobalt leaching R^2 values were relatively low across all models, particularly at lower temperatures. At 25°C, the highest R^2 was only 0.2209 (Film Diffusion), indicating poor model fit. As temperature increased to 40°C and 60°C, the R^2 values improved slightly, product layer diffusion showing the best fit (R^2 = 0.4949). However, no single mechanism dominates, suggesting that cobalt leaching may be governed by a combination of rate-controlling steps rather than a single SCM mechanism. The cobalt mixed control graphs are shown below (**Figure 7-4**). Nonetheless the data does not adequately fit a straight line as required by the linearized models. As such the cobalt data was fitted to a shrinking particle model coupled with pseudo second order kinetics (SPM-PSO) (**see section 7.4**)

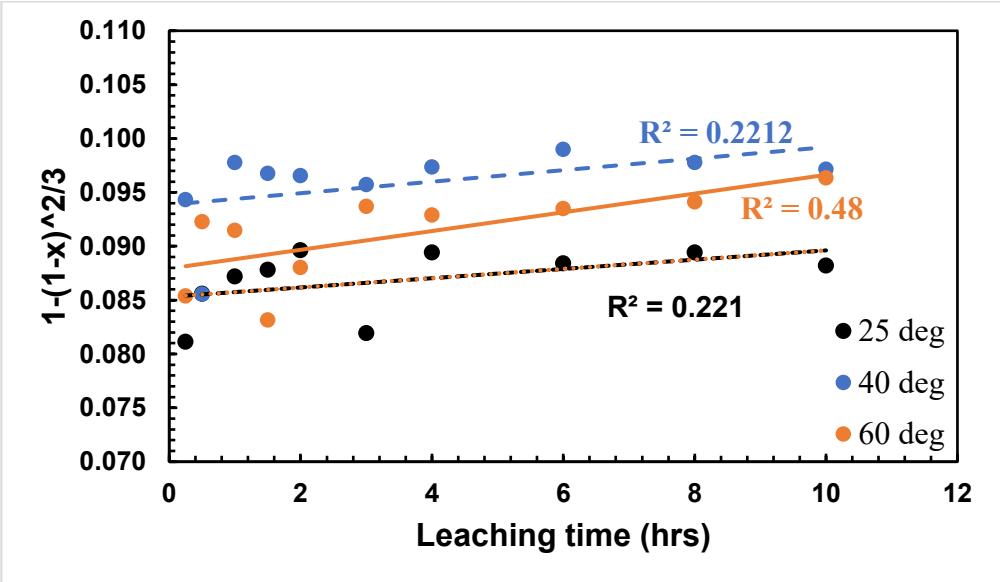


Figure 7-4 Plots of $1-(1-x)^{2/3}$ vs time for Co Dissolution at 25℃ to 60 ℃

Copper Leaching Kinetics

In contrast to nickel and cobalt, copper leaching exhibits a significantly better fit to SCM models, particularly at higher temperatures. At 25°C, the highest R^2 is 0.6097 (Product Layer Diffusion), already indicating a reasonable correlation. As

temperature increases, model fit improves further, with R^2 values exceeding 0.97 at 60°C across all models. The highest R^2 (0.9803) is observed for product layer diffusion (**see Figure 7-5**), suggesting that at elevated temperatures, copper leaching is predominantly controlled by diffusion through the solid product layer, though mixed control (R^2 = 0.9705) cannot be ruled out (**see Figure 7-6**).

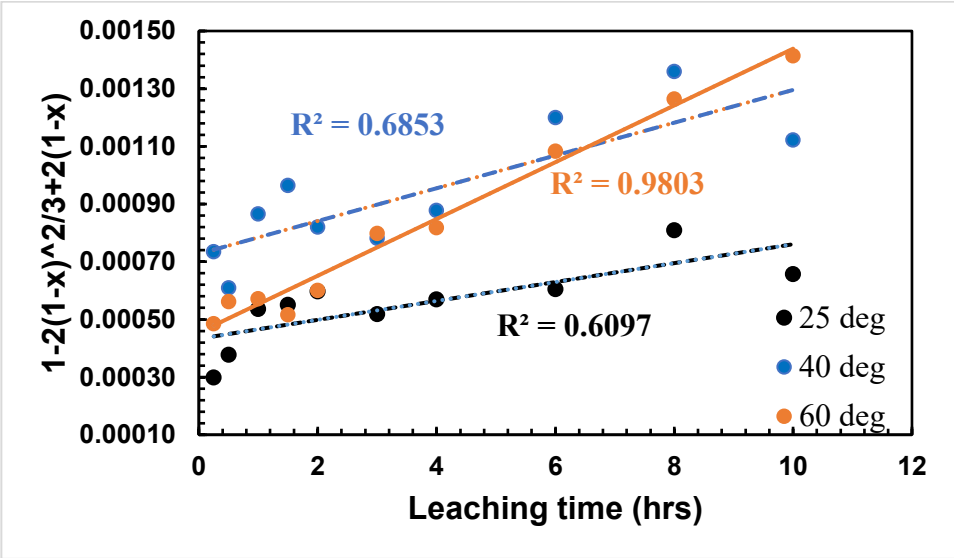


Figure 7-5 Plot of $1 - 3(1-x)^{2/3} + 2(1-x)$ vs time for Cu Dissolution at 25℃ to 60 ℃

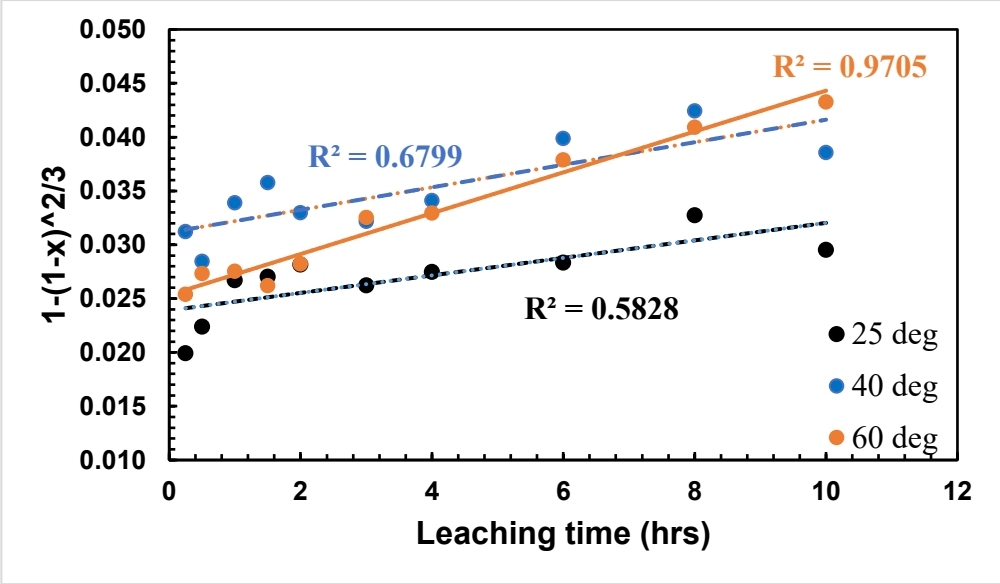


Figure 7-6 Plot of $1 - (1-x)^{1/3}$ vs time for Cu Dissolution at 25℃ - 60℃

Nickel Leaching kinetics

The kinetic analysis of nickel leaching revealed a generally poor fit to the SCM, particularly at lower temperatures. At 25°C, the highest R^2 value was only 0.1539 for the film diffusion model, indicating that none of the traditional SCM mechanisms adequately described the leaching process. This suggests that nickel dissolution at low temperatures may not be governed by a single rate-limiting step but rather by a more complex reaction mechanism. As the temperature increased to 40°C, the R^2 values improved slightly, with the best correlation observed for product layer diffusion (R^2 = 0.2934), though the overall fit remained weak. At 60°C, the highest R^2 was 0.4351 for the product layer diffusion model, followed closely by the surface reaction model (R^2 = 0.4229), suggesting that as temperature increases, the model becomes more predictable and may shift towards a surface reaction or diffusion-controlled mechanism. However, the lack of a single dominant model across all temperatures indicates that nickel leaching is likely governed by mixed control, where multiple rate-limiting steps contribute to the overall kinetics, see **Figure.7-7**

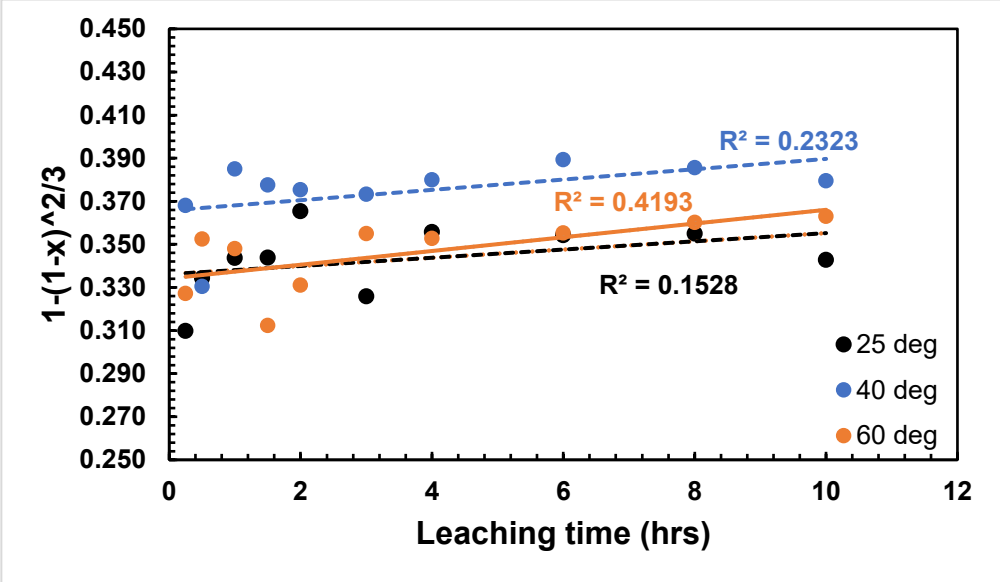


Figure 7-7 Plot of $1-(1-x)^{2/3}$ vs time for Ni Dissolution at 25℃ - 60℃

Similar to cobalt kinetics the nickel data does not adequately fit a straight line as required by the linearized models. As such it was fitted to a SPM-PSO (see **section 7.4**)

7.3.4 Discussion

The low R-squared values for the Ni and Co dissolution across all temperatures indicate that the SCM, as applied here, does not accurately capture the rate-controlling mechanisms. Several factors could explain this discrepancy. The assumption of homogeneous, isothermal particles may not hold due to surface irregularities, agglomeration, or non-uniform heat transfer. The dissolution process may involve overlapping mechanisms (e.g., diffusion and chemical reaction control) that are not captured by the simplified SCM equations (Dong, Mazzarino and Alexiadis, 2021). However, fitting the data to a mixed control model did not improve the R-squared values (see **table 7-1** and **Figure 7-7)**.

It is also possible that variations in particle size could lead to non-uniform reaction rates, further complicating the kinetic behaviour. The slight improvement in R-squared values at higher temperatures across the different regimes suggests that elevated temperatures enhance reaction kinetics up to a certain point (<60℃), likely by increasing the diffusivity of species or decreasing the activation energy of the surface reaction. However, these improvements were insufficient to conclusively identify the rate-controlling step.

The stark contrast in copper's dissolution behaviour is evident. The high R^2 values, especially at 60°C, suggest that the dissolution process is well-described by all three models, indicating a possible mixed-control mechanism. This implies that the dissolution rate is influenced by a combination of film diffusion, surface reaction, and product layer diffusion, rather than a single rate-limiting step.

The significant increase in R^2 values with temperature for copper suggests that temperature strongly influences the kinetics of all three processes. The near-unity R^2 values at 60°C indicate that all three mechanisms may be contributing substantially to the overall dissolution rate at this temperature.

Understanding the kinetics of Ni and Co dissolution is critical for optimizing leaching processes in hydrometallurgy. The poor fit to the SCM suggests that potential industrial processes relying on similar assumptions may not achieve optimal efficiency. Future studies should consider using alternative kinetic models, such as empirical approaches, to better describe the system. Particle properties need to be investigated further by employing techniques such as SEM and XRD to examine particle morphology and verify assumptions of homogeneity.

The following sections explored an alternative kinetic model followed up by the Arrhenius equation to calculate activation energies and determine or verify the rate controlling regime.

7.4 Shrinking Particle Model Coupled with Pseudo-Second-Order Kinetics

The generic kinetic models commonly used to describe metallurgical leaching processes were found to be inadequate in fitting the dissolution kinetic data presented in **Section 7.2**. Models that include power law kinetics, 0 to 3rd order chemical-controlled kinetics, one-to-three-dimensional diffusion-controlled kinetics, contracting area/volume models, and nucleation models (e.g. Avrami–Erofeyev or Prout–Tompkins) have shown limitations when applied to similar systems (Khawam and Flanagan, 2006; Carlesi et al., 2022).

Recent studies have demonstrated that models incorporating a logarithmic time function (see **Equation 7.4**) are better suited for fitting data of this nature, especially in systems where solute concentration and diffusion dynamics evolve significantly over time (Cao *et al.*, 2006).

$$\left(1-(1-\alpha)^{1/3}\right)^2 = k\ln(t) \quad \textbf{(7.4)}$$

Here, α represents the converted fraction. Cao et al., (2006) attributed the logarithmic term to a variable diffusion coefficient inversely related to time, caused by the effect of solute concentration on solution viscosity, particularly in non-agitated systems. Although this offers an empirical basis for the model, the physical justification remains incomplete. Addressing this limitation requires further investigation into the interplay between diffusion, viscosity, and solute concentration.

To improve the representation of the dissolution process, a hybrid model combining the shrinking particle concept with pseudo-second-order kinetics (SPM-PSO) was developed. This model accounts for the pseudo second order increase in the concentration of metallic chloride complexes in the solvent while incorporating saturation constraints (Kumar, Khaddour and Gupta, 2010). The model is expressed in its nonlinear and linearized forms as **Equations (7.5)** and **(7.6),** respectively:

$$\frac{1}{(\alpha_s-\alpha)}-\frac{1}{\alpha_s}=kt \quad \textbf{(7.5)}$$

$$\frac{1}{\alpha}=\frac{1}{\alpha_S}+\left[\frac{1}{k\alpha_s}\right]\frac{1}{t} \quad \textbf{(7.6)}$$

In these equations, α_s denotes the maximum achievable conversion fraction at saturation, and *k* represents the apparent kinetic constant. A detailed derivation of the model, including assumptions and explanation of *k* are provided in **Appendix C** and Carlesi et al. (2022). The linearized form enables regression analysis for parameter estimation.

7.5 Results and Discussion

Cobalt kinetics

The kinetic data for cobalt was fitted to the proposed SPM-PSO model in the temperature range 25-60℃, see **figure 7-8 and 7-9**

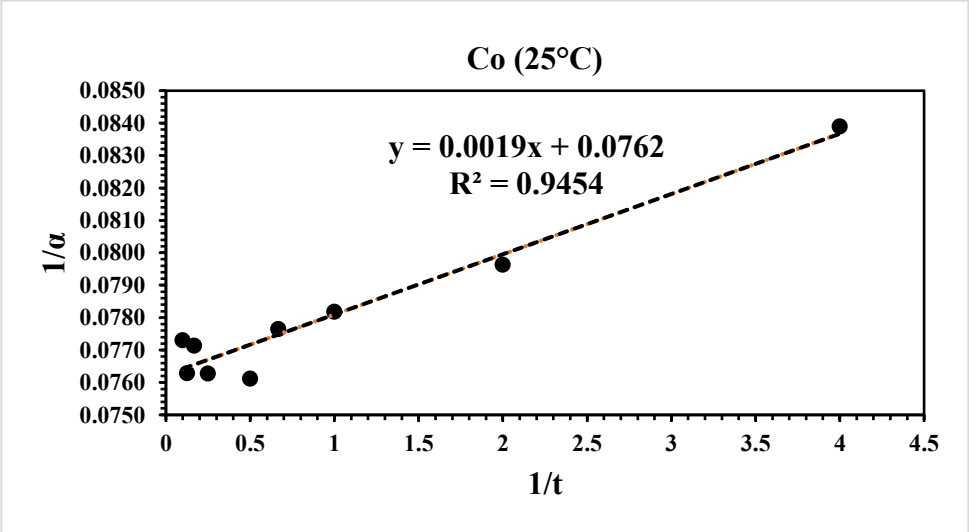


Figure 7-8 Plot of $\frac{1}{\alpha}$ vs $\frac{1}{t}$ for the proposed SPM-PSO Co kinetic model at 25℃

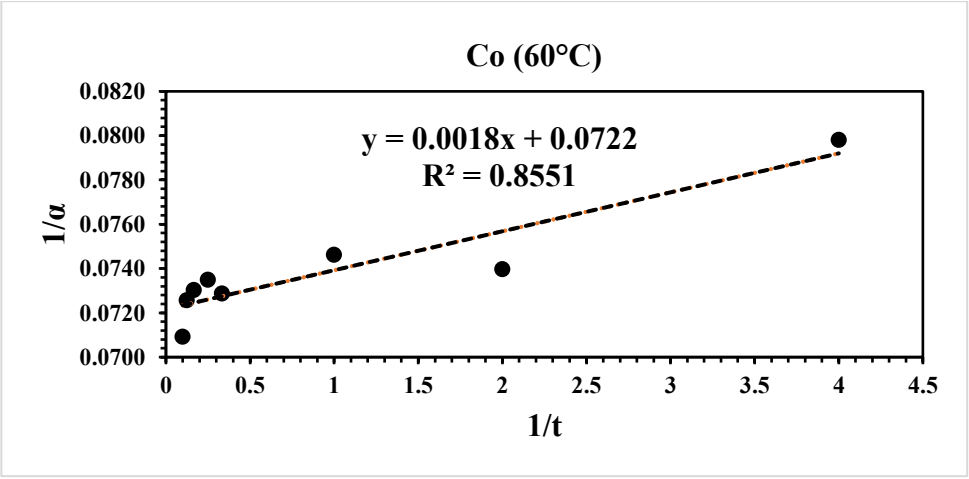


Figure 7-9 Plot of $\frac{1}{\alpha}$ vs $\frac{1}{t}$ for the proposed SPM-PSO Co kinetic model at 60℃

The coefficient of determination was high at 25 °C (0.9454) and 60 °C (0.8551) indicating a very good fit to the proposed model. A summary of key model parameters is shown in **table 7-2** below. At 40 °C, the data had more scatter and R^2 was significantly lower at 0.5577, suggesting a weaker linear fit under these conditions. However, overall, the SPM-PSO fitted the cobalt kinetic data better than the previously proposed SCM. The data in **table 7-2** was used to predict a maximum dissolution fraction or recovery for cobalt and within the studied temperature range predicted maximum cobalt recovery was 13.12-14.26%. This is in line with experimental observations.

Table 7-2 Summary of cobalt SPM-PSO fit results

Temperature	**25°C**	**40°C**	**60°C**
Slope (m) of linear regression	0.0019	0.0006	0.0018
Intercept [C]	0.0762	0.0701	0.0722
Maximum dissolution fraction [α_s]	13.12	14.26	13.85
Apparent Kinetic Constant (k) (h^{-1})	40.11	116.83	40.111
Coefficient of determination (R^2)	0.9454	0.5577	0.8551

Nickel kinetics

Figures 7-10 to **7-11** present the fits of **Equation 7-6** to experimental data at 25°C, and 60°C, with the corresponding kinetic parameters summarized in **Table 7-3**. The SPM-PSO model consistently provided better fits compared to the standard shrinking core model (SCM) across all studied temperatures, as indicated by higher R^2 values. However, the fit at 40°C (R^2 = 0.548) was weaker than those at 25°C (R^2 = 0.837) and 60°C (R^2 = 0.840) respectively. This discrepancy could result from experimental uncertainties, which warrant further investigation.

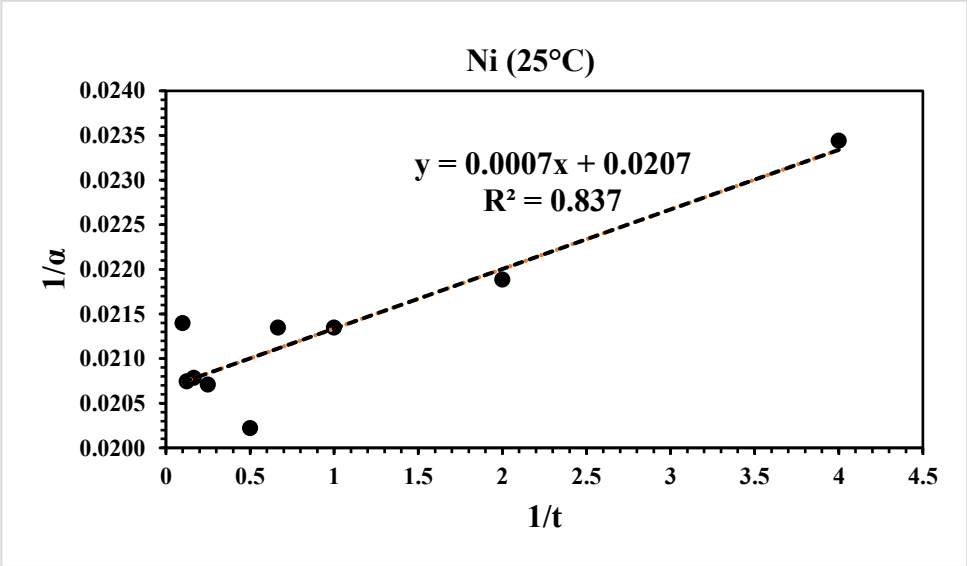


Figure 7-10 Plot of $\frac{1}{\alpha}$ vs $\frac{1}{t}$ for the proposed SPM-PSO Ni kinetic model at 25℃

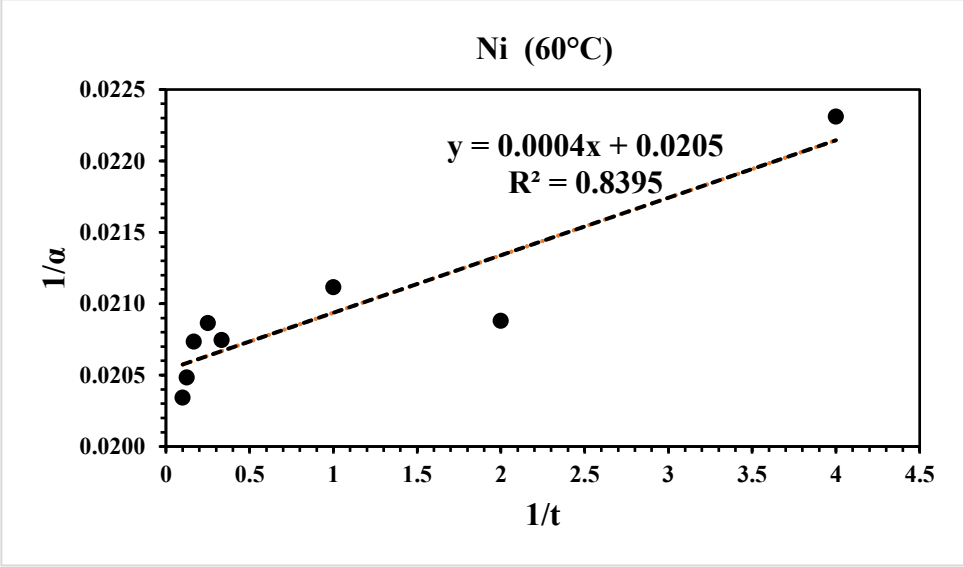


Figure 7-11 Plot of $\frac{1}{\alpha}$ vs $\frac{1}{t}$ for the proposed SPM-PSO Ni kinetic model at 60℃

Table 7-3 Summary of nickel SPM-PSO fit results

Temperature (°C)	Slope (*m*)	Intercept (*C*)	α_s (%)	k (h^{-1})	R^2
25	0.0007	0.0207	48.31	29.57	0.837
40	0.0003	0.0194	51.55	64.67	0.548
60	0.0004	0.0205	48.78	51.25	0.840

The theoretical maximum nickel recovery at saturation ranged from 48.31% at 25°C to 51.55% at 40°C, which aligned well with the observed experimental data. The apparent kinetic constant (k) increased with temperature up to 40°C but slightly decreased at 60°C. This deviation may reflect changes in solute-solvent interactions or diffusion dynamics at higher temperatures. These trends align with previous studies indicating complex temperature dependencies in agitated systems (Carlesi et al., 2022). Nonetheless further exploration of how solution properties such as viscosity and particle size distribution evolve during leaching is needed.

7.6 Activation Energy

The apparent rate constants (k) were determined from the dissolution experiments conducted at various temperatures (see **Table 7-2** to **7-3**). These rate constants were used to construct an Arrhenius plot enabling the analysis of the temperature dependence of the reaction rate and the calculation of activation energy *(E_a)*. The relationship between k and temperature is expressed by the *Arrhenius equation*:

$$k = Ae^{\frac{E_a}{RT}} \quad \textbf{(7.4)}$$

where:

- k is the rate constant,
- A is the pre-exponential factor,
- E_a is the activation energy (J/mol),

- R is the universal gas constant (8.314 J/mol·K)
- T is the temperature (K).

To facilitate plotting, the equation was linearized by taking the natural logarithm of **Equation (7.4):**

$$lnk = lnA - \frac{E_a}{RT} \quad \textbf{(7.5)}$$

This linear form allows *lnk* to be plotted against *1/T* and the slope of the resulting straight line ($m = -\frac{E_a}{R}$) was used to calculate the apparent activation energy.

7.6.1 Results and Discussion

The linear form of **equation 7.4** was used to plot *lnk* against *1/T*, as shown in **Figure 7-12** to **7-13**. Examination of the cobalt Arrhenius plot did not give a satisfactory straight line, as the R^2 value was too low. As previously discussed, the copper SCM plots could not be differentiated in terms of a dominating control mechanism hence the apparent rate constants from all the SCM plots were used to generate Arrhenius plots (see **Figure 7-13**).

The activation energy for the nickel dissolution was calculated to be 12.24 $kJmol^{-1}$ using the slope of the line of best fit. The low activation energy suggests that the dissolution process is controlled by mass transport rather than by chemical reactions. In diffusion-controlled processes, the activation energy is typically low (below 20 $kJmol^{-1}$). By contrast, reactions controlled by chemical processes involving surface reactions or bond-breaking, typically exhibit higher activation energies, usually above 20−40 kJ/mol. Mass transport control indicates that the energy barrier for dissolution is minimal and is primarily governed by the movement of species (e.g., nickel ions and chloride complexes) through the

solvent. Consequently, improvements in factors affecting mass transport, such as agitation, liquid-to-solid ratio, or solvent diffusivity, would significantly enhance the dissolution rate.

To confirm the role of mass transport, additional experiments could be conducted by varying agitation rates or the liquid-to-solid ratio to observe their impact on the dissolution rate. Such studies would validate the hypothesis that mass transport is the rate-limiting step. The role of these individual factors on metal recovery was explored in previous chapters entailing screening of significant factors by use of statistical methods such as Analysis of Variance (ANOVA). In those experiments temperature and agitation rate were identified as insignificant factors. However, the pulp density or liquid to solid ratio was identified as a critical factor influencing nickel extraction.

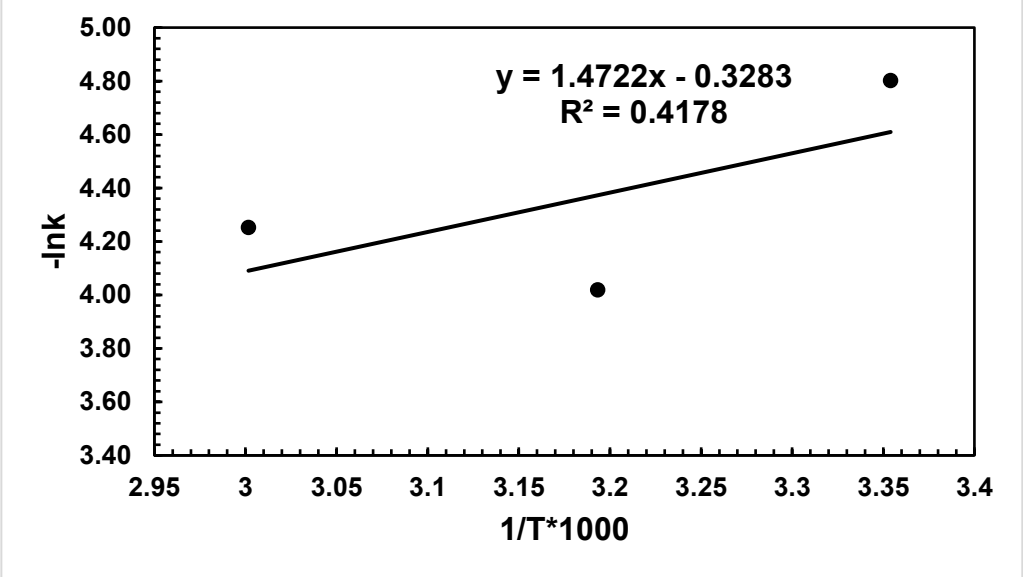


Figure 7-12 Arrhenius plot showing the linear relationship between *lnk* and *1/T* for Ni extraction in the DES, ethaline (1ChCl:2EG).

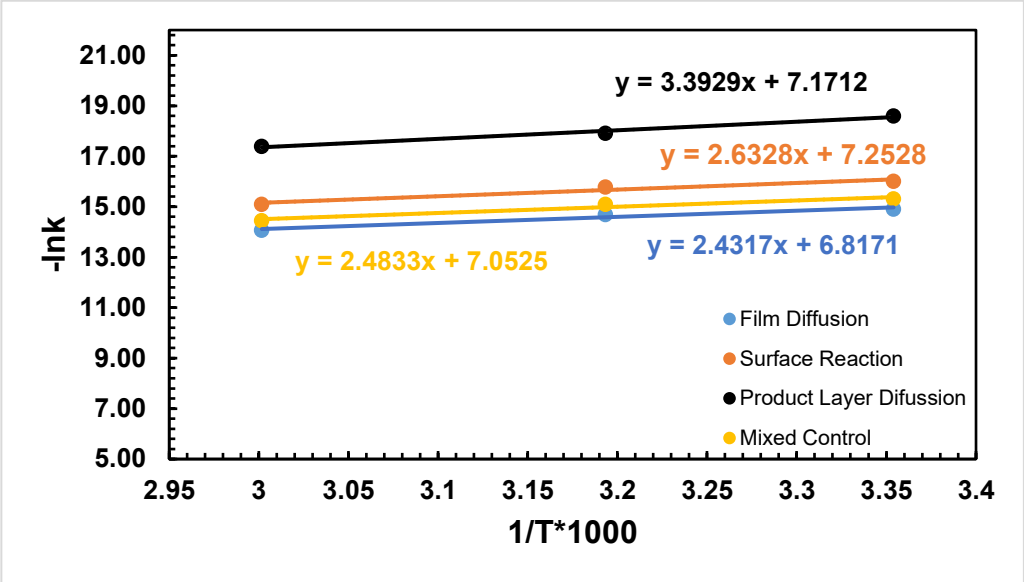


Figure 7-13 Arrhenius plot showing the linear relationship between lnk and 1/T for Cu extraction in the DES, ethaline (1ChCl:2EG).

The activation energies for the copper dissolution were calculated to be 20.22 $kJmol^{-1}$, 21.89 $kJmol^{-1}$,28.21 $kJmol^{-1}$ and 20.65 $kJmol^{-1}$ for film diffusion, chemical reaction, product layer diffusion and mixed control respectively. Typically, activation energies under 20 $kJmol^{-1}$ indicate diffusion control, while values between 20 $kJmol^{-1}$ and 40 kJ/mol suggest a mixed-control mechanism (Faraji *et al.*, 2022). Activation energies exceeding 40 kJ/mol are associated with chemical reaction rate control. Based on this criterion, the dissolution of copper from the concentrate material is governed by a mixed control mechanism equally dominated by both product layer diffusion and surface reactions. This validates the relatively low recoveries of copper across all experiments. This can be explained by the fact that the leaching system employs ethaline as the lixiviant, which has a high viscosity thus potentially limits the diffusion (mass transfer) of the reactants and reaction products to and from the particle surface.

7.7 Summary

This chapter presented a kinetic analysis of nickel, copper, and cobalt leaching from a sulphide concentrate using ethaline, a DES, as the lixiviant. The results and discussion were structured around three primary areas: extraction profiles, kinetic modelling, and alternative models and mechanisms. In terms of extraction profiles, nickel recovery peaked at 54.97% at 90°C but declined over time, likely due to solvent instability or reprecipitation, with optimal recoveries occurring within the first one to two hours of leaching. Cobalt recovery remained low, reaching a maximum of 16%, though its stable recovery at higher temperatures suggested less dependence on temperature variation compared to nickel. Copper dissolution was minimal at 6.4% and decreased with increasing temperature, indicating the potential for selective nickel recovery. For kinetic modelling, the Shrinking Core Model (SCM) was applied to evaluate rate-controlling mechanisms. The SCM fitted the copper data well with R^2 values exceeding 0.97 however the SCM yielded poor fits to the experimental data for Ni and Co. Consequently, alternative models were explored, with the hybrid Shrinking Particle Model coupled with Pseudo-Second-Order Kinetics (SPM-PSO) providing better data fits ($R^2 > 0.8$ at some temperatures), effectively accounting for dynamic diffusion and saturation effects. Additionally, Arrhenius analysis indicated a low activation energy of 12.24 kJ/mol for nickel dissolution, confirming that the process was primarily controlled by mass transport. For copper the leaching kinetics were governed by a mixed control mechanism.

CHAPTER EIGHT

CONCLUSIONS AND RECOMMENDATIONS

8.1 Conclusions

8.1.1 Introduction

The leaching of metals from sulphide minerals in deep eutectic solvents is not well understood however, the consensus is that it probably relies on the following fundamental mechanisms: (1) protonation reactions facilitated by the acidic nature of some DESs, (2) dissolution of metal ions through complexation with DES components and (3) redox reactions.

The main aim of this study was to expand on these principles to evaluate the feasibility of using choline chloride based DESs as sustainable and effective media for the leaching of copper-nickel sulphide concentrate. Sulphide minerals contain valuable metals however, due to their high sulphur content when processed by conventional techniques they tend to form noxious gases and acidic effluents which are detrimental to the environment and often require costly pollution abatement technologies.

The findings of this study suggest that DESs, particularly those based on choline chloride, enhance metal solubilization by promoting selective dissolution mechanisms thus forming stable metal-ion complexes. This approach offers a potential pathway for efficient and environmentally benign metal recovery from complex sulphide ores.

To investigate this possibility, the aims and objectives of this study were defined as:

i. To collect and characterize base metal flotation concentrate samples to establish their chemical and mineralogical composition.

ii. Investigation of parameters which promote Ni, Cu and Co dissolution in sulphide concentrate using the DES.

iii. To conduct solvent selection or comparison experiments, to identify the lixiviant that demonstrates the highest extraction of nickel, copper and cobalt.

iv. To establish the optimal conditions for extraction of nickel, copper, and cobalt by employing the most effective lixiviant (i.e., optimization studies).

v. Derivation of a conceptual reaction kinetic model for Ni, Cu and Co dissolution

8.1.2 Screening of significant factors and solvent alternatives

The chemical leaching of copper-nickel sulphide ore concentrate with eutectic mixtures of choline chloride and various hydrogen bond donors (ethylene glycol, urea and malonic acid) provided a better insight into the DES leaching process. The results presented in this study have shown that the extent of nickel dissolution is not highly dependent on the type of leaching media or hydrogen bond donor. The three solvents studied, ethaline, reline and maline showed similar maximal recoveries of nickel ie.54.98% ,54.76% and 53.76%. All solvent showed selective leaching properties towards nickel while cobalt and copper recoveries were low to moderate across all solvents. However, considering the effect of co-dissolution of other metals with nickel, ethaline exhibited slightly better selectivity. Additionally, the highest nickel recovery achieved was 56.34% in ethaline, using a higher-resolution full factorial design

The highest copper recovery achieved was 19.61% in maline whilst ethaline and reline had lower recoveries of 5.35% and 5.29% respectively. The relatively high recovery of copper in maline suggests opportunities for sequential or targeted leaching stages, which could maximize overall process efficiency. On the other hand, solvent choice seemed to have little impact on cobalt extraction with

recovery remaining relatively similar across all solvents i.e., EG (14.77%), U (16.05%) and MA (14.59%).

The lack of variation in recovery trends suggests that leaching efficiency alone is not a sufficient criterion for solvent selection. Instead, it should be combined with consideration of desirable solvent properties, such as viscosity. The choice of ethaline for further optimization was based on this consideration including its slightly better leaching performance.

Five variables were investigated for their effect on metal recovery i.e., temperature, pulp density, stirring rate, leaching time, and diluent ratio. The partial factorial designs for all solvents produced insignificant nickel recovery models due to the low resolution of the designs. The high resolution full factorial design for ethaline showed that pulp density was the most significant factor influencing nickel recovery, with lower pulp densities generally favouring higher recoveries. The stirring rate though not a significant factor was involved in a 3-way interaction with temperature and leaching time. High settings of stirring rate favoured high nickel recoveries which suggested the dissolution process might be mass transfer limited. Leaching temperature was a non-significant factor indicating high recoveries could be obtained even at near ambient conditions. The two highest nickel recoveries (55.55% and 56.34%) were obtained at 25℃. Leaching time did not have a significant effect on extraction, as high nickel recoveries (56.34%) could be achieved in 1 hour, indicating relatively fast kinetics. Extended leaching times (4 hrs) led to reduced recoveries (47.86%) under similar conditions.

The inclusion of ethylene glycol as a diluent for reducing viscosity in the two solvents reline and maline did not have a significant effect on metal recovery. The highest nickel recoveries for reline and maline were obtained in neat solutions i.e., 54.76% and 53.76% respectively. The results highlight ethaline's potential for efficient and selective nickel recovery, establishing a foundation for subsequent optimization and greener metallurgical processes.

8.1.3 Parameter Optimization

Response Surface Methodology, a statistically driven optimization approach, was employed for parameter optimization. with ethaline chosen as a lixiviant. Ethaline was selected because it demonstrated higher leaching recoveries than reline and maline in the screening study. A statistical experimental design called custom I-optimal design was used to limit the number of runs, but being adequate to describe the one variable leaching process. The experimental data were analysed, leading to the development of a suitable predictive empirical second-order model. This model, representing the nickel recovery process, was formulated as a function of pulp density. Model validity was checked using fit statistics, analysis of variance (ANOVA), and diagnostic plots based on residual analysis, which insured that convergence at the optimal factor settings was accomplished.

The results indicated that pulp density and its quadratic terms were statistically significant for influencing metal recovery, with lower pulp densities generally leading to higher nickel recovery. Numerical optimization was utilized to determine the optimal conditions for maximizing nickel recovery while minimizing the co-dissolution of iron and cobalt. Within the studied conditions, the statistically derived optimization model predicted maximum recoveries of 58.12% nickel, 16.68% cobalt, and 4.28% iron. The corresponding optimal conditions were identified as a 0.5% pulp density, 1-hour leaching time, 600 rpm stirring rate, and a leaching temperature of 25°C.

For verification of the predicted optimal conditions, confirmatory tests were conducted. The observed nickel recoveries were 58.16% and 59.06%, respectively. This indicates a strong correlation between the predicted and experimental results, with a relative error of less than 1.6%. This study has shown that a eutectic mixture of choline chloride and ethylene glycol can be used to selectively leach nickel sulphides achieving relatively high nickel recoveries in a single stage leach operation whilst minimising co-dissolution of associated metallic values.

8.1.4 Kinetic study

To determine the reaction regime governing the leaching of copper-nickel sulphide ore concentrate, both the shrinking core model (SCM) and activation energy studies were performed. A precise understanding of the dissolution process is crucial for scaling up from laboratory to industrial equipment.

The extraction profiles showed nickel recovery peaked at 54.97% at 90°C but declined over time due to solvent instability or reprecipitation. Optimal nickel recoveries occurred within 1–2 hours of leaching. Cobalt recovery was low peaking at 16% and stable across the temperature range indicating less of a dependence on temperature variation. Copper recovery was very low (6.4%) and decreased with temperature. The low cobalt and copper recoveries indicated potential for selective nickel recovery.

The SCM fitted the copper data well with R^2 values exceeding 0.97 and leaching kinetics were found to be governed by a mixed control mechanism. However, the SCM yielded poor fits to the experimental data for Ni and Co. Consequently, alternative models were explored, with the hybrid Shrinking Particle Model coupled with Pseudo-Second-Order Kinetics (SPM-PSO) providing better data fits ($R^2 > 0.8$ at some temperatures), effectively accounting for dynamic diffusion and saturation effects. Additionally, Arrhenius analysis indicated a low activation energy of 12.24 kJ/mol for nickel dissolution, confirming a mass transport-controlled process. This is consistent with observations made in the screening and optimization studies were pulp density and to a lesser extent stirring rate were identified as critical factors for controlling nickel recovery. Pulp density affects the rate of mass transfer and the contact between ore particles and lixiviants during leaching. High pulp densities generally limit lixiviant contact with ore particles. Stirring increases the rate of diffusion and mass transfer of chemical species.

8.1.5 Potential Application in Industry

This study has demonstrated the potential application of ethaline, a DES, for the commercial processing of sulphide ores. The key findings include relatively fast leaching kinetics, with efficient nickel dissolution achieved in under one hour, and low energy consumption due to the process operating near room temperature (~25°C). These attributes make ethaline a highly attractive alternative to conventional hydrometallurgical techniques, which often require elevated temperatures and prolonged processing times.

The leaching efficiency of ethaline, however, is highly dependent on pulp density, highlighting the need for precise optimization of process parameters to achieve maximum recovery rates. This dependency suggests that ethaline-based leaching systems may perform best under controlled feed conditions, ensuring the optimal balance between solvent volume and ore mass.

Ethaline's ability to process sulphide ores with minimal energy requirements and rapid dissolution kinetics is particularly advantageous for regions with limited access to high-energy infrastructure. Additionally, the selective leaching capability of ethaline allows for efficient recovery of nickel while reducing the dissolution of gangue materials, which contributes to waste minimization and improved downstream processing.

Moreover, the use of ethaline can be extended to other challenging materials beyond sulphide ores, such as complex polymetallic ores, low-grade sulphide tailings, and refractory materials. Its environmentally benign nature and potential to dissolve a wide range of metal sulphides without extensive pretreatment could lead to its adoption in industries focused on sustainable and energy-efficient resource recovery. This makes ethaline-based processing a promising candidate for advancing circular economy practices in the mining and metallurgical sectors.

8.2 Recommendations

Based on the insights gained from this work, the following recommendations for future studies are suggested.

8.2.1 Inert Atmosphere Experiments

DESs are highly hygroscopic, and their exposure to moisture can significantly alter their physicochemical properties, potentially impacting leaching efficiency and reaction mechanisms. To mitigate this, it is recommended that leaching experiments be conducted in controlled environments, such as glove boxes or Schlenk setups, to prevent moisture contamination.

Future studies should focus on performing leaching experiments under an inert atmosphere (e.g., nitrogen or argon) to evaluate how moisture exclusion affects the dissolution kinetics and overall process performance. These controlled environments will help ensure the stability of the DES and minimize unintended side reactions that may arise from exposure to atmospheric moisture.

Comparative analyses of leaching conducted in inert versus open-air conditions will provide valuable insights into how moisture control influences leaching efficiency and process dynamics. Such investigations may lead to optimized reaction control regimes, enhanced metal recovery efficiencies, and more accurate kinetic models for industrial applications.

Exploring the role of inert atmosphere setups will not only ensure consistency in experimental conditions but also advance the development of standardized handling protocols for DESs in industrial applications. This research direction is crucial for optimizing the use of DESs in processing sulphide ores and expanding their applicability across diverse ore types.

8.2.2 Multiple Leaching Stages

This study has demonstrated the potential of ethaline, for processing sulphide ores, with a maximum nickel recovery of approximately 59% achieved under single stage leaching conditions. While promising, this recovery rate suggests that there is room for improvement, and multi-stage leaching experiments are recommended as a potential pathway to enhance nickel extraction.

Future research should focus on designing sequential leaching experiments where fresh DES or optimized leaching conditions are applied in each stage. Sequential leaching may improve the dissolution of residual nickel in the ore by exposing previously unreacted surfaces or breaking down refractory phases that inhibit complete recovery in a single stage. Furthermore, multi-stage leaching could offer insights into selective metal recovery, enabling tailored extraction of other valuable metals present in the ore. By investigating the effectiveness of sequential leaching, future studies can provide a pathway for optimizing nickel recovery beyond the current 59% and extend the applicability of DES-based processing to other complex sulphide ores. In addition, future studies may explore whether combining different DES in varying ratios within sequential leaching stages could further enhance efficiency and selectivity.

8.2.3 Oxidative Leaching

Oxidative leaching experiments are recommended as a potential pathway to enhance metal dissolution and recovery rates. Future research should explore the incorporation of oxidizing agents, such as hydrogen peroxide, iodine, ferric and cupric ions into the leaching system to evaluate their effect on the dissolution kinetics of complex sulphide minerals. Oxidative leaching may facilitate the breakdown of refractory sulphide phases, allowing for more efficient recovery of nickel and copper. The impact of oxidative conditions on the physicochemical properties of ethaline, such as viscosity should also be assessed to ensure the long-term economic and operational feasibility of the process.

REFERENCES

Abbott, A.P., Capper, G., Davies, D.L., Rasheed, R.K. and Tambyrajah, V., 2003. Novel solvent properties of choline chloride/urea mixtures. *Chemical communications*, (1), pp.70-71.

Abbott, A.P., Boothby, D., Capper, G., Davies, D.L. and Rasheed, R.K., 2004. Deep eutectic solvents formed between choline chloride and carboxylic acids: versatile alternatives to ionic liquids. *Journal of the American Chemical Society*, *126*(29), pp.9142-9147.

Abbott, A.P., Capper, G., Davies, D.L., Rasheed, R.K. and Shikotra, P., 2005. Selective extraction of metals from mixed oxide matrixes using choline-based ionic liquids. *Inorganic chemistry*, *44*(19), pp.6497-6499.

Abbott, A.P., Capper, G., Davies, D.L., McKenzie, K.J. and Obi, S.U., 2006. Solubility of metal oxides in deep eutectic solvents based on choline chloride. *Journal of Chemical & Engineering Data*, *51*(4), pp.1280-1282.

Abbott, A.P., Collins, J., Dalrymple, I., Harris, R.C., Mistry, R., Qiu, F., Scheirer, J. and Wise, W.R., 2009. Processing of electric arc furnace dust using deep eutectic solvents. *Australian journal of chemistry*, *62*(4), pp.341-347.

Abbott, A.P., Frisch, G., Gurman, S.J., Hillman, A.R., Hartley, J., Holyoak, F. and Ryder, K.S., 2011. Ionometallurgy: designer redox properties for metal processing. *Chemical Communications*, *47*(36), pp.10031-10033.

Abbott, A.P., Al-Bassam, A.Z., Goddard, A., Harris, R.C., Jenkin, G.R., Nisbet, F.J. and Wieland, M., 2017. Dissolution of pyrite and other Fe–S–As minerals using deep eutectic solvents. *Green Chemistry*, *19*(9), pp.2225-2233.

Abbott, A.P., Frisch, G. and Ryder, K.S., 2008. Metal complexation in ionic liquids, *Annual Reports Section" A"(Inorganic Chemistry)*, 104, pp. 21–45.

Abbott, A.P. and McKenzie, K.J., 2006. Application of ionic liquids to the electrodeposition of metals, *Physical Chemistry Chemical Physics*, 8(37), pp. 4265–4279.

El Achkar, T., Greige-Gerges, H. and Fourmentin, S., 2021. Basics and properties of deep eutectic solvents: a review, *Environmental chemistry letters*, 19, pp. 3397–3408.

Adebayo, A.O., Ipinmoroti, K.O. and Ajayi, O.O., 2003. Dissolution kinetics of chalcopyrite with hydrogen peroxide in sulphuric acid medium', *Chemical and biochemical engineering quarterly*, 17(3), pp. 213–218.

Agilent Technologies., 2021. *Microwave Plasma Atomic Emission Spectroscopy (MPAES):*

Application eHandbook. January 2021.

Analytics, S.S.D., 2017. User Guide to MODDE: Version 12. *Sartorius Stedim Data: Umeå, Sweden*.

Anggara, S., Bevan, F., Harris, R.C., Hartley, J.M., Frisch, G., Jenkin, G.R. and Abbott, A.P., 2019. Direct extraction of copper from copper sulfide minerals using deep eutectic solvents. *Green Chemistry*, *21*(23), pp.6502-6512.

Antony, J., 2023. *Design of experiments for engineers and scientists*. Elsevier.

van Aswegen, P.C., Van Niekerk, J. and Olivier, W., 2007. The BIOX™ process for the treatment of refractory gold concentrates. In *Biomining* (pp. 1-33). Berlin, Heidelberg: Springer Berlin Heidelberg.

Barnes, S.J., Holwell, D.A. and Le Vaillant, M., 2017. Magmatic sulfide ore deposits. *Elements*, *13*(2), pp.89-95.

Bartow, V.,1953. Axel Fredrick Cronstedt, *Journal of Chemical Education*, 30(5), p. 247.

Bidari, E., Winardhi, C.W., Godinho, J.R.D.A. and Frisch, G., 2024. Role of oxidants in metal extraction from sulfide minerals in a deep eutectic solvent. *ACS omega*, *9*(12), pp.14592-14603.

Binnemans, K. and Jones, P.T., 2017. Solvometallurgy: an emerging branch of extractive metallurgy. *Journal of Sustainable Metallurgy*, *3*(3), pp.570-600.

Binnemans, K. and Jones, P.T., 2023. Ionic liquids and deep-eutectic solvents in extractive metallurgy: mismatch between academic research and industrial applicability. *Journal of Sustainable Metallurgy*, *9*(2), pp.423-438.

BITRI., 2023. *Mineralogical Investigation of One Copper and Nickel Bearing Flotation Concentrate Samples from Botswana (Prepared by Phuti Moloto, SGS)*. Gaborone.

Bloecher Jr, F.W., 1950. *Lyometallurgical tests of marysvale uranium ores* (No. MITG-252). Massachusetts Inst. of Tech., Watertown, Mass. Mineral Engineering Lab.

Box, G.E.P., Hunter, J.S. and Hunter, W.G., 2005. Statistics for experimenters, in *Wiley series in probability and statistics*. Wiley Hoboken, NJ.

Box, G.E., Hunter, W.H. and Hunter, S., 1978. *Statistics for experimenters* (Vol. 664). New York: John Wiley and sons.

Box, G.E.P. and Wilson, K.B., 1951. Series b (methodological), *Journal of the Royal Statistical Society*, 13(1), pp. 1–45.

Bruce, E., Sepúlveda, R., Castillo, J. and Saldana, M., 2024. Effect of Incorporation of Sulfation

in Columnar Modeling of Oxidized Copper Minerals on Predictions of Leaching Kinetics. *Metals*, *14*(6), p.708.

Cao, Y., Harjanto, S., Shibayama, A., Naitoh, I., Nanami, T., Kasahara, K., Okumura, Y. and Fujita, T., 2006. Kinetic study on the leaching of Pt, Pd and Rh from automotive catalyst residue by using chloride solutions. *Materials transactions*, *47*(8), pp.2015-2024.

Carlesi, C., Harris, R.C., Abbott, A.P. and Jenkin, G.R., 2022. Chemical dissolution of chalcopyrite concentrate in choline chloride ethylene glycol deep eutectic solvent. *Minerals*, *12*(1), p.65.

Cassetta, A., 2015. X-ray diffraction (XRD). In *Encyclopedia of Membranes* (pp. 1-3). Springer, Berlin, Heidelberg.

Chagnes, A., 2019. Advances in hydrometallurgy. *Metals*, *9*(2), p.211.

Chen, W., Jiang, J., Lan, X., Zhao, X., Mou, H. and Mu, T., 2019. A strategy for the dissolution and separation of rare earth oxides by novel Brønsted acidic deep eutectic solvents. *Green chemistry*, *21*(17), pp.4748-4756.

Chong, E., 2013. An Introduction to Optimization. Wiley.

Coker, A.K., 2001. *Modeling of chemical kinetics and reactor design*. Gulf Professional Publishing.

Coleman, T., Branch, M.A. and Grace, A., 1999. Optimization toolbox, *For Use with MATLAB. User's Guide for MATLAB 5, Version 2, Release II*.

Córdoba, E.M., Muñoz, J.A., Blázquez, M.L., González, F. and Ballester, A., 2008. Leaching of chalcopyrite with ferric ion. Part I: General aspects. *Hydrometallurgy*, *93*(3-4), pp.81-87.

Dean, A., Voss, D. and Draguljić, D., 2017. Response surface methodology. In *Design and analysis of experiments* (pp. 565-614). Cham: Springer International Publishing.

Delgado-Mellado, N., Larriba, M., Navarro, P., Rigual, V., Ayuso, M., García, J. and Rodríguez, F., 2018. Thermal stability of choline chloride deep eutectic solvents by TGA/FTIR-ATR analysis. *Journal of Molecular Liquids*, *260*, pp.37-43.

Denysschen, D.F. and Wagner, B.N., 2009. Pre-concentration of low-grade lateritic sulphide nickel ore. In *Base Metals Conference* (pp. 291-306).

Dhavalikar, M.K., 1997. Meluhha—The Land of Copper. *South Asian Studies*, *13*(1), pp.275-279.

Dixon-Warren, N., 2017. *BCL Limited (In Liquidation) And Tati Nickel Mining Company (Proprietary) Limited (In Provisional Liquidation) (Collectively Referred To As The BCL Group): Proposed Disposal Of The BCL Group – BCM, Botswana Chamber of Mines, Mining and*

Exploration. Available at: https://www.bcm.org.bw/proposed-disposal-of-the-bcl-group/ (Accessed: 30 January 2022).

Dong, L., Mazzarino, I. and Alexiadis, A., 2021. Development of Solid–Fluid Reaction Models—A Literature Review, *ChemEngineering 2021, Vol. 5, Page 36*, 5(3), p. 36.

Ebrahimi, E., Safari, H., Rezaee, M., Rezaei, A. and Abdollahi, H., 2023. An environmentally friendly method for extraction of cobalt and molybdenum from spent catalysts using deep eutectic solvents (DESs). *Environmental Science and Pollution Research*, *30*(39), pp.90243-90255.

Ekosse, G.I.E., 2007. Influenza/common cold within the Selebi Phikwe nickel-copper exploitation environment, Botswana. *African Journal for Physical Health Education, Recreation and Dance*, *13*(4), pp.473-490.

Entezari-Zarandi, A. and Larachi, F., 2019. Selective dissolution of rare-earth element carbonates in deep eutectic solvents. *Journal of Rare Earths*, *37*(5), pp.528-533.

Faraji, F., Alizadeh, A., Rashchi, F. and Mostoufi, N., 2022. Kinetics of leaching: a review. *Reviews in Chemical Engineering*, *38*(2), pp.113-148.

Haschke, M., Flock, J. and Haller, M., 2021. *X-ray fluorescence spectroscopy for laboratory applications* (pp. 14-of). Weinheim, Germany: Wiley-VCH.

Fogler, H.S., 2016. Elements of Chemical Reaction Engineering, 5th edition, *Boston, Massachusetts, USA: Prentice Hall*.

Free, M.L., 2013. *Hydrometallurgy: fundamentals and applications*. John Wiley & Sons.

Fuerstenau, M.C., Jameson, G.J. and Yoon, R.H. eds., 2007. *Froth flotation: a century of innovation*. SME.

García Álvarez, J., 2014. Deep eutectic solvents and their applications as new green and biorenewable reaction media. *Handbook of Solvents, Vol. 2, 2nd ed.: Use, Health, and Environment*.

Gbor, P.K. and Jia, C.Q., 2004. Critical evaluation of coupling particle size distribution with the shrinking core model. *Chemical Engineering Science*, *59*(10), pp.1979-1987.

Gericke, M., Neale, J.W. and Van Staden, P.J., 2009. A Mintek perspective of the past 25 years in minerals bioleaching. *Journal of the Southern African Institute of Mining and Metallurgy*, *109*(10), pp.567-585.

Gupta, A. and Yan, D.S., 2006. Introduction to mineral processing design and operation. *Perth, Australia*, pp.564-570.

Gupta, C.K., 2006. *Chemical metallurgy: principles and practice*. John Wiley & Sons.

Habashi, F., 1997. *Handbook of extractive metallurgy*. Wiley-VCH.

Habashi, F.,1999. *Kinetics of metallurgical processes*. Métallurgie Extractive Québec Québec, QC, Canada.

Habashi, F., 2013. Extractive metallurgy and national policy.

Haghbakhsh, R., Duarte, A.R.C. and Raeissi, S., 2021. Viscosity Investigations on the Binary Systems of (1 ChCl:2 Ethylene Glycol) DES and Methanol or Ethanol, *Molecules*, 26(18), p. 5513.

Hansen, B.B., Spittle, S., Chen, B., Poe, D., Zhang, Y., Klein, J.M., Horton, A., Adhikari, L., Zelovich, T., Doherty, B.W. and Gurkan, B., 2020. Deep eutectic solvents: a review of fundamentals and applications. *Chemical reviews*, *121*(3), pp.1232-1285.

Harris, B., 2019. The future of Ni-Co-Cu processing in the age of lithium-ion batteries. In *ALTA conference proceedings* (Vol. 21).

Heckert, N.A., Filliben, J.J., Croarkin, C.M., Hembree, B., Guthrie, W.F., Tobias, P. and Prinz, J., 2002. Handbook 151: Nist/sematech e-handbook of statistical methods.

Holdich, R., 2020. *Fundamentals of particle technology*. MidlandIT.

Hottinger Bruel & Kjaer Inc., 2024. *Response Surface Methods for Optimization*. Available at: https://help.reliasoft.com/reference/experimentr_design_and_analysis/doe/response_surface_methods_for_optimization.html (Accessed: 10 December 2024).

House, J.E. ,2007. *Principles of chemical kinetics*. Academic press.

Hu, Z. and Qi, L., 2014. 15.5-Sample digestion methods, *Treatise on geochemistry*, 1, pp. 87–109.

Huang, P. and Zhang, Y., 2018. Electrodeposition of nickel coating in choline chloride-urea deep eutectic solvent, *Int. J. Electrochem. Sci*, 13, pp. 10798–10808.

Jafari, M., Shafaie, S.Z., Abdollahi, H. and Entezari-Zarandi, A., 2022. Green recycling of spent Li-ion batteries by deep eutectic solvents (DESs): Leaching mechanism and effect of ternary DES. *Journal of Environmental Chemical Engineering*, *10*(6), p.109014.

Jangir, A.K., Nain, A.K. and Kuperkar, K., 2021. Insight into structural properties and molecular interactions of maline (choline chloride+ malonic acid) and 1, 4-butanediol based pseudo-binary mixture: A thermophysical, spectral, and simulation portrayal, *Journal of Molecular Liquids*, 334, p. 116050.

Jenkin, G.R., Al-Bassam, A.Z., Harris, R.C., Abbott, A.P., Smith, D.J., Holwell, D.A., Chapman, R.J. and Stanley, C.J., 2016. The application of deep eutectic solvent ionic liquids for environmentally friendly dissolution and recovery of precious metals. *Minerals Engineering*, *87*,

pp.18-24.

Khawam, A. and Flanagan, D.R., 2006. Solid-State Kinetic Models: Basics and Mathematical Fundamentals, *The Journal of Physical Chemistry B*, 110(35), pp. 17315–17328. Available at: https://doi.org/10.1021/jp062746a.

Khuri, A.I. and Mukhopadhyay, S., 2010. Response surface methodology, *Wiley interdisciplinary reviews: Computational statistics*, 2(2), pp. 128–149.

Kimball, R.B. and Ewing, R.A., 1957. *Uranium recovery from ores with hydrochloric acid and acetone*. U.S. Patent 2,800,387.

Kumar, K.V., Khaddour, I.A. and Gupta, V.K., 2010. A Pseudo Second-Order Kinetic Expression for Dissolution Kinetic Profiles of Solids in Solutions', *Industrial & Engineering Chemistry Research*, 49(16), pp. 7257–7262.

Lange, K., 2013. *Optimization*. Springer Science & Business Media.

Lekakh, S.N., Rawlins, C.H., Robertson, D.G., Richards, V.L. and Peaslee, K.D., 2008. Kinetics of aqueous leaching and carbonization of steelmaking slag. *Metallurgical and Materials Transactions B*, *39*(1), pp.125-134.

Levenspiel, O., 1999. Chemical Reaction Engineering, John Wiley and Sons Inc. *USA*, *675*.

Li, X. *et al.*, 2022. Effect of Mechanical Activation on the Leaching Process of Rare Earth Metal Yttrium in Deep Eutectic Solvents, *Applied Sciences*, 12(16), p. 8253.

Lottermoser, B. and Lottermoser, B.G., 2010. Sulfidic mine wastes. In *Mine wastes: Characterization, treatment and environmental impacts* (pp. 43–117). Berlin, Heidelberg: Springer Berlin Heidelberg.

Lu, Z.Y. *et al.*, 2000. Studies of pentlandite leaching in mixed oxygenated acidic chloride-sulfate solutions, *Hydrometallurgy*, 56(1), pp. 63–74.

Maier, W.D., Barnes, S.J., Chinyepi, G., Barton Jr, J.M., Eglington, B. and Setshedi, I., 2008. The composition of magmatic Ni–Cu–(PGE) sulfide deposits in the Tati and Selebi-Phikwe belts of eastern Botswana. *Mineralium Deposita*, *43*(1), pp.37-60.

Manjong, N.B., Usai, L., Burheim, O.S. and Strømman, A.H., 2021. Life cycle modelling of extraction and processing of battery minerals—a parametric approach. *Batteries*, *7*(3), p.57.

Masloboev, V.A., Seleznev, S.G., Svetlov, A.V. and Makarov, D.V., 2018. Hydrometallurgical processing of low-grade sulfide ore and mine waste in the Arctic regions: Perspectives and challenges. *Minerals*, *8*(10), p.436.

Mcrae, M.E., 2016. 2016 Minerals Yearbook: Nickel. *US Geological Survey*.

Meng, X. and Han, K.N., 1996. The principles and applications of ammonia leaching of metals—a review. *Mineral Processing and Extractive Metullargy Review*, *16*(1), pp.23-61.

Missen, R.W., 1999. In Mims CA, Saville BA, *Introduction to chemical reaction engineering and kinetics*.

Montgomery, D.C., 2017. *Design and analysis of experiments*. John wiley & sons.

Motswaiso, F.S., Nakamura, K., Watanabe, N. and Komai, T., 2019. Geochemical investigation of metals and trace elements around the abandoned Cu-Ni mine site in Selibe Phikwe, Botswana. *Journal of Geoscience and Environment Protection*, *7*(5), pp.275-293.

Mulaba-Bafubiandi, A.F. and Medupe, O., 2007. An assessment of pentlandite occurrence in the run of mine ore from BCL mine (Botswana) and its impact on the flotation yield. In *Proc. of the fourth Southern African conference on base metals, Swakopmund, Namibia, SAIMM* (pp. 57-76).

Natarajan, K.A. (ed), 2018. Chapter 7 - Bioleaching of Zinc, Nickel, and Cobalt. *Biotechnology of Metals*. Amsterdam: Elsevier, pp. 151–177.

Nkrumah, P.N., Echevarria, G., Erskine, P.D. and van der Ent, A., 2022. Farming for battery metals. *Science of the Total Environment*, *827*, p.154092.

Ochromowicz, K. and Leśniewicz, T., 2018. Optimization of laterites leaching by application of sequential design of experiments', *Physicochemical Problems of Mineral Processing*, 54(2), pp. 343–354.

Otunniyi, I.O., Oabile, M., Adeleke, A.A. and Mendonidis, P., 2016. Copper activation option for a pentlandite–pyrrhotite–chalcopyrite ore flotation with nickel interest. *International Journal of Industrial Chemistry*, *7*(3), pp.241-248.

Panayotova, M. and Panayotov, V., 2020. Recovery of valuable metals from mining and mineral processing waste. In *E3S Web of Conferences* (Vol. 211, p. 02009). EDP Sciences.

Paynter, J.C., 1973. A review of copper hydrometallurgy. *Journal of the Southern African Institute of Mining and Metallurgy*, *74*(4), pp.158-172.

Radetzki, M., 2009. Seven thousand years in the service of humanity—the history of copper, the red metal. *Resources Policy*, *34*(4), pp.176-184.

Raghavan, S. and Fuerstenau, D.W., 1993. A lyometallurgical process for leaching copper from chrysocolla. In *Hydrometallurgy fundamentals, technology and innovations, Proceedings of the Milton E., Wordsworth (IV) Int. Symposium on Hydrometallurgy* (pp. 283-297).

Golroudbary, S.R., Kraslawski, A., Wilson, B.P. and Lundström, M., 2023. Assessment of environmental sustainability of nickel required for mobility transition. *Frontiers in Chemical Engineering*, *4*, p.978842.

Rao, S., Zou, X., Wang, S., Lu, Y., Shi, T., Hsu, H.Y., Xu, Q. and Lu, X., 2019. Electrodeposition of Ni-Cu alloy films from nickel matte in deep eutectic solvent. *Materials Chemistry and Physics*, *232*, pp.6-15.

Reuter, M.A..,2021. Process principles in minerals and materials production–with a focus on metal production and recycling by PC Hayes, 2021, eBook edition: http://peterhayesmetallurgy. com, ISBN: 978-0-6486989-5-1. Print edition: https://www. amazon. com. au. ISBN: 978-0-64', *Mineral Processing and Extractive Metallurgy*, 130(4), pp. 433–434.

Riekkola-Vanhanen, M., 2013. Talvivaara mining company–From a project to a mine. *Minerals Engineering*, *48*, pp.2-9.

Rodriguez Rodriguez, N., Machiels, L. and Binnemans, K., 2019. p-Toluenesulfonic acid-based deep-eutectic solvents for solubilizing metal oxides. *ACS Sustainable Chemistry & Engineering*, *7*(4), pp.3940-3948.

Saari, P. and Riekkola-Vanhanen, M., 2012. Talvivaara bioheapleaching process. *Journal of the Southern African Institute of Mining and Metallurgy*, *112*(12), pp.1013-1020.

Sairinen, R., Tiainen, H. and Mononen, T., 2017. Talvivaara mine and water pollution: An analysis of mining conflict in Finland. *The Extractive Industries and Society*, *4*(3), pp.640-651.

Saldaña, M., Gálvez, E., Robles, P., Castillo, J. and Toro, N., 2022. Copper mineral leaching mathematical models—A review. *Materials*, *15*(5), p.1757.

Samadov, A.U., Khojiev, S.T., Buzurkhanova, F.S. and Ruziev, Z.N., 2018. Perspective method of smelting low-sulfur copper concentrates. In *НАУЧНЫЕ ДОСТИЖЕНИЯ И ОТКРЫТИЯ СОВРЕМЕННОЙ МОЛОДЁЖИ* (pp. 38-41).

Shengo, L.M., 2021. Potentially exploitable reprocessing routes for recovering copper and cobalt retained in flotation tailings. *Journal of Sustainable Metallurgy*, *7*(1), pp.60-77.

Simwaka, M., Gumbie, M., Moswate, P., Keitshokile, D.C. and Dzinomwa, G., 2009. Milestones in the Improvement of Concentrator Nickel And Copper Recoveries at BCL. In *Proceedings Base Metals Conference the Southern African Institute of Mining and Metallurgy, Kasane* (pp. 27-31).

Smit, D.S., 2001. *The leaching behaviour of a Ni–Cu–Co sulphide ore in an oxidative pressure–acid medium* (Doctoral dissertation, Potchefstroom University for Christian Higher Education).

Smith, E.L., Abbott, A.P. and Ryder, K.S., 2014. Deep eutectic solvents (DESs) and their applications. *Chemical reviews*, *114*(21), pp.11060-11082.

Streli, C., Wobrauschek, P. and Kregsamer, P., 2016. 'X-ray fluorescence spectroscopy, applications', in *Encyclopedia of Spectroscopy and Spectrometry*. Elsevier, pp. 707–715. Available at: https://doi.org/10.1016/B978-0-12-803224-4.00315-0.

Tian, G.-C., Jian, L.I. and Hua, Y.-X., 2010. Application of ionic liquids in hydrometallurgy of nonferrous metals, *Transactions of Nonferrous Metals Society of China*, 20(3), pp. 513–520.

Topçu, M.A., Rüşen, A. and Küçük, Ö.Z.K.A.N., 2021. Treatment of copper converter slag with deep eutectic solvent as green chemical. *Waste Management*, *132*, pp.64-73.

Tripathi, N., Peek, E. and Stroud, M., 2011. Advanced process modeling at the BCL smelter: Improving economic and environmental performance. *Jom*, *63*(1), pp.63-67.

Ultra Jr, V.U. and Manyiwa, T., 2021. Influence of mycorrhiza and fly ash on the survival, growth and heavy metal accumulation in three Acacia species grown in Cu–Ni mine soil. *Environmental Geochemistry and Health*, *43*(4), pp.1337-1353.

Vallance, C., 2008. *Reaction Kinetics lecture notes*, *University of Oxford*. Available at: https://vallance.chem.ox.ac.uk/pdfs/KineticsLectureNotes.pdf (Accessed: 4 November 2024).

Weeks, M.E., 1932. The discovery of the elements. III. Some eighteenth-century metals. *Journal of chemical education*, *9*(1), p.22.

Whitcomb, P. and Oehlert, G.W., 2007. Graphical selection of effects in general factorials, in *Fall Technical Conference*, pp. 2036–2037.

Wills, B.A. and Finch, J.A., 2016. *Wills' Mineral Processing Technology, An Introduction to the Practical Aspects of Ore Treatment and Mineral Recovery*. 8th edn. Oxford: Elsevier Ltd.

Xie, G. *et al.*,2023. A critical review of the enhanced recovery of rare earth elements from phosphogypsum, *Molecules*, 28(17), p. 6284.

Xie, Y., Xu, Y., Yan, L. and Yang, R., 2005. Recovery of nickel, copper and cobalt from low-grade Ni–Cu sulfide tailings. *Hydrometallurgy*, *80*(1-2), pp.54-58.

Yadav, A. and Pandey, S., 2014. Densities and viscosities of (choline chloride+ urea) deep eutectic solvent and its aqueous mixtures in the temperature range 293.15 K to 363.15 K, *Journal of Chemical & Engineering Data*, 59(7), pp. 2221–2229.

Zhu, X.L., Xu, C.Y., Tang, J., Hua, Y.X., Zhang, Q.B., Liu, H., Wang, X. and Huang, M.T., 2019. Selective recovery of zinc from zinc oxide dust using choline chloride based deep eutectic solvents. *Trans. Nonferrous Met. Soc. China*, *29*(10), pp.2222-2228.

Zürner, P. and Frisch, G., 2019. Leaching and selective extraction of indium and tin from zinc flue dust using an oxalic acid-based deep eutectic solvent. *ACS Sustainable Chemistry & Engineering*, *7*(5), pp.5300-5308.

APPENDIX A

PARTICLE SIZE ANALYSIS AND ORE CONCENTRATE COMPOSITION

Table A1. Sieve Analysis data for BCL flotation Concentrate

Sieve(mm)	retained weight (g)	retained %	cumulative weight (g)	cumulative %	% Passing
25	18.5	2	18.5	2	98
19	34.5	3	53	5	95
12.5	71.5	7	124.5	12	88
9.5	65.5	7	190	19	81
6.3	99.5	10	289.5	29	71
4.5	83.0	8	372.5	37	63
3.15	89.0	9	461.5	46	54
2.00	114	11	575.5	57	43
1.7	28.0	3	603.5	60	40
1.12	91.5	9	695	69	31
0.710	81.0	8	776	77	23
0.500	39	4	815	81	19
0.355	41	4	856	85	15
0.250	42.5	4	898.5	90	10
0.160	41.5	4	940	94	6
-0.160	62.5	6	1002.5	100	0

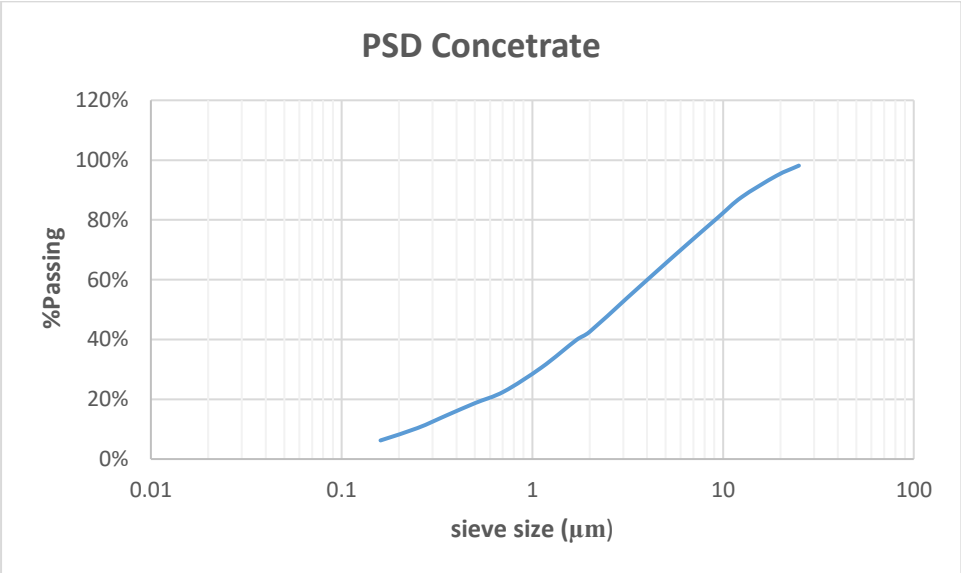


Figure A1. Sieve analysis plot of the head sample.

Preparation of 2 acid solution

A 4 mL aliquot of concentrated HCl was transferred into a glass beaker and slowly mixed with 8 mL of concentrated nitric acid using a magnetic stir bar.

Digestion Protocol

Approximately 0.5000g of a homogenized sample was weighed out and transferred into a 250 mL glass beaker equipped with a watch glass. Then 12 mL of the two-acid solution was added to the sample beaker and was allowed to digest on a hot plate for 3 hours at a temperature of 110℃. The digestion mixture was allowed to evaporate to near dryness and diluted with 20 mL of 2% (v/v) nitric acid. The solution was filtered into a 100 mL volumetric flask and diluted to the mark with deionised water. This digestion procedure was carried out in four replicates. The four solutions were then taken for analysis using MPAES.

Table A2. Determination of metal composition after 2-acid (1HCl:2HNO_3) digestion.

Solution label (Replicates)	**% Metal Content**		
	Cu	Ni	Co
C1	3.10	6.58	0.85
C3	2.86	6.35	0.84
C4	3.00	6.59	0.88
Mean	2.98±0.10	6.51± 0.11	0.86 ± 0.015

Elemental Compositions (of minerals of interest)

The elemental compositions of the Ni-bearing minerals by quantifying the present elements from their analysed spectra data are shown in Table A3. Based on the elemental compositions of the different/varying maufite phases, the reported maufite could also be regarded as a spinel phase. The spectra for the Ni-bearing spinel had too low intensity counts to be elementally quantified

Table A3 The (average) Elemental Compositions of Ni-bearing minerals, determined from spectra.

	S	Fe	Ni
Pentlandite (phase 1):	32.7%	30.5%	36.8%
Pentlandite (phase 2):	33.5%	1.7%	64.9%

	O	Mg	Al	Si	S	Fe	Ni
Pentlandite in Silicates (phase 1):	48.3%	12.9%	5.5%	15.7%	1.6%	15.7%	0.3%
Pentlandite in Silicates (phase 2):	43.6%	6.3%	0.6%	18.0%	11.4%	19.8%	0.3%

	O	Mg	Al	Si	Fe	Ni
Maufite (phase 1):	50.5%	13.5%	6.6%	16.8%	8.1%	4.7%

	O	Mg	Al	Si	Fe	Ni	Ti
Maufite (phase 2):	48.9%	10.3%	6.2%	19.7%	13.9%	0.6%	0.04%

	O	Na	Al	Si	Fe	Ni	K	Ca
Maufite (phase 3):	44.3%	3.7%	15.2%	26.7%	1.1%	0.0%	3.2%	5.8%

	O	Na	Al	Si	Fe	Ni	K	Ca
Maufite (phase 4):	46.4%	5.7%	12.5%	29.3%	0.8%	0.0%	2.2%	3.0%

	S	Fe	Ni
Pyrite (Ni):	53.9%	43.7%	2.5%

	S	Fe	Ni
Violarite:	41.5%	21.7%	36.8%

Similarly, the elemental compositions of the Cu-bearing minerals by quantifying the present elements from their analysed spectra data are shown in Table A4.

Table A4 The (average) Elemental Compositions of Cu-bearing minerals, determined from spectra.

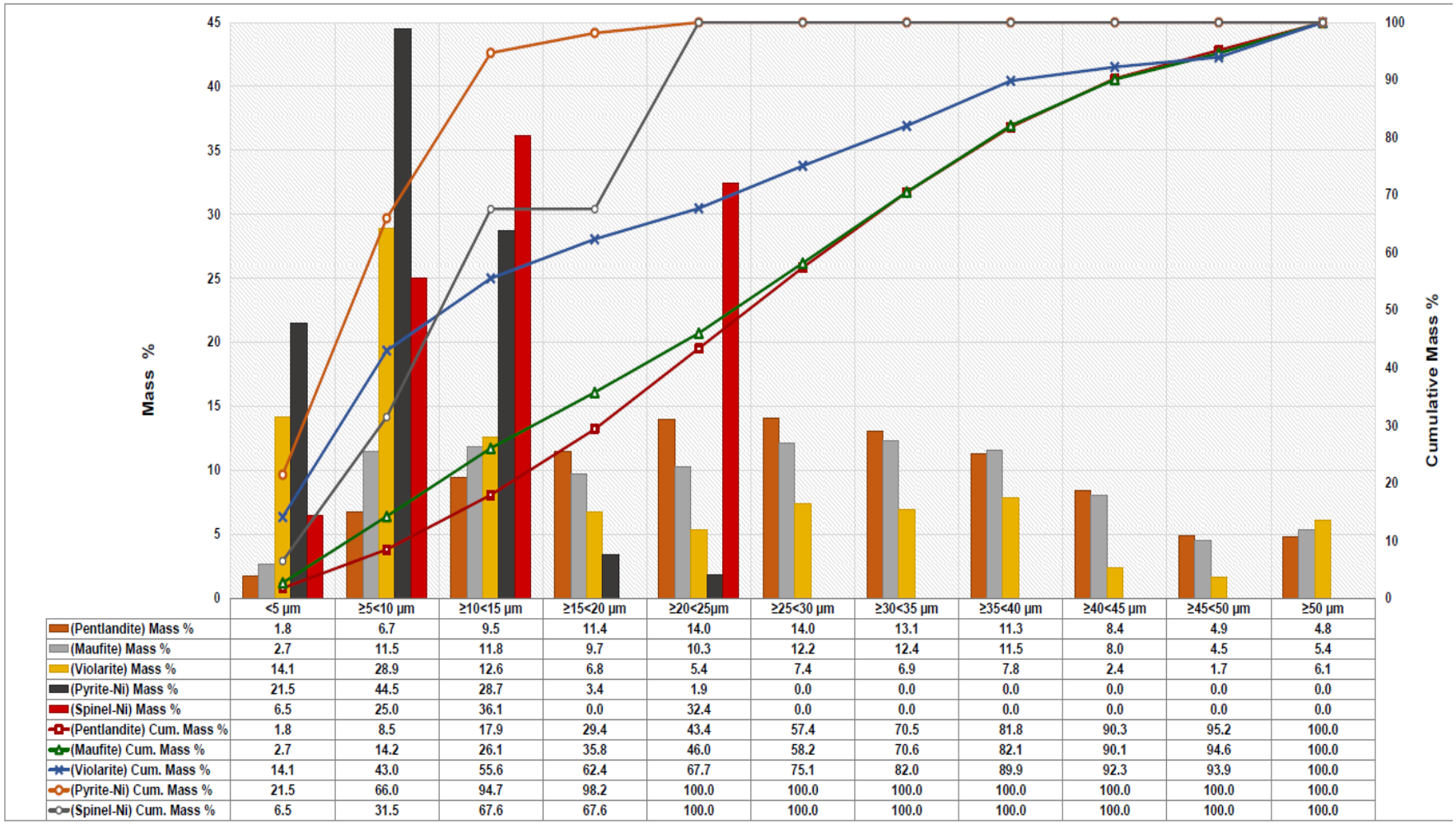
	S	Fe	Cu
Chalcopyrite:	35%	30%	35%

	S	Fe	Cu
Bornite:	26%	11%	63%

	S	Fe	Cu
Cubanite:	35%	41%	23%

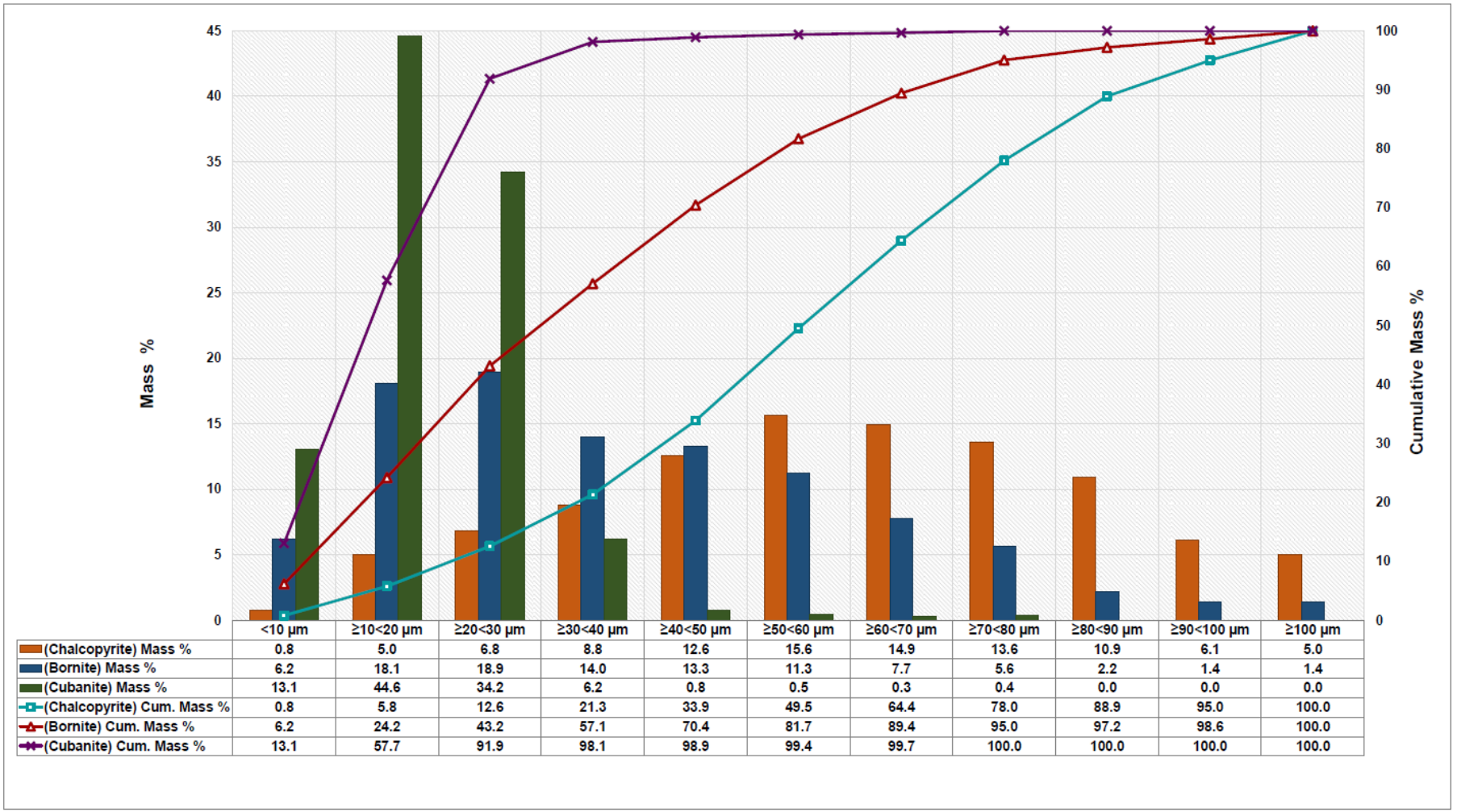
Grain Size Distribution (GSD) of Ni and Cu-bearing minerals

The GSD data for the minerals of interest is shown in **Figure B3** and **Figure B4**. The GSD of grains were considered in isolation; the data is given as the mass percent of mineral grains which fall into each size class. A mineral grain is that which consists of a single mineral type



	<5 µm	≥5<10 µm	≥10<15 µm	≥15<20 µm	≥20<25µm	≥25<30 µm	≥30<35 µm	≥35<40 µm	≥40<45 µm	≥45<50 µm	≥50 µm
(Pentlandite) Mass %	1.8	6.7	9.5	11.4	14.0	14.0	13.1	11.3	8.4	4.9	4.8
(Maufite) Mass %	2.7	11.5	11.8	9.7	10.3	12.2	12.4	11.5	8.0	4.5	5.4
(Violarite) Mass %	14.1	28.9	12.6	6.8	5.4	7.4	6.9	7.8	2.4	1.7	6.1
(Pyrite-Ni) Mass %	21.5	44.5	28.7	3.4	1.9	0.0	0.0	0.0	0.0	0.0	0.0
(Spinel-Ni) Mass %	6.5	25.0	36.1	0.0	32.4	0.0	0.0	0.0	0.0	0.0	0.0
(Pentlandite) Cum. Mass %	1.8	8.5	17.9	29.4	43.4	57.4	70.5	81.8	90.3	95.2	100.0
(Maufite) Cum. Mass %	2.7	14.2	26.1	35.8	46.0	58.2	70.6	82.1	90.1	94.6	100.0
(Violarite) Cum. Mass %	14.1	43.0	55.6	62.4	67.7	75.1	82.0	89.9	92.3	93.9	100.0
(Pyrite-Ni) Cum. Mass %	21.5	66.0	94.7	98.2	100.0	100.0	100.0	100.0	100.0	100.0	100.0
(Spinel-Ni) Cum. Mass %	6.5	31.5	67.6	67.6	100.0	100.0	100.0	100.0	100.0	100.0	100.0

Figure A2 GSD data for the Ni-bearing samples.



	<10 µm	≥10<20 µm	≥20<30 µm	≥30<40 µm	≥40<50 µm	≥50<60 µm	≥60<70 µm	≥70<80 µm	≥80<90 µm	≥90<100 µm	≥100 µm
(Chalcopyrite) Mass %	0.8	5.0	6.8	8.8	12.6	15.6	14.9	13.6	10.9	6.1	5.0
(Bornite) Mass %	6.2	18.1	18.9	14.0	13.3	11.3	7.7	5.6	2.2	1.4	1.4
(Cubanite) Mass %	13.1	44.6	34.2	6.2	0.8	0.5	0.3	0.4	0.0	0.0	0.0
(Chalcopyrite) Cum. Mass %	0.8	5.8	12.6	21.3	33.9	49.5	64.4	78.0	88.9	95.0	100.0
(Bornite) Cum. Mass %	6.2	24.2	43.2	57.1	70.4	81.7	89.4	95.0	97.2	98.6	100.0
(Cubanite) Cum. Mass %	13.1	57.7	91.9	98.1	98.9	99.4	99.7	100.0	100.0	100.0	100.0

Figure A3 GSD data for the Cu-bearing samples

APPENDIX B

SAMPLE CALCULATIONS

% Metal composition

The metal grade in the ore concentrate was calculated as a percentage of the total mass of the concentrate. The composition was determined using the Agilent 4200 Microwave-Plasma Atomic Emission Spectrophotometer (MP-AES) after digestion of concentrate with a two-acid solution (1:2 molar ratio of HCl and HNO_3 mixture).

Example (Ni grade)

$$\%\ Ni\ composition = \frac{mass\ of\ Ni\ in\ Solution}{mass\ of\ the\ \ concentrate\ sample} \times 100\%$$

Mass of ore concentrate weighed (g)	= 0.5063
Volume of dilute digestion solution (ml)	= 250
Ni (ppm) in solution by MPAES (replicates)	= 66.62, 63.80 and 66.76
Dilution factor	= 2
Unit Conversion factor (ppm to g/mL)	= $1*10^{-6}$
Total Ni dissolved (g)	= $66.62\ x1*10^{-6}*2*250$ = 0.03331 g
% Ni composition	= (0.03331/0.5063) x100 = 6.58%
Average % Ni composition (3 replicates)	= (6.58+6.35+6.59) /3 = 6.52$\pm$0.11%

% Metal recovery

The % metal recovery after the leaching of ore concentrates was calculated as a percentage of metal in the liquid phase (lixiviant) to that in the solid phase (concentrate). The recovery was determined using the Agilent 4200 Microwave-Plasma Atomic Emission Spectrophotometer (MP-AES) after leaching of concentrate with binary or ternary DES mixtures i.e., ethaline (1ChCl:2EG), reline (1ChCl:2U: nEG), and maline (1ChCl:1MA: nEG), with "n" ranging from 0 to 3 moles.

Example (Ni recovery)

$$\%\ Ni\ recovery = \frac{mass\ of\ Ni\ in\ Solution}{mass\ of\ Ni\ in\ \ concentrate} \times 100\%$$

Mass of ore concentrate weighed (g)	= 0.5000
% Ni composition in concentrate	= 6.51
Mass of Ni in concentrate (g)	= 6.51% of 0.5000 = 0.03255
Volume of dilute leach solution (ml)	= 100
Ni (ppm) in solution by MPAES	= 16.68
Dilution factor	= 10
Unit Conversion factor (ppm to g/mL)	= $1*10^{-6}$
Mass of Ni dissolved (g)	= 16.68 $x1*10^{-6}*10*100$ = 0.0167 g
% Ni recovery	= (0.0167/0.03255) $x100$ = 51.24 %

Determination of Activation Energies

The activation energy (E_a) was determined using the Arrhenius equation:

$$k = Ae^{\frac{E_a}{RT}}$$

Taking the natural logarithm on both sides:

$$lnk = lnA - \frac{E_a}{RT}$$

Sample data (Nickel)

T (°C)	T(K)	1/T	1/T*1000	k (h^{-1})	k, s^{-1}	lnk	| lnk |
25	298.15	0.00335	3.35	29.6	0.00821	-4.802	4.802
40	313.15	0.00319	3.19	64.7	0.01796	-4.019	4.019
60	333.15	0.003	3.00	51.3	0.01424	-4.252	4.252

The rate constants (k) for Ni dissolution were determined using the SPM-PSO kinetic model.

Plotting *lnk vs 1/T*

To determine E_a, we plot *lnk* against *1/T*. The slope of the linear regression line is given by:

$$slope = \frac{E_a}{R}$$

Equation of linear regression from the Arrhenius plot is given below:

$$y = 1.4722x - 0.3283$$

$$1.4722 = \frac{E_a}{8.314}$$

$$E_a = 12.24\ kJ/mol$$

Hence the calculated activation energy for the process was 12.24 kJ/mol indicating a diffusion-controlled process.

Preparation of Choline Chloride-Based DES

General Formula for DES Preparation

A typical DES is prepared by mixing choline chloride (ChCl) with a hydrogen bond donor (HBD) in a specific molar ratio, usually 1:2 (ChCl:HBD). The general approach to calculating the required mass and volume is as follows:

The mass of each component is determined using:

$$m = nxM$$

Where:

- m = mass (g)
- n = number of moles
- M = molar mass (g/mol)

For liquid components, volume is calculated using:

$$V = \frac{m}{\rho}$$

Where:

- V = volume (mL)
- ρ = density (g/mL)

Example (Ethaline: ChCl + Ethylene Glycol, 1:2 Molar Ratio)

Component properties

- Choline Chloride (solid)
    - Molar Mass: 139.62 g/mol
- Ethylene Glycol (Liquid)
    - Molar Mass: 62.07 g/mol
    - Density: 1.11 g/mL

Mass and volume calculation for 1 mol ChCl:

- ChCl mass:

$$m_{ChCl} = 1 \times 139.62 = 139.62\ g$$

- Ethylene Glycol mass:

$$m_{EG} = 2 \times 62.07 = 124.14\ g$$

- Ethylene volume:

$$V_{EG} = \frac{124.14}{1.11} = 111.8\ mL$$

The components are then weighed out and mixed using the preparation procedure.

APPENDIX C

DERIVATION OF SPM-PSO KINETIC MODEL

The leaching kinetic model derivation is described below, adopted from Carlesi et al., 2022)

The dissolution kinetics were modelled with the following considerations

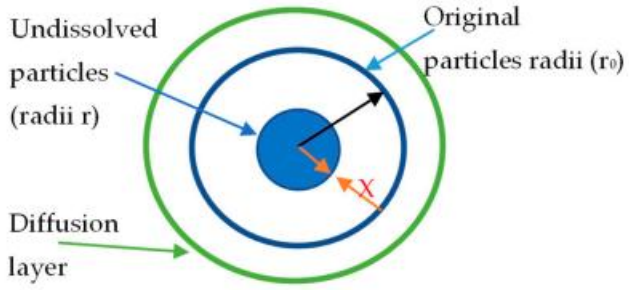


Figure C1 Diagram of an ideal mineral particle undergoing leaching

The mineral is viewed as a collection of particles with initial radii r_0 that undergo leaching, causing their radii to decrease uniformly over time (r as a function of time).

$$r = r_0 - x \tag{C1}$$

Taking into account the volume of a sphere and α as the molar fraction of the particle that has undergone reaction, the unreacted fraction is given by

$$1 - \alpha = \left(\frac{(r_0 - x)}{r_0}\right)^3$$

$$(1 - \alpha)^{\frac{1}{3}} = 1 - \frac{x}{r_0}$$

$$x = r_0\left[1 - (1 - \alpha)^{\frac{1}{3}}\right] \tag{C2}$$

$$\frac{dx}{d\alpha} = -\frac{r_0}{3}(1 - \alpha)^{-\frac{2}{3}} \tag{C3}$$

The shrinking of the particle radius is connected to its dissolution, which results in the release of a mass (m) of copper/nickel/cobalt. This process leads to a rise in the metal concentration within the liquid phase over time (t).

$$\left(\frac{1}{M}\right) * \frac{dm}{dt} = L * \frac{dc}{dt} \quad \textbf{(C4)}$$

The molar concentration of copper/nickel/cobalt in the liquid phase is denoted by ***c***. The molecular weight of the metallic species is symbolized by ***M***. The volume of the liquid phase in which the metal is dissolved is represented by ***L***. The metal loss from the solid is expressed by:

$$\frac{1}{M} * \frac{dm}{dt} = \frac{\rho dV_s}{Mdt} = \frac{4\pi\rho dr^3}{3Mdt} \quad \textbf{(C5)}$$

In this equation, ρ represents the density of the mineral. V_s is for the volume of the spherical solids. The chain rule of differentiation was applied to express the above equation in terms of *dx/dt*:

$$\frac{dr^3}{dt} = \frac{dr^3}{dx} * \frac{dx}{dt}$$

Applying **Equation C1** we get

$$\frac{dr^3}{dx} = \frac{d(r_0 - x)^3}{dx} = -3(r_0 - x)^2$$

Furthermore, substituting this result into Equation (A4):

$$\frac{1}{M} * \frac{dm}{dt} = \frac{(-4\pi\rho * (r_0 - x)^2 dx)}{Mdt} \quad \textbf{C6}$$

This molar flux of copper/nickel/cobalt transfers into the liquid phase, and assuming the liquid phase concentration follows a pseudo-second-order behaviour, it can be expressed as:

$$\frac{dc}{dt} = kD * (c_S - c)^2 \quad \textbf{C7}$$

In this equation, c_s is the saturation concentration of copper/nickel in the liquid phase. The term k_D denotes the rate constant for the pseudo-second-order reaction. The converted fraction α is expressed in terms of the liquid phase concentration as:

$$\alpha = a * \left(\frac{cL}{S}\right)$$

$$\alpha_S = a * \left(\frac{c_s L}{S}\right)$$

Where S represents the total moles of metal contained in the solid phase, and a is an experimentally determined constant that establishes the relationship between the liquid-to-solid ratio and the converted fraction.

Substituting into **Equation** (**C7**)

$$\frac{dc}{dt} = k_D * \left(\frac{S}{aL}\right)^2 * (\alpha_s - \alpha)^2 \quad \textbf{(C8)}$$

Furthermore, by substituting Equations (C6) and (C8) into Equation (C4), we obtain:

$$\frac{(-4\pi\rho * (r_0 - x)^2 dx)}{M dt} = k_D * \left(\frac{S}{a}\right)^2 * \frac{1}{L}(\alpha_s - \alpha)^2$$

By rearranging and simplifying we get,

$$\frac{dx}{dt} = (-k^*)\frac{(\alpha_s - \alpha)^2}{(r_0 - x)^2} \quad \textbf{(C9)}$$

where

$$k^* = \frac{\left(M\, k_D \left(\frac{S}{a}\right)^2\right)}{(4\pi\rho\, L)}$$

Furthermore, substituting x from Equation (C2) into Equation (C9) yields:

$$\frac{dx}{dt} = (-k^*) \times \frac{(\alpha_s - \alpha)^2}{\left[r_0 - r_0\left(1 - (1-\alpha)^{\frac{1}{3}}\right)\right]^2} = (-k^*) \times \frac{(\alpha_s - \alpha)^2}{\left(\left(r_0(1-\alpha)^{\frac{1}{3}}\right)^2\right)} \quad \textbf{(C10)}$$

Finally, by applying the chain rule of differentiation once more and incorporating Equations (C3) and (C10), the expression for the converted fraction as a function of time can be derived:

$$\frac{d\alpha}{dt} = \left(\frac{d\alpha}{dx}\right) * \left(\frac{dx}{dt}\right) = \left(\frac{-3}{r_0}\right)(1 - \alpha)^{\frac{2}{3}} \times \frac{(-k^*(\alpha_s - \alpha)^2)}{\left(r_0^2(1 - \alpha)^{\frac{2}{3}}\right)} = \frac{(3\,k^*(\alpha_s - \alpha)^2)}{r_0^3}$$

$$\frac{d\alpha}{(\alpha_s - \alpha)^2} = \frac{(3\,k^*)}{r_0^3}dt = kdt$$

Taking into account a new overall constant ***k*** and performing the integration:

$$\int_0^{\alpha} \frac{d\alpha}{(\alpha_s - \alpha)^2} = \int_0^t kdt$$

An expression is derived that, when rearranged, enables the correlation of experimental data (α, t) and allows for the determination of the overall constant ***k***, as well as the theoretical maximum dissolution fraction α_s. This fraction depends on factors such as the particle's initial radius, temperature, fluid dynamic conditions (e.g., stirring), and the initial liquid-to-solid ratio (solvent-to-mineral).

$$\frac{1}{(\alpha_s - \alpha)} - \frac{1}{\alpha_s} = kt$$

$$\frac{1}{\alpha} = \frac{1}{\alpha_S} + \left[\frac{1}{k\alpha_s}\right]\frac{1}{t}$$